Vortex dynamics in two-dimensional Josephson junction arrays

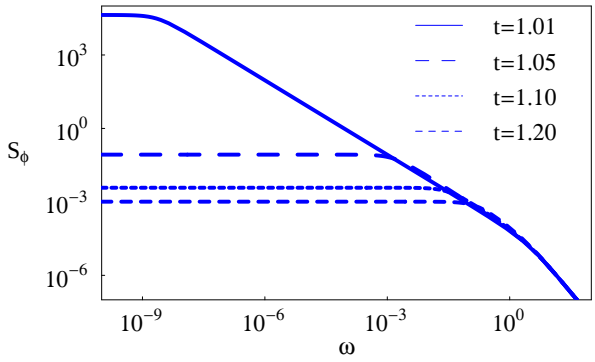

Md. Ashrafuzzaman

Université de Neuchâtel

Thèse présentée par Md. Ashrafuzzaman
à la Faculté des Sciences
de l'Université de Neuchâtel
pour l'obtention du titre de Docteur ès sciences.

sous la direction du

professeur Hans Beck

de l'Université de Neuchâtel.

Université de Neuchâtel, 2000 Neuchâtel, Switzerland,

Preface

This thesis treats vortex dynamics in two-dimensional Josephson junction arrays. We have considered both regular and diluted arrays of superconducting islands and have treated the dynamics of thermally excited vortices and antivortices in these arrays using classical calculations. Some parts of this thesis are already published and the rest of the work is in process of being published or will be submitted shortly. Every chapter consists of its conclusion separately, therefore the final conclusions are very short or it can be considered as short summary of all the conclusions.

Md. Ashrafuzzaman

Dedication

I dedicate this thesis

To my parents
To the school going children of Bangladesh

Contents

1 Introduction **1**

1.1 Josephson junction arrays 1
1.2 The Berezinskii - Kosterlitz - Thouless scenario 4
1.3 The Dynamics of JJA 5
1.3.1 Equation of motion for the phases 5
1.3.2 Microscopic derivation of the coupling constants 7
1.4 Vortex dynamics - Classical equations of motion 7

2 Vortex-Antivortex Pair Dynamics in Regular two-dimensional Josephson junction arrays : averaging over pair length distribution **11**

2.1 Theoretical approach and basic definitions 12
2.1.1 Pair relaxation picture - unscreened and screened Coulomb interaction 12
2.1.2 Bormann's approaches to dielectric function 18
2.1.3 Calculation of flux noise 19
2.2 Results 27
2.3 Conclusions 32

3 Partial structure Factors in a binary mixture of vortices and antivortices in two-dimensional Josephson junction arrays **35**

3.1 Basic definitions 35
3.2 Results 39
3.3 Conclusions 41

4 Vortex/Antivortex free dynamics in diluted two-dimensional Josephson junction arrays **55**

4.1 Introduction 55
4.2 The multiple trapping model 58
4.2.1 The multiple trapping equations 58
4.2.2 The vortex mobility 60
4.2.3 Binding energy for circular holes 62
4.3 Electrodynamic response of the array 63
4.3.1 Resistance and Inductance 63
4.3.2 Flux noise 66

4.4 Results 67
4.5 Summary and conclusions 75

5 Vortex Dynamics in two-dimensional Josephson junction arrays : Fokker-Planck Approach 79
5.1 Theoretical approach and basic definitions 79
5.1.1 Fokker-Planck equation for vortex dynamics in JJAs when vortices and antivortices are considered to be massless particles - overdamped limit 80
5.1.2 Fokker-Planck equation for vortex dynamics in JJAs when vortices and antivortices are considered to be massive particles . . . 88
5.1.3 Massive vortex antivortex pair dynamics 89
5.1.4 Vortex antivortex pair dynamics in one dimension 90
5.1.5 Vortex antivortex pair dynamics in two-dimension 100
5.2 Conclusions 101

6 Vortex-Antivortex Pair Dynamics in Regular two-dimensional Josephson junction arrays : Averaging over pair life time distribution 103
6.1 Theoretical approach and basic definitions 103
6.2 Conclusions 112

7 Summary and discussion 113

A Bibliography 117

Chapter 1

INTRODUCTION

Vortex dynamics in Josephson junction arrays (JJAs) has been an interesting field of research during last decades. Aiming at explaining some important aspects of the dynamical phenomena of JJAs in presence of thermally created vortices and antivortices in the arrays we have been working in our project during several years. We have given some possible theoretical analysis of some experimental data observed in recent years and have also given only the theoretical analysis of some other parameters which are experimentally unobserved but related to vortex dynamics in JJAs. In doing so we have sometimes used established theories or proposed new formulas and techniques and also used the Monte Carlo simulation of XY model. In our research we have mainly focused on calculating the vortex charge density correlator and using this we have discussed other parameters like flux noise, vortex dielectric function, conductance of the array etc. for both regular and disordered JJAs.

Before going to the detailed explanations on our actual research in the next few chapters we shall now focus on some aspects of Josephson junction arrays, Berezinskii-Kosterlitz-Thouless transition, vortex dynamics etc. in some details.

1.1 Josephson junction arrays

Two-dimensional (2D) Josephson junction arrays (JJA) offer a unique opportunity for studying a variety of topics in 2D physics, such as phase transitions, non-linear dynamics, percolation, frustration and disorder, in relatively ≪clean≫ experimental realisation. Fabrication of arrays and their basic physical properties have been described in various articles [1], [2]. A JJA consists of islands, positioned in some periodic or irregular arrangement, that become superconducting below a given transition temperature T_c^o. Below this temperature each island l is characterized by its superconducting wave function

$$\psi = |\psi_l| e^{i\theta_l} \tag{1.1}$$

with its amplitude and its phase. For all practical purposes one can assume that $|\psi_l|$ has the same value in each island, such that the phase is the only relevant variable. The islands are linked to each other by the Josephson coupling. The potential energy

of the array is then given by

$$H = \sum_{\langle ll' \rangle} J_{ll'}[1 - \cos(\theta_l - \theta_{l'})] \tag{1.2}$$

The sum can usually be restricted to nearest neighbors in the array and the Josephson coupling J is related to the critical current I_c by

$$J = \frac{\hbar}{2e} I_c \tag{1.3}$$

If the array is placed in a perpendicular magnetic field the phase differences in (1.2) have to be replaced by the $\ll$ gauge invariant $\gg$ combination

$$\phi_{ll'} = \theta_l - \theta_{l'} - A_{ll'} \tag{1.4}$$

where $A_{ll'}$ is the line integral

$$A_{ll'} = \frac{2e}{\hbar} \int_l^{l'} d\mathbf{r} \cdot \mathbf{A}(\mathbf{r}) \tag{1.5}$$

of the applied vector potential. Most of our subsequent calculations will be based on the assumption of a large magnetic penetration depth. Then any vector potential appearing in our equations describes an applied external electromagnetic field, whereas internal field fluctuations are neglected.

When the phases of neighboring islands differ from each other a supercurrent

$$K_{ll'} = J_{ll'} \sin \phi_{ll'} \tag{1.6}$$

flows through the junction (l, l') and the two islands get charged. The electrostatic energy

$$E_{ll'} = \frac{1}{2} \sum_{ll'} Q_l (C^{-1})_{ll'} Q_{l'} \tag{1.7}$$

has to be added to (1.2). Here Q_l is the charge of island l, related to the excess number δN_l of Cooper pairs by $Q_l = 2e\delta N_l$, and $C_{ll'}$ is the capacitance matrix of the array. Its diagonal elements determine the charging energy with respect to ground and the nearest neighbor elements represent the junction capacitance. The excess number δN_l can be identified with a canonical momentum P_l conjugate to the phase [1,3,4]:

$$[P_l, \theta_{l'}] = \frac{\hbar}{i} \delta_{ll'} \tag{1.8}$$

The electrostatic energy (1.7) thus plays the role of a (non-local) kinetic energy that has to be added to the potential energy (1.2) yielding thus the complete Hamiltonian

$$H = \frac{1}{2} \sum_{ll'} (2e)^2 P_l (C^{-1})_{ll'} P_{l'} + \sum_{\langle ll' \rangle} J_{ll'} (1 - \cos \phi_{ll'}) \tag{1.9}$$

of the array on which our equations of motion will be based in subsection 1.3.

Much work has been done in order to elucidate the thermodynamic properties of (1.9) which is indeed a challenging problem of statistical mechanics. The simplest case taking into account only the potential energy (1.2) in zero applied field is the classical XY-model in 2 dimensions. In its ground state all the ≪spins≫ are parallel, respectively all the phases θ_l are equal. This system allows to study the critical behaviour of a 2D system with a complex order parameter. It gives rise to the well-known Berezinski-Kosterlitz-Thouless phase transition [5,6] bringing in the basic concept of vortex excitations. The basic features are summarized in the following subsection.

The full form (1.9) adds two complications:

a) A JJA in an applied magnetic field corresponds to the ≪frustrated≫ XY-model. Owing to the additional term $A_{ll'}$ in the coupling energy the phase configuration in the ground state is more complicated - corresponding to magnetic field induced vortices - and the energy per bond is less negative than $-2J$. The effect of $A_{ll'}$ is measured in terms of the flux threading through an elementary cell of the array, the ≪frustration parameter≫ f

$$f = \frac{1}{2\pi} \sum_{\langle ll' \rangle} A_{ll'} \tag{1.10}$$

the sum running over the bonds going around the cell. For simple - rational - values of f the ground state phase pattern is known (see [1] and the references given there). For certain f-values interesting infinite degeneracies have been found in triangular arrays [7] The behavior at finite temperatures, in particular the various kinds of phase transitions that a frustrated array is supposed to undergo is less well understood [1].

b) Owing to the commutation relations (1.8) the full Hamiltonian (1.9) describes a quantum system, sometimes called ≪quantum XY-model≫ although its operator algebra is, of course, different from the XY-model describing quantum spins. Quantum fluctuations, surviving even at $T = 0$, add to the thermal fluctuations of the phases already present in the classical XY-model. They tend to counteract the tendency to ≪topological≫ phase order which is characteristic of the 2D classical system. Taking into account only the charging energy with respect to ground the capacitance matrix has the form $C_{ll'} = C\delta_{ll'}$ and the influence of charging energy can be expressed in terms of the ratio

$$\alpha = \frac{(2e)^2}{2CJ} \tag{1.11}$$

The corresponding phase diagram (with and without dissipation) has been studied by various methods. Approximating the cosine phase interaction by a quadratic form in the phase differences corresponds to the ≪selfconsistent harmonic approximation≫ [4,8,9]. One finds that the critical temperature decreases with increasing α and finally vanishes at a critical threshold α_c on the order of 6. The same conclusion is drawn from Quantum Monte Carlo calculations [10]. The quantum model including dissipation is presumably also relevant for describing the superconductor-insulator transition occuring at the underdoped limit of cuprate superconductors [11]. It has been shown

[12] that dissipation may lead to a new universality class characterized by an effective non-ohmic dissipation.

1.2 The Berezinskii - Kosterlitz - Thouless scenario

Treating each phase θ_l as a classical variable ranging between 0 and 2π the Hamiltonian (1.2) describes the classical 2D XY-model, the phase angle giving the direction of a classical spin of unit length at site l. Its thermodynamic properties are governed by the Berezinskii-Kosterlitz-Thouless (BKT) transition. The lowest energy configuration corresponds to all phases being equal, corresponding to the ≪ferromagnetic≫ ground state of the spins at $T = 0$. For any $T > 0$ this long range order is replaced by ≪topological≫ order due to thermal fluctuations [13]. Besides small amplitude variations, which give rise to ≪spin waves≫ in the dynamic generalization of (1.2), the main finite temperature configurations are given by thermally excited vortices (V) and antivortices (A). Their interaction varies essentially logarithmically with their distance. They thus behave like a 2D Coulomb gas. In the absence of frustration the latter is neutral (equal number of V and A). According to the BKT scenario, V and A are bound in pairs below the transition temperature T_{BKT}. When T grows above T_{BKT} more and more pairs with large separations dissociate yielding an increasing number of ≪ free ≫ V and A. The mean distance between the latter is given by the BKT correlation length ξ with its particular T-dependence

$$\xi(T) = \xi_o \; exp(\frac{b}{\sqrt{T/T_{BKT} - 1}}) \tag{1.12}$$

where ξ_o is a prefactor of the order of the lattice constant and b a parameter of order one. The topological order below T_{BKT} is characterized by a power-law spatial decay of phase (spin) correlations :

$$\langle e^{i(\theta_l - \theta_{l'})} \rangle = (\frac{|l - l'|}{a})^{-\frac{k_B T}{2\pi J(T)}} \tag{1.13}$$

with a coupling constant $J(T)$ renormalized by thermal fluctuations, and a finite helicity modulus Λ expressing the ≪phase stiffness≫ of the system. Λ is given by the variation of the free energy of the system with respect to a ≪phase twist≫ :

$$\Lambda = (\frac{\partial^2 F(\alpha)}{\partial \alpha^2})_{\alpha=0} \tag{1.14}$$

where the free energy

$$F(\alpha) = -k_B T \ln \int d[\theta] \quad e^{-\beta H[\theta,\alpha]} \tag{1.15}$$

is evaluated by imposing the boundary condition

$$\theta(na, Na) = \theta(na, 0) + \alpha \tag{1.16}$$

relating the phase $\theta(n,m)$ on a given column n of the array at the lower and the upper boundary, respectively, the lattice sites being parametrized in units of the lattice constant a by (na, ma). $\wedge$ has a particular temperature dependence. Starting from its $T = 0$ value, where it is given by the coupling constant J, it is a deacreasing function of temperature, since thermal fluctuations make the phase system softer. At T_{BKT} it jumps from a universal value

$$\wedge_c = \frac{2}{\pi} k_B T_{BKT} \tag{1.17}$$

to zero.

Above the transition temperature the phase correlation function decays exponentially with the BKT correlation length given by (1.12).

In the frustrated case there are magnetic field induced V (or A, depending on the sign of the field) already in the ground state. The thermal vortex antivortex (VA) pairs coexist with the latter. The precise nature of the corresponding phase transition in the presence of frustration is still a matter of debate, see ch. 8 of ref. [1].

The precise link between the XY-Hamiltonian (1.2) expressed in terms of the phases and the 2D Coulomb gas can be formalized by transforming it into a vortex representation with the help of a dual transformation [14, 15]. This procedure allows - at least approximately - to separate the spin wave contribution to the partition function and yields the vortex Hamiltonian

$$H_c = \frac{1}{2} \sum_{RR'} (m(R) - f) V_c(R - R')(m(R') - f) \tag{1.18}$$

The sum runs over the plaquettes of the array, $m(R)$ being the vorticity of plaquette R (in practice $m = 0$, 1 or -1). The interaction potential V_c depends logarithmically on the distance, at least for large values of the latter. The frustration f acts on the Coulomb gas of A and V as a $\ll$ background charge $\gg$. The precise critical behaviour of the BKT transition is obtained by introducing length scale dependent screening, which yields renormalization group equations [1,13,14] for the relevant parameters of the Coulomb system, namely its dielectric constant, related to the phase stiffness $\wedge$ and its fugacity.

A very extensive review of the BKT transition and the Coulomb gas model has been published by Minnhagen [17]. Other review articles, such as [18,19], are more directly concerned with dynamic properties of JJAs. In order to interpret correctly measurements on JJAs in the light of the BKT scenario one should, however, bear in mind that the latter (as critical phenomena in general) is in principle valid for the thermodynamic limit of an infinitely large system.

1.3 The Dynamics of JJA

1.3.1 Equation of motion for the phases

In order to derive equations of motion for a JJA we start from our Hamiltonian (1.9) involving Josephson coupling and electrostatic energy. It is useful for later purposes to

include a possible coupling of the array to external currents I_l flowing into (or out of) site l

$$H_1 = \sum_l I_l \theta_l \tag{1.19}$$

The resulting canonical equations read

$$\dot{\theta}_l = \frac{\partial H}{\partial P_l} = (2e)^2 \sum_{l'} (C^{-1})_{ll'} P_{l'} \tag{1.20}$$

$$\dot{P}_l = -\frac{\partial H}{\partial \theta_l} = -\sum_{l'} J_{ll'} \sin(\theta_l - \theta_{l'}) - I_l \tag{1.21}$$

Due to (1.6) and (1.8) the second equation is the continuity relation expressing charge conservation at each site of the array, the right hand side being the sum of supercurrents and external current flowing into site l.

Dissipation, due to normal current between islands and from islands to ground, is now easily added to the charge conservation expressed by (1.21) which then reads [16]:

$$\dot{P}_l = -\sum_{l'} J_{ll'} \sin(\theta_l - \theta_{l'}) - \sum_{l'} (R^{-1})_{ll'} (\frac{\hbar}{4\pi e})^2 (\dot{\theta}_l - \dot{\theta}_{l'}) - R_o^{-1} (\frac{\hbar}{4\pi e})^2 \dot{\theta}_l - I_l \tag{1.22}$$

Here we have introduced the matrix $R_{ll'}$ of junction resistances and the resistance R_o to ground, and we have used the Josephson relation between the time derivative of the phase and a corresponding voltage. Equations (1.20) and (1.22) correspond to a description of the array in terms of an effective circuit involving capacitive, resistive and Josephson ($\ll$ inductive $\gg$) elements. Neglecting the $\ll$local $\gg$ charging energy and normal current (ie between a given site and the ground) yields the so-called $\ll$ Resistively and capacitively shunted junction (RCSJ) model $\gg$.

Capacitive effects are important for ultrasmall superconducting islands. The interplay between charge and phase fluctuations lowers the superconducting transition temperature and can drive it completely to zero, leading thus to a quantum superconductor-insulator transition, as discussed in subsection 1.1. We will mostly concentrate on dynamic phenomena of $\ll$ classical arrays $\gg$ for which charging effects are unimportant. This corresponds to a motion without inertial acceleration and thus equation (1.22) with the left hand equal to zero will determine our phase dynamics. The two most frequently used equations of motion are then distinguished according to the type of phase damping involved, corresponding to the type of normal current dissipation :

a. Resistively shunted junction - RSJ - dynamics

Only the $\ll$ bond damping $\gg$ (the second term in (1.22)) is kept, describing dissipation by currents flowing through the junctions. This dynamics is therefore also called $\ll$ total current conserved $\gg$. With R_J being the junction resistance the RSJ equation for the phases then reads :

$$\dot{\theta}_l = -\sum_{l'} G_{ll'} (\frac{4\pi e}{\hbar})^2 \frac{1}{R_J} [\sum_{l''} J_{l'l''} \sin(\theta_{l'} - \theta_{l''}) + I_{l'}] \tag{1.23}$$

Here we have introduced the Green function of the lattice which allows to write the sum over bond differences of the phase θ as a sum over sites :

$$\sum_{l'}(\theta_l - \theta_{l'}) = \sum_{l'}(G^{-1})_{ll'}\theta_{l'} \tag{1.24}$$

b. Time dependent Landau-Ginzburg - TDGL - dynamics

Taking into account only site damping due to losses to the ground (only R_o is considered in (1.22)) yields the simpler ≪relaxational≫ equation of motion

$$\dot{\theta}_l = -(\frac{4\pi e}{\hbar})^2 \frac{1}{R_o}[\sum_{l'} J_{ll'} \sin(\theta_l - \theta_{l'}) + I_l] \tag{1.25}$$

This corresponds to the usual time dependent Landau-Ginzburg equation representing ≪ nonconserved ≫ dynamics (charges are ≪ lost ≫ by currents going to the ground).

In the presence of an electromagnetic field the phase differences occurring in the various current expressions have to be replaced by the corresponding ≪ gauge invariant ≫ combinations with the applied vector potential, as indicated in (1.4).

Dynamic equations, such as (1.24) or (1.25) can now be used for various analytical considerations, such as the derivation of an equation of motion for the center of a vortex or the calculation of dynamic linear response functions. They are also at the basis of numerical simulations of equilibrium dynamics and of the response of the array to very strong driving currents.

1.3.2 Microscopic derivation of the coupling constants

The various coupling constants (resistances, capacitances and Josephson couplings) of the RCSJ model describe the physical properties of single Josephson junctions. They can be derived from a microscopic transfer Hamiltonian, describing the coupling between the two superconducting islands through a normal metal or an insulator by a tunneling interaction and including Coulomb repulsion between electrons. Besides numerous earlier publications on the physics of Josephson junctions useful reviews, focussing in particular on very small junctions which can now be fabricated, have been given by Schön and Zaikin [20] and by Simanek [4]. Using either an imaginary time or a real time representation the quantum mechanical partition function can be rewritten in terms of an action involving the phase difference between the two superconductors. Its dynamics is indeed governed by a capacitance and by generalized dissipation and Josephson coupling terms.

1.4 Vortex dynamics - Classical equations of motion

Vortex excitations are the main elements determining the physical properties of a JJA, in particular in connection with the Berezinskii-Kosterlitz-Thouless scenario. Thus it is important to account for them explicitly in dynamic calculations. A classical equation of motion for a vortex configuration can be found, in analogy with the way the dynamics

of localized excitations in magnetic models is treated [21]. We start from one of our general equations of motion for the phases of the array derived in subsection 1.3.1 which can be transformed into an equation for the bond supercurrent given by (1.6). In order to prepare a continuum description of the array it is useful to number each site (of a square array) by an integer I and to attach a horizontal and a vertical bond to each site, distinguished by the index $s = x$ or y, respectively. The bond current $K_{ll'}$ (1.6) is then replaced by $K_s(I)$ and the phase difference (1.4) by $\phi_s(I)$.

Our equations of motion for the phases, derived in subsection 1.3, can be used for determining the time evolution of K_s

$$C_o \frac{\partial^2 K_s(I)}{\partial t^2} = -E_s(I) \sum_{s'I'} \{ J M_{ss'}(I - I') K_{s'}(I') + \eta_{ss'}(I - I') \dot{\phi}_s(I') \} \tag{1.26}$$

where $E_s(I) = \cos \phi_s(I)$ and the $\ll$dynamical matrix$\gg$ M ensures the correct coupling between bonds.

In equation 1.26 we have specialized to the case of a local capacity, but we still admit both types of damping discussed in subsection 1.3.1 :

$$\eta_{ss'}(I - I') = \begin{cases} \delta_{ss'} \delta_{II'} \eta_L & \text{for local damping} \\ M_{ss'}(I - I') \eta_T & \text{for bond damping} \end{cases} \tag{1.27}$$

The friction constants are proportional to the inverse resistances showing up in (1.22), ie the ground (local damping), respectively the bond resistance (bond damping).

A moving vortex is now introduced by a trial solution[22]

$$\phi_s(I,t) = \phi_s^{(v)}(I,t) + \varphi_s(I,t) \tag{1.28}$$

where

$$\phi_s^{(v)}(I,t) = arc \sin K_s^{(v)}(I|\mathbf{R}(t)) \tag{1.29}$$

The first term represents the circular symmetric $\ll$hedge hog$\gg$ phase pattern with a time dependent center $\mathbf{R}(t)$ and the second contribution describes deviations from this form. The form (1.27) is substituted into the phase equation of motion (1.26) yielding an equation for the bond currents $K_s^{(v)}$ forming the vortex pattern

$$\begin{aligned} C_o \frac{\partial^2 K_s^{(v)}(I)}{\partial t^2} &= -E^s(I) \sum_{s'I'} \{ J M_{ss'}(I - I') [E_{s'}(I') \varphi_{s'}(I') + K_{s'}^{(v)}(I')] \\ &\quad + \eta_{ss'}(I - I') \frac{\partial}{\partial t} arc \sin K_{s'}^{(v)}(I') \} \end{aligned} \tag{1.30}$$

We have neglected the small deformation field φ wherever it multiplies terms involving $\phi_s^{(v)}$. The first term on the right hand side of (1.30), involving the dynamical matrix M, represents the Peierls force acting on the moving vortex which originates in the discrete lattice structure of the JJA. Indeed, the potential energy of the phase pattern

of the vortex increases when its geometrical center moves away from the middle of a plaquette. It reaches its maximum value when the vortex center crosses the bond separating two adjacent plaquettes. The height E_B of this energy barrier depends on the lattice structure : $E_B \approx 0.199J$ for the square and $E_B \approx 0.043J$ for the triangular array [23]. Going over from the discrete lattice to a continuum and integrating out the phase variables in a suitable way (see [21] and [22] for more details) allows to obtain a Newtonian equation for the center $\mathbf{R}$ of the vortex

$$M_v \ddot{\mathbf{R}} = -\Gamma \dot{\mathbf{R}} - 2\pi q a J \hat{z} \times \vec{\varphi} \tag{1.31}$$

The parameter $q = \pm 1$ determines the sign of the excitation (V or A). The vortex mass M_v is expressed in terms of the grain capacity C_o and $a \ll$ core radius $\gg b$ of the vortex patterns (which can be taken of the order ot the lattice constant a) :

$$M_v = C_o \frac{20\pi}{9} (\frac{b}{a})^2 \tag{1.32}$$

Obviously, in the absence of an underlying discrete lattice structure there is no more energy barrier for the moving vortex. The two types (1.27) of dissipation, although yielding different equations for the phase field, lead to the same friction term in (1.31), the respective friction constants being only quantitatively different :

$$\Gamma = \begin{cases} \eta_L \frac{20\pi}{9} (\frac{b}{a})^2 & \text{for local damping} \\ \eta_L \frac{2\pi}{9} (\frac{b}{a})^2 & \text{for bond damping} \end{cases} \tag{1.33}$$

One should stress here that different calculations may yield different results for friction constant and mass: ≪simple≫ calculations like the above skteched trial function approach yield a ≪bare≫ mass, whereas taking into account the coupling of the vortex configuration with thermal fluctuations introduce a renormalization to mass and friction, which can even be (logarithmically) divergent due to the 2D ≪substrate≫, see, for example, [24]. The second term on the right hand side of (1.31) can be interpreted in different ways : it can represent the force acting on the vortex when a supercurrent, given by a phase gradient $\vec{\varphi} = \nabla\theta$, is flowing through the sample. It is usually called "Lorentz force" [1,25-27], in analogy to the force a current-carrying wire experiences in a perpendicular magnetic field. In our later calculations we will insert into equation (1.3) the phase gradient $\nabla\theta$ resulting from the presence from another vortex located at $\mathbf{R}_1$ in order to introduce the effect of V-V interaction in the equation of motion :

$$M_v \ddot{\mathbf{R}} = -\Gamma \dot{\mathbf{R}} + q_1 q_2 a^2 J^2 \frac{\mathbf{R} - \mathbf{R}_1}{(\mathbf{R} - \mathbf{R}_1)^2} \tag{1.34}$$

When capacitive effects in the array can be neglected (for sufficiently large capacities or for low enough frequencies) the mass term disappears from (1.31).

We have given above some introductory analysis of the vortex dynamics in Josephson junction arrays in two-dimension. In the subsequent chapters we are going to explain in details of different types of vortex dynamics in JJAs. There we shall explain

vortex antivortex pair dynamics and free dynamics in and without presence of disorder in the array.

In chapter 2, some aspects of vortex-antivortex (VA) pair dynamics and flux noise will be explained in details. We shall consider the dynamics above the Berezinskii-Kosterlitz-Thouless transition temperature T_{BKT} and will develop a possible form of the vortex charge density correlation function which is related to response function. The vortex mobility for VA pair dynamics will be derived from averaging the VA pair distribution function through the modification of AHNS approach [28] and the free V/A dynamical mobility will be taken from the calculation using the Mori technique. Finally we shall develop a formula for calculating the flux noise using this generalised response function.

Chapter 3 will be devoted to the study of the structure factor and some related probability distribution functions in a vortex antivortex system in a Josephson junction array at finite temperature using Monte Carlo simulation of XY model for the temperature dependent vortex density and projections in a periodic array in two dimension.

In chapter 4, we shall explain vortex or antivortex free dynamics in a diluted Josephson junction array. The free vortex dynamics and the effects of missing superconducting sites in the array will be explained using the multiple trapping model (MTM). The frequency dependent conductance of the disordered array in presence of vortices will be explained in details.

Chapter 5 will focus on calculating the vortex density correlator using a Fokker Planck equation for the time-dependent probability distribution function of vortices and antivortices. Here the time dependent phenomena of the vortex antivortex interaction and making and breaking of the pairs of the particles (V and A) will be explained in details.

In chapter 6 we shall explain vortex-antivortex pair dynamics through the consideration of a VA pair life time distribution. Contrary to the consideration of VA pair length distribution as will be explained in chapter 2 we shall devote chapter 6 in describing VA pair dynamics where we consider that there are VA pairs whose survival periods are different and in fact we can consider a distribution of VA pair life time in their dynamics in JJAs and susceptibility, dielectric functions etc will be calculated.

Finally in chapter 7 we shall give some concluding remarks on our research methodologies and the summary of the results.

Chapter 2

Vortex-Antivortex Pair Dynamics in Regular two-dimensional Josephson junction arrays : averaging over pair length distribution

In this chapter, some aspects of vortex-antivortex (VA) pair dynamics and flux noise will be explained in details.

Below the Berezinskii-Kosterlitz-Thouless (BKT) transition temperature T_{BKT} of a Josephson junction array (JJA) the thermally excited vortices and antivortices exist as pairs of different sizes. At T_{BKT} the longest vortex antivortex (VA) pairs dissociate, and for each pair a free vortex (V) and a free antivortex (A) are produced. With the increase of the temperature T from T_{BKT} more and more pairs dissociate and simultaneously more and more vortices and antivortices become free. So above T_{BKT} the thermodynamical phenomena of a JJA consists of both VA pair dynamics and V and A free dynamics. In this chapter we shall discuss VA pair dynamics in detail and will develop a possible form of the vortex charge density correlation function which is related to response function. We have proposed a generalized form of the average vortex mobility in a JJA through addition of the mobilities of the VA pair dynamics and V/A free dynamics for calculating the response function. The vortex mobility for VA pair dynamics is derived from averaging the VA pair distribution function through the modification of Ambekaokar et. al. (AHNS) expression [28] and the free V/A dynamical mobility is taken from the calculation using the Mori technique. Finally we have developed a formula for calculating the flux noise [29] using this generalised response function.

2.1 Theoretical approach and basic definitions

There are two types of approaches [30] which we have adopted here in our comparable investigations of the vortex antivortex pair dynamics in two dimensional (2D) Coulomb gas:

Pair relaxation picture - without screening

Pair relaxation picture - with screening

In this section we shall also explain a different approach for calculating the dielectric function for the vortex antivortex system from the proposal made by Dierk Bormann [31]. Then we shall develop a theoretical method for calculating the flux noise in the pick up coil due to vortex antivortex dynamics in the Josephson junction arrays.

2.1.1 Pair relaxation picture - unscreened and screened Coulomb interaction

Berezinskii-Kosterlitz-Thouless (BKT) scenario [5,6] of superfluidity in two dimensions (2D) and Kosterlitz's subsequent quantitative calculations of the static properties of a superfluid [13] suggest that in the superfluid state, smoothly varying phase fluctuations coexist with a dilute gas of bound vortex antivortex pairs. With increasing temperatures, a finite fraction of the pairs dissociates, destroying the superfluidity and causing a transition to a normal phase. Afterwards the results obtained by José et al. [14] suggest that the model used by Kosterlitz, as well as the results obtained by him, provide a universal long-wavelength description of 2D superfluidity. These theories predict that the superfluid density drops discontinuously to zero by a universal amount as the temperature is raised to the transition temperature (T_{BKT}). Since both the superfluid density and the dissipation contribute to the inertia and absorption of energy of a ^4He film, precise experimental tests of the physical ideas described above require theoretical predictions for the dissipation which has been theoretically explained by Ambegaokar et al. (AHNS). AHNS analysis of the vortex motion builds on the BKT picture of the static properties, and has been aided by an analogy with the dynamics of a plasma, confined between capacitor plates and subjected to an oscillating electric field, in which charges move by diffusion. Contribution from free vortices and bound pairs enter in the various regimes. The problem is defined by a set of Langevin equations for the particle motion where vortices and antivortices have been considered as particles of negligible masses that is the dynamics is considered in the overdamped limit.

The *polarizability* of a vortex antivortex pair of fixed length, in overdamped limit where in the dynamics of vortices and antivortices in a JJA the particles (V and A) are considered to be massless, is defined by

$$\chi(z) = \frac{q_0^2}{z\Gamma + f} \tag{2.1}$$

where Γ is the friction, z is the complex frequency and $f = V'' = \frac{\partial^2 V(r)}{\partial r^2}$ is the effective stiffness which is proportional to the potential $V(r)$ between the particles. $V(r)$ is the

Coulomb interaction between two charged particles (V and A) where $q_0(-q_0)$ is the charge of a vortex (antivortex). The unscreened form of $V(r)$ in 2D is

$$V(r) = -q_0^2 \ln(r/a) \tag{2.2}$$

with a being the lattice constant. So $V' = -\frac{q_0^2}{r}$, $V'' = \frac{q_0^2}{r^2} = \frac{q_0^2}{a^2}(\frac{a}{r})^2$. If we now let $l = \ln(r/a)$ we get $V(l) = q_0^2 l$ and $V''(l) = \frac{q_0^2}{a^2}e^{-2l}$ and

$$f(l) = \frac{q_0^2}{a^2}e^{-2l} \tag{2.3}$$

If we now introduce the length dependent screening in the Coulomb interaction between the particles we get

$$Potential: \qquad V_{sc}(l) = \frac{q_0^2 l}{\hat{\epsilon}(l)} \tag{2.4}$$

$$Force\ constant: \qquad \hat{f}(l) = \frac{f}{\hat{\epsilon}(l)} = \frac{q_o^2}{a^2}\frac{e^{-2l}}{\hat{\epsilon}(l)} \tag{2.5}$$

Here $\hat{\epsilon}(l)$ follows the following arguments (from Renormalization group (RG) theory [1,13,14]):

$$0 \le l \le l_\xi : \hat{\epsilon}(l) \text{ is given by RG equation}$$
$$l = l_\xi : \hat{\epsilon}(l_\xi) = \infty$$

with $l_\xi = \ln\frac{\xi}{a}$, ξ is the BKT correlation length of a VA pair.

Putting $z = -i\Omega$ and rearranging a little bit we finally get the definition for the *polarizability* of a VA pair in the case of length dependent screening in the Coulomb interaction between the particles is

$$\chi(\omega, l) = \frac{q_o^2 a^2}{k_B T}\frac{1}{-i\omega + B(l)} \tag{2.6}$$

where $B(l) = \frac{q_0^2}{k_B T}\frac{e^{-2l}}{\hat{\epsilon}(l)}$ and we have chosen a different scaled real frequency $\omega = \frac{\Omega}{\omega_a}$ with $\omega_a = \frac{k_B T}{\Gamma a^2}$.

According to AHNS [28] we have modified the problem of calculating the frequency dependent dynamic charge susceptibility (average pair polarizability) $\bar{\chi}(\Omega)$ of vortex antivortex dipolar system like

$$\bar{\chi}(z) = \int_a^\xi dr\ rp(r)\chi(z, r) \tag{2.7}$$

$p(r)$ is the probability of finding VA pair at size r.

In the case of unscreened Coulomb interaction the frequency dependent average dynamic charge susceptibility takes the following form

$$\bar{\chi}(\Omega) = \int_a^\xi d(r/a)\ (r/a)p(r)\frac{q_0^2}{-i\Omega\Gamma + \frac{q_o^2}{r^2}} \tag{2.8}$$

where we have considered that the length of a VA pair can be distributed between the lowest limit a and the highest limit ξ which is the KT correlation length

$$\xi(T) = a\ exp(\frac{b}{\sqrt{T/T_{BKT} - 1}}) \tag{2.9}$$

where b is of the order of unity. A simple form for the probability distribution $p(r)$, in the case of unscreened Coulomb interaction, is

$$p(r) = A(r/a)^{-4\frac{T_{BKT}}{T}} \tag{2.10}$$

The proportionality constant A can be calculated from the relation

$$\int_1^c dx\ xp(x) \doteq 1 \tag{2.11}$$

and is given by

$$A = \frac{2 - 4\frac{T_{BKT}}{T}}{c^{2-4\frac{T_{BKT}}{T}} - 1} \tag{2.12}$$

Here $c = \xi/a$ is the dimensionless KT correlation length of a VA pair.

Using equations (2.9-2.12) and rearranging equation (2.8) we obtain

$$\begin{aligned}\bar{\chi}(\omega) &= \frac{4\frac{T_{BKT}}{T} - 2}{1 - c^{2-4\frac{T_{BKT}}{T}}} \frac{q_0^2 a^2}{k_B T} \int_1^c dx \frac{x^{3-4\frac{T_{BKT}}{T}}}{4 - i\omega x^2} \\ &= \frac{4\frac{T_{BKT}}{T} - 2}{1 - c^{2-4\frac{T_{BKT}}{T}}} \frac{q_0^2 a^2}{k_B T} \int_1^c dx \frac{x^{1-4\frac{T_{BKT}}{T}}}{-i\omega + 4/x^2}\end{aligned} \tag{2.13}$$

where Boltzmann's constant k_B and BKT transition temperature T_{BKT} are related to the superconducting coupling constant J by

$$k_B T_{BKT} \approx J \tag{2.14}$$

Now letting $l = \ln x$ and $\ln c = l_2$, the upper cut-off for the correlation length where VA pairs cross from interaction zone over to repulsive zone (where the pairs dissociate) in equation (2.13), we get

$$\bar{\chi}(\omega) = \frac{4\frac{T_{BKT}}{T} - 2}{1 - c^{2-4\frac{T_{BKT}}{T}}} \frac{q_0^2 a^2}{k_B T} \int_0^{l_2} dl \frac{e^{l(2-4\frac{T_{BKT}}{T})}}{-i\omega + 4e^{-2l}} \tag{2.15}$$

where q_0, the charge of a vortex follows from the Josephson coupling constant J through

$$q_0 = \sqrt{2\pi J} \tag{2.16}$$

When the dynamic charge susceptibility $\bar{\chi}(\omega)$ is known, we can calculate the frequency dependent dielectric function $\epsilon(\omega)$ through the following relation

$$\epsilon(\omega) = 1 + 2\pi \frac{n}{2} \bar{\chi}(\omega) \tag{2.17}$$

where n is the density of vortices and antivortices in the array.

Using equation (2.15) the expression for dielectric function at equation (2.17) becomes

$$\epsilon(\omega) = 1 + 2\pi q_0^2 n \frac{4^{\frac{T_{BKT}}{T}} - 2}{1 - c^{2-4\frac{T_{BKT}}{T}}} \frac{a^2}{2k_B T} \int_1^c dx \frac{x^{3-4\frac{T_{BKT}}{T}}}{4 - i\omega x^2} \tag{2.18}$$

The above expression for dielectric function can be reexpressed like

$$\epsilon(\omega) = 1 + \int_1^c dx \ \phi(x,T) \frac{1}{4 - i\omega x^2} \tag{2.19}$$

where the probability function $\phi(x,T)$ for the dielectric function is given by

$$\phi(x,T) = 2\pi q_0^2 n \frac{4^{\frac{T_{BKT}}{T}} - 2}{1 - c^{2-4\frac{T_{BKT}}{T}}} \frac{a^2}{2k_B T} x^{3-4\frac{T_{BKT}}{T}} \tag{2.20}$$

Now changing the variable in the integral in equation (2.18) like $l = \ln x$ where $x = r/a$ we get the rearranged form of the equation (2.18)

$$\epsilon(\omega) = 1 + \int_0^{l_2} dl \ \phi(l,T) \frac{1}{-i\omega + 4e^{-2l}} \tag{2.21}$$

where the new probability function $\phi(l,T)$ is given by the following equation

$$\phi(l,T) = 2\pi q_0^2 n \frac{4^{\frac{T_{BKT}}{T}} - 2}{1 - c^{2-4\frac{T_{BKT}}{T}}} \frac{a^2}{2k_B T} e^{l(2-4\frac{T_{BKT}}{T})} \tag{2.22}$$

Now we come back to the case where the Coulomb interaction between the particles is screened by the length dependent dielectric function. In this case $\chi(\omega, l)$ follows from equation (2.6) and the frequency dependent average dynamic charge susceptibility $\bar{\chi}(z = -i\Omega)$ of VA dipolar system takes the following form

$$\bar{\chi}(z) = \int_a^\xi dr \ r\bar{p}(r)\chi(z,r) \tag{2.23}$$

where $\bar{p}(r)$ is the probability of finding VA pair at size r in screened Coulomb interaction $\hat{V}(r) = V(r)/\hat{\epsilon}(r)$ and is given by

$$\bar{p}(r) = \frac{e^{-\beta\hat{V}(r)}}{\bar{A}} \tag{2.24}$$

$$\bar{A} = \int_a^\xi dr \ re^{-\beta\hat{V}(r)} = a^2 \int_0^{l_\xi} dl \ e^{2l - \beta V_{sc}(l)} \equiv a^2 A \tag{2.25}$$

With all these and making some rearrangements we get the expression for the average pair susceptibility

$$\bar{\chi}(\omega) = \frac{q_o^2 a^2}{k_B T} \int_0^{l_\xi} dl \frac{\phi_1(l)}{-i\omega + B(l)} \tag{2.26}$$

$$\phi_1(l) = \frac{1}{A'} e^{2l-\beta V_{sc}(l)}, \qquad \beta = \frac{1}{k_B T} \tag{2.27}$$

$$A' = \int_0^{l_\xi} dl e^{2l-\beta V_{sc}(l)} = \int_0^{l_\xi} dl e^{2l-4l(1-t(l))} \tag{2.28}$$

Here we have used Renormalization group (RG) theory for the interaction $V_{sc}(l)$. According to RG we get (for details see in [1,13,14,17])

$$t(l) = c\ ctg(\phi - 2cl), \qquad c = \sqrt{|t_o^2 - y_o^2|},\ \phi = arc\cos(\frac{t_o}{y_o}) \tag{2.29}$$

with $0 < \phi < \pi$ and the expression for t_o and y_o in $t(l)$ as follows

$$t_o = 1 - 1/\tau, \qquad y_o = \frac{2\pi}{\tau} e^{-\pi/\tau} \tag{2.30}$$

where τ is given by

$$\tau = \frac{4k_B T}{q_0^2}, \quad so\ , \tau_c = \frac{4k_B T_{BKT}}{q_0^2} \tag{2.31}$$

The value of τ_c is calculated using the condition that at the transition temperature

$$t_o = -y_o \tag{2.32}$$

We now get the relation

$$V_{sc}(l) = \frac{q_0^2 l}{\epsilon(l)} = q_0^2 l\tau(1 - t(l)) = 4k_B T l(1 - t(l)) \tag{2.33}$$

where we have used the following relation for the length dependent dielectric function

$$\epsilon(l) = \frac{1}{\tau(1 - t(l))} \tag{2.34}$$

So the final expression for $\phi_1(l)$ is

$$\phi_1(l) = \frac{e^{2l-4l(1-t(l))}}{\int_0^{l_\xi} dl e^{2l-4l(1-t(l))}} \tag{2.35}$$

Similarly using the RG equations (as before) we get the expression for $B(l)$

$$B(l) = 4e^{-2l}(1 - t(l)) \tag{2.36}$$

The dielectric function for the VA system (pair dynamics) in the case of screened Coulomb interaction then takes the following form

$$\epsilon(\omega) = 1 + 2\pi q_0^2 n \frac{a^2}{2k_B T} \int_0^{l_\xi} dl \frac{\phi_1(l)}{-i\omega + B(l)} \tag{2.37}$$

Pair Life Time

Susceptibility: $\chi(z) = \frac{A}{z\Gamma+f}$ which yields $\chi(t) \sim e^{-\frac{f}{\Gamma}t}$
since $\int_0^\infty dt e^{-zt}\frac{A}{\Gamma}e^{-\frac{f}{\Gamma}t} = \frac{A}{\Gamma}\frac{1}{z+f/\Gamma} = \frac{A}{z\Gamma+f}$

We now consider that a VA pair can not survive for ever. It has rather a finite life time τ' [30]. After this life time the pair dissociate. Considering this finite life time the VA pair polarizability is modified as

$$\hat{\chi}(t) = \frac{A}{\Gamma}e^{-f/\Gamma t}e^{-t/\tau'} \; so \; \hat{\chi}(z) = A\frac{1}{z\Gamma + f + \Gamma/\tau'(r)}$$

Screened Coulomb interaction

For a pair of size r we have proposed the following form for the pair life time

$$\frac{1}{\tau'(r)} = \omega_o e^{-\beta[V(r_2)-V(r)]} = \omega_o e^{\beta q_o^2[\frac{\ln(r_2/a)}{\epsilon(r_2)} - \frac{\ln(r/a)}{\epsilon(r)}]} \tag{2.38}$$

where ω_o is a free parameter representing an attempt frequency for pairs trying to escape the barrier up to the maximum of the potential, at the distance r_2, by thermal excitation. More specifically r_2 is the distance where the vortex-antivortex attraction ceases and falls into a repulsive (non attractive) zone. In the Coulomb interaction in the above equation we have considered the vortex and antivortex are having opposite (namely positive and negative) components of charges.

Now as $f(r) = \frac{q_0^2}{r^2} = \frac{4k_BT_{BKT}}{r^2}$ through some intermediate calculations we get the expression for the susceptibility $\hat{\chi}(\omega)$ as follows

$$\hat{\chi}(\omega) = \frac{q_0^2a^2}{k_BT}\int_0^{l_2} dl \frac{\phi_1(l)}{-i\omega + 4e^{-2l}(1-t(l)) + \nu_o e^{-4\frac{T_{BKT}}{T}(\frac{l_2}{\epsilon(l_2)} - \frac{l}{\epsilon(l)})}} \tag{2.39}$$

with $\nu_o = \omega_o/\omega_a$, is the scaled frequency (inverse of the life time for a VA pair).

Unscreened Coulomb interaction

$\frac{1}{\tau'(r)} = \omega_o e^{-\beta\Delta E}$ where $\Delta E = V(r) - V(\xi) = q_0^2 \ln(\xi/r)$ so we get

$$\frac{1}{\tau'(r)} = \omega_o e^{-\beta q_0^2 \ln(\xi/r)} = \omega_o(\xi/r)^{-\beta q_0^2} = \omega_o(\xi/r)^{-4\frac{T_{BKT}}{T}} \tag{2.40}$$

So the expression for susceptibility is

$$\hat{\chi}(\omega) = \frac{4\frac{T_{BKT}}{T} - 2}{1 - c^{2-4\frac{T_{BKT}}{T}}}\frac{q_0^2a^2}{k_BT}\int_0^{l_2} dl \frac{e^{l(2-4\frac{T_{BKT}}{T})}}{-i\omega + 4e^{-2l} + \nu_o e^{-4\frac{T_{BKT}}{T}(l_2-l)}} \tag{2.41}$$

2.1.2 Bormann's approaches to dielectric function

There are two approaches through which Dierk Bormann [31] calculated the dielectric function $\epsilon(\omega)$ of paired vortex antivortex system. In the first approach he calculated directly the dielectric function and in the second approach he calculated the inverse of the dielectric function. The ways he did them are explained bolow.

a) Bormann's 1st approach

Bormann reformulated the AHNS expression for calculating the dielectric function, $\epsilon(\Omega)$ for bound pairs like this

$$\epsilon(\Omega) = 1 + \int_a^{\xi} dr \frac{d\epsilon(r)}{dr} \frac{1}{1 - i\Omega\tau(r)} \tag{2.42}$$

where the scale dependent dielectric constant $\epsilon(r)$ is determined by the KT flow equations. The factor $\frac{1}{1-i\Omega\tau(r)}$ in the integral describes the relaxation of an individual pair of size r. The expression for the relaxation time $\tau(r)$ can be obtained from an analysis of the single-pair problem and is given as follows

$$\tau(r) \approx \frac{r^2\epsilon(r)\Gamma}{3.5q^2} \tag{2.43}$$

Now using $l = \ln\frac{r}{a}$ i.e.,$l_\xi = \ln\frac{\xi}{a}$, $\omega = \Omega/\omega_a$ where $\omega_a = \frac{k_B T}{\Gamma a^2}$ and rearranging the above expressions we get the final form of dielectric function for bound pairs like this

$$\epsilon(\omega) = 1 + \int_0^{l_\xi} dl \frac{2c^2/\tau}{(1-t(l))^2(1+(\phi-2cl)^2)} \frac{1}{1 - i\omega\frac{e^{2l}}{14(1-t(l))}} \tag{2.44}$$

where we have used the relation for the scale dependent dielectric function $\epsilon(l)$ with $t(l)$.

Now we can reexpress equation (2.44) for dielectric function $\epsilon(\omega)$ like the following

$$\epsilon(\omega) = 1 + \int_0^{l_\xi} dl\,\phi(l,\tau) \frac{1}{1 - i\omega\frac{e^{2l}}{14(1-t(l))}} \tag{2.45}$$

where the probability function $\phi(l,\tau)$ for dielectric function $\epsilon(\omega)$ is given by

$$\phi(l,\tau) = \frac{2c^2/\tau}{(1-t(l))^2(1+(\phi-2cl)^2)} \tag{2.46}$$

b) Bormann's 2nd approach

In the second approach Bormann reformulated the AHNS expression for calculating the dielectric function, $\epsilon(\Omega)$ for bound pairs like this

$$1/\epsilon(\Omega) = 1 + \int_a^{\xi} dr \frac{d[1/\epsilon(r)]}{dr} \frac{1}{1 - i\Omega\tau(r)} \tag{2.47}$$

where all the parameters here follow Bormann's first approach except the inverse of the scale dependent dielectric function $\epsilon(r)$ is taken here in the integrand and thus the whole expression in the right hand side of the above equation gives us the inverse of the dielectric function for the dipolar VA systems. So following the other rearrangements explained in the column of Bormann's 1st approach we can reformulate the expression here in Bormann's 2nd approach like this

$$1/\epsilon(\omega) = 1 + \int_0^{l_\xi} dl\phi'(l,\tau)\frac{1}{1 - i\omega\frac{e^{2l}}{14(1-t(l))}} \tag{2.48}$$

where the probability function $\phi'(l,\tau)$ for the inverse of the dielectric function $1/\epsilon(\omega)$ is given by

$$\phi'(l,\tau) = -\tau\frac{2c^2}{1 + (\phi - 2cl)^2} \tag{2.49}$$

We have, in our comparable studies of the dielectric function, also used the above Bormann's two approaches of calculating dielectric function. We have got some similarities and discrepancies between our approach and Bormann's which will be explained in the results section.

2.1.3 Calculation of flux noise

In this subsection we shall calculate the flux [29] in the pick up coil which is placed at a certain height from a Josephson junction array (JJA) where the thermally created vortices and antivortices are moving.

Considering the displacement current negligible, Ampere's law

$$\nabla \times \mathbf{B} = \mu_0(\varepsilon_0\partial_t\mathbf{E} + \mathbf{J}) \tag{2.50}$$

where $\mathbf{E}$ is the electric field, becomes

$$\nabla \times \mathbf{B} = \mu_0\mathbf{J} \tag{2.51}$$

The relation

$$\nabla \cdot (\nabla \times \mathbf{B}) = 0 \tag{2.52}$$

implies, for the current density J

$$\nabla \cdot \mathbf{J} = 0 \tag{2.53}$$

and for the charge density ρ, in the static case, using the continuity equation

$$\partial_t\rho = 0 \tag{2.54}$$

Maxwell's equations become

$$\begin{aligned} \nabla \cdot \mathbf{E} &= \tfrac{\rho}{\epsilon_0} \\ \nabla \times \mathbf{E} + \partial_t\mathbf{B} &= 0 \\ \nabla \cdot \mathbf{B} &= 0 \end{aligned} \tag{2.55}$$

Introducing vector potential ($\mathbf{A}$) and scalar potential (ϕ) by the definitions $\mathbf{B} = \nabla \times \mathbf{A}$ and $\mathbf{E} = -\partial_t \mathbf{A} - \nabla\phi$ and using equations (2.51-2.53) we get the following relation in Fourier space

$$\begin{aligned} \phi(\mathbf{k}) &= \frac{\rho(\mathbf{k})}{\epsilon_0 k^2} \\ \mathbf{A}(\mathbf{k},\omega) &= \frac{\mu_0 \mathbf{J}(\mathbf{k},\omega)}{k^2} \end{aligned} \tag{2.56}$$

In the case of quasistatic approximation we neglect dynamic field and charge fluctuations as well as radiation effects. In a conducting medium, the static charge distribution ρ is completely screened so we can assume

$$\rho \equiv \phi \equiv 0 \tag{2.57}$$

Therefore the electromagnetic fields are entirely specified in terms of the current $\mathbf{J}$(defined by equation (2.56)), magnetic field $\mathbf{B}$ and electric field $\mathbf{E}$ where

$$\mathbf{B} = i\mathbf{k} \times \mathbf{A} \tag{2.58}$$

and

$$\mathbf{E} = i\omega\mathbf{A} \tag{2.59}$$

Now consider a conducting film (vortex and antivortex are at z=0 plane) with internal current density

$$\mathbf{J^{in}}(\mathbf{r}) = \delta(r_\perp)\mathbf{J}(\mathbf{r}_{||}) \tag{2.60}$$

where $\mathbf{r}$ decomposes into two components, one parallel to the V-A plane $r_{||}$ and the other is $r_\perp$ which is perpendicular to the V-A plane that is along the Z-axis.

$$\mathbf{r} := (\mathbf{r}_{||}, \mathbf{r}_\perp) \tag{2.61}$$

We know by definition the flux through some area is the total lines of force flowing through that area. So the flux that comes out perpendicular to the V-A plane and flows through the loop of the the pick up coil is defined as

$$\phi = \int \mathbf{B}.d\mathbf{S} = \int \nabla \times \mathbf{A} \cdot d\mathbf{S} = \oint d\mathbf{r} \cdot \mathbf{A} \tag{2.62}$$

Here we have used Stoke's theorem and to calculate the flux through the pick up coil we have to do the closed integral along the loop of the pick up coil.

Flux can also be expressed in terms of the characteristic function of the coil i.e., in the pick up coil the flux is expressed as

$$\phi = \int d^3r \boldsymbol{\chi} \cdot \mathbf{A}(\mathbf{r}) \tag{2.63}$$

Here $r \in$ loop of the pick up coil and magnetic potential ($\mathbf{A}$) is in the pick up coil due to current ($\mathbf{J}$) in the plane of V-A. The characteristic function of the pick up coil χ is defined as

$$\boldsymbol{\chi}(\mathbf{r}) = \mathbf{e}_\perp \times \frac{\mathbf{r}_{||}}{r_{||}} \delta(r_{||} - R)\delta(r_\perp - d) \tag{2.64}$$

Here R is the radius of the pick up coil and d is the perpendicular distance of the pick up coil from the V-A plane and $\mathbf{e}_\perp$ is unit vector along Z-axis [33].

The characteristic function just describes the current distribution of a unit current flowing along the closed wire path describing the coil.

Now we calculate the vector potential due to currents in the plane. Using Fourier transformation we get

$$\begin{aligned}\mathbf{A}(\mathbf{r}) &= \int d^3k \quad e^{i\mathbf{k}.\mathbf{r}}\mathbf{A}(\mathbf{k}) \\ &= \int d^2k_\parallel \quad e^{i\mathbf{k}_\parallel\cdot\mathbf{r}_\parallel}\int dk_\perp \quad e^{ik_\perp r_\perp}\frac{\mu_0\mathbf{J}(\mathbf{k}_\parallel)}{k_\parallel^2+k_\perp^2} \\ &= \mu_0 2\pi\int d^2k_\parallel \quad e^{i\mathbf{k}_\parallel\cdot\mathbf{r}_\parallel}\frac{e^{-k_\parallel r_\perp}}{2k_\parallel}\mathbf{J}(\mathbf{k}_\parallel)\end{aligned} \tag{2.65}$$

In particular the vector potential in the plane of the array is

$$\mathbf{A}(\mathbf{r}_\parallel) = 2\pi\mu_0\int d^2k_\parallel e^{i\mathbf{k}_\parallel\cdot\mathbf{r}_\parallel}\frac{\mathbf{J}(\mathbf{k}_\parallel)}{2|\mathbf{k}_\parallel|} \tag{2.66}$$

which in Fourier transformation can be written as

$$\mathbf{A}(\mathbf{k}_\parallel) \equiv \frac{1}{(2\pi)^2}\int d^2r_\parallel e^{-i\mathbf{k}_\parallel\cdot\mathbf{r}_\parallel}\mathbf{A}(\mathbf{r}_\parallel) = \frac{\pi\mu_0}{|\mathbf{k}_\parallel|}\mathbf{J}(\mathbf{k}_\parallel) \tag{2.67}$$

Using eqn.(2.64) and (2.65-2.67) we get from eqn. (2.63)

$$\begin{aligned}\phi &= \pi\mu_0\int d^3r\int d^2k_\parallel \quad e^{i\mathbf{k}_\parallel\cdot\mathbf{r}_\parallel}e^{-k_\parallel r_\perp}\frac{\mathbf{J}(k_\parallel)}{k_\parallel}\cdot(\mathbf{e}_\perp\times\frac{\mathbf{r}_\parallel}{r_\parallel})\delta(r_\parallel-R)\delta(r_\perp-d) \\ &= \pi\mu_0\int r_\parallel dr_\parallel\int dr_\perp\int d\theta\int d^2k_\parallel e^{ik_\parallel r_\parallel cos\theta}e^{-k_\parallel r_\perp}\frac{J(k_\parallel)}{k_\parallel}cos\theta\delta(r_\parallel-R)\delta(r_\perp-d) \\ &= \pi\mu_0 R\int d^2k_\parallel(\int d\theta cos\theta e^{ik_\parallel Rcos\theta})e^{-k_\parallel d}\frac{J(k_\parallel)}{k_\parallel} \\ &= i2\pi^2\mu_0 R\int d^2k_\parallel J_1(k_\parallel R)e^{-k_\parallel d}\frac{J(k_\parallel)}{k_\parallel}\end{aligned} \tag{2.68}$$

Here we have used

$$\int d\theta cos\theta e^{ik_\parallel Rcos\theta} = 2\pi i J_1(k_\parallel R) \tag{2.69}$$

where $J_1(k_\parallel R)$ is Bessel function.

Now we shall derive the expression for $J(k_\parallel)$. We know 2D Ginzburg Landau (GL) free energy functional in the London limit is

$$H = \int d^2r_\parallel\frac{g^*}{2m^*}|\hbar\nabla_\parallel\theta - e^*\mathbf{A}|^2 + \frac{1}{2\mu_0}\int d^3r|\mathbf{B}-\mathbf{B}^{ex}|^2 \tag{2.70}$$

where two dimensional condensate wave function, $\psi = |\psi_\infty| e^{i\theta}$, $\theta \rightarrow phase$, $n_s^* = |\psi_\infty|^2 \rightarrow$ 2D no. density of Cooper pairs, m^* and e^* are mass and charge of the Cooper pairs respectively.
In plane the magnetic penetration depth is

$$\lambda_{||} := \frac{2m^*}{\mu_0 n_s^* e^{*2}} \tag{2.71}$$

and the flux quantum is

$$\phi_0 = \frac{2\pi\hbar}{e^*} \tag{2.72}$$

and the vector potential is

$$\mathbf{A} := \mathbf{A^{in}} + \mathbf{A^{ex}} \tag{2.73}$$

Therefore eqn.(2.70) becomes

$$H = \frac{1}{\mu_0 \lambda_{||}} \int d^2 r_{||} |\frac{\phi_0}{2\pi} \nabla_{||} \theta - \mathbf{A}^{ex} - \mathbf{A}^{in}|^2 + \frac{1}{2\mu_0} \int d^3 r |\mathbf{B^{in}}|^2 \tag{2.74}$$

Minimizing H with respect to $\mathbf{A^{in}}$ (no field fluctuations)

$$0 \doteq \frac{\delta H}{\delta \mathbf{A}^{in}(\mathbf{r})} = -\frac{2}{\mu_0 \lambda_{||}} \delta(r_\perp) (\frac{\phi_0}{2\pi} \nabla_{||} \theta - \mathbf{A}^{ex} - \mathbf{A}^{in})(r_{||}) + \frac{1}{\mu_0} \nabla \times \mathbf{B^{in}}(\mathbf{r}) \tag{2.75}$$

Now we know

$$\nabla \times \mathbf{B}^{in} \approx \mu_0 \mathbf{J}^{in} \tag{2.76}$$

Using eqn.(2.60), and (2.75,2.76) we get the link between current and vector potential (London equation) as follows

$$\mathbf{J} \doteq \frac{2}{\mu_0 \lambda_{||}} (\frac{\phi_0}{2\pi} \nabla_{||} \theta - \mathbf{A}^{ex} - \mathbf{A}^{in}) \tag{2.77a}$$

which can be reexpressed as

$$\mathbf{J}(\mathbf{r}_{||}) = \frac{2}{\mu_0 \lambda_{||}} (\mathbf{J}_\theta - \mathbf{A}(\mathbf{r}_{||})) \tag{2.77b}$$

where $\mathbf{J}_\theta = \frac{\phi_0}{2\pi} \nabla_{||} \theta$. Now to make vortex degrees of freedom explicit we write the phase gradient as a sum of it's longitudinal and transverse parts:

$$\nabla_{||} \theta = \nabla_{||} \vartheta - \mathbf{e}_\perp \times \nabla_{||} \Phi_v \tag{2.78}$$

Here $\vartheta \rightarrow$ a real, single valued field, $\Phi_v \rightarrow$ electrostatic potential for vorticity i.e., it obeys the two dimensional(2D) Poisson eqn.

$$\nabla_{||}^2 \Phi_v = 2\pi \rho_v \tag{2.79}$$

where

$$\rho_v(\mathbf{r}_{\|}) := \sum_l q_l \delta^2(\mathbf{r}_{\|} - \mathbf{R}_l) \tag{2.80}$$

Using eqn.(2.79) we can rewrite eqn.(2.78) in Fourier space as

$$\nabla_{\|}\theta(k_{\|}) = ik_{\|}\vartheta(\mathbf{k}_{\|}) - 2\pi i \frac{\mathbf{e}_{\perp} \times \mathbf{k}_{\|}}{k_{\|}^2}\rho_v(k_{\|}) \tag{2.81}$$

Using eqn.(2.81) we get from eqn.(2.77) the transverse part of the internal current as

$$J_T(k_{\|}) = \frac{2}{\mu_0\lambda_{\|}}(\phi_0\frac{\rho_v}{k_{\|}} - A_T^{ex} - A_T^{in}) \approx \frac{2}{\mu_0\lambda_{\|}}\phi_0\frac{\rho_v(k_{\|})}{k_{\|}} \tag{2.82}$$

We have used above approximation as we are dealing the case without applied field and the internal field is neglected.

In equation (2.68) we shall now use the expression in eqn. (2.82) for $J(k_{\|})[\approx J_T(k_{\|})]$

$$\begin{aligned}\phi &= \pi\mu_0 R\frac{2}{\mu_0\lambda_{\|}}\phi_0(2\pi i)\int d^2k_{\|}\frac{J_1(k_{\|}R)}{k_{\|}^2}e^{-k_{\|}d}\rho_v(k_{\|}) \\ &= i\phi_0 4\pi^2\frac{R}{\lambda_{\|}}\int d^2k_{\|}\frac{J_1(k_{\|}R)}{k_{\|}^2}e^{-k_{\|}d}\rho_v(k_{\|})\end{aligned} \tag{2.83}$$

This is the total flux in the pick up coil due to vortices and antivortices in the V-A plane(Z=0 plane).

Now flux-flux correlation is

$$\begin{aligned}\langle\delta\phi(t)\delta\phi(0)\rangle = (-i)(i)(2\pi)^4(\frac{R}{\lambda_{\|}})^2\int d^2k_{\|}\int d^2k_{\|}^{'} \\ \frac{J_1(k_{\|}R)J_1(k_{\|}^{'}R)}{k_{\|}^2k_{\|}^{'2}}e^{-(k_{\|}+k_{\|}^{'})d}\langle\delta\rho_v(k_{\|},t)\delta\rho_v^*(k_{\|}^{'},0)\rangle\end{aligned} \tag{2.84}$$

$$As \qquad \langle\delta\rho_v(k_{\|},t)\delta\rho_v^*(k_{\|}^{'},0)\rangle = \varphi_{\rho\rho}(k_{\|},t)\delta_{k_{\|},k_{\|}^{'}} \tag{2.85}$$

where $\varphi_{\rho\rho}(k_{\|},t)$ is the dynamic vortex density correlation function at time t. We get

$$\langle\delta\phi(t)\delta\phi(0)\rangle = 16\pi^4\frac{R^2}{\lambda_{\|}^2}\int d^2k_{\|}\frac{|J_1(k_{\|}R)|^2}{k_{\|}^4}e^{-2k_{\|}d}\varphi_{\rho\rho}(k_{\|},t) \tag{2.86}$$

We shall now consider the case of quasistatic screening. Taking into account the internal field we get from eqnuation (2.77) through Fourier transformation

$$\mathbf{J}(\mathbf{k}_{\|}) = \frac{2}{\mu_0\lambda_{\|}}(\mathbf{J}_\theta(\mathbf{k}_{\|}) - \mathbf{A}(\mathbf{k}_{\|})) \tag{2.87}$$

Using equation (2.67) we can rewrite this equation as

$$\mathbf{J}(\mathbf{k}_{\|}) = \frac{2}{\mu_0\lambda_{\|}}(\mathbf{J}_\theta(\mathbf{k}_{\|}) - \frac{\pi\mu_0}{|\mathbf{k}_{\|}|}\mathbf{J}(\mathbf{k}_{\|})) \tag{2.88}$$

from which we get

$$\mathbf{J}(\mathbf{k}_{\|}) = \frac{2}{\mu_0\lambda_{\|}}\frac{\lambda_{\|}k_{\|}}{1+\lambda_{\|}k_{\|}}\phi_0\frac{\rho_v(k_{\|})}{k_{\|}} \tag{2.89}$$

Using this value for $J(k_{\|})$ in original expression of the total flux ϕ (eqn. 2.68) we get

$$\begin{aligned}\phi &= \mu_0 R 2\pi^2 i\int d^2k_{\|}\frac{2\phi_0}{\mu_0\lambda_{\|}}\frac{\lambda_{\|}k_{\|}}{1+\lambda_{\|}k_{\|}}\frac{J_1(k_{\|}R)}{k_{\|}^2}e^{-k_{\|}d}\rho_v(k_{\|}) \\ &= \phi_0 R 4\pi^2 i\int d^2k_{\|}\frac{J_1(k_{\|}R)}{k_{\|}(1+\lambda_{\|}k_{\|})}e^{-k_{\|}d}\rho_v(k_{\|})\end{aligned} \tag{2.90}$$

So the flux-flux correlation is

$$\begin{aligned}\langle\delta\phi(t)\delta\phi(0)\rangle &= 16\pi^4R^2\phi_0^2\int d^2k_{\|}\int d^2k_{\|}^{'}\frac{J_1(k_{\|}R)J_1(k_{\|}^{'}R)}{(1+\lambda_{\|}k_{\|})(1+\lambda_{\|}k_{\|}^{'})} \\ &\quad \frac{1}{k_{\|}k_{\|}^{'}}e^{-(k_{\|}+k_{\|}^{'})d}\langle\delta\rho_v(k_{\|},t)\delta\rho_v^*(k_{\|}^{'},0)\rangle\end{aligned} \tag{2.91}$$

or,

$$\begin{aligned}&\langle\delta\phi(t)\delta\phi(0)\rangle \\ &= 16\pi^4R^2\phi_0^2(2\pi)\int_0^\infty\frac{dk_{\|}}{k_{\|}}\frac{|J_1(k_{\|}R)|^2}{(1+\lambda_{\|}k_{\|})^2}e^{-2k_{\|}d}\varphi_{\rho\rho}(k_{\|},t)\end{aligned} \tag{2.92}$$

Phenomenological expression for $\varphi_{\rho\rho}(\mathbf{k}_{\|},\mathbf{t})$

We shall try to calculate an expression for $\varphi_{\rho\rho}(k_{\|},t)$ through a phenomenological approach [34]. Equation of continuity of charge

$$\frac{\partial\rho(\mathbf{r},t)}{\partial t} + \nabla\cdot\mathbf{j}_\rho(\mathbf{r},t) = 0 \tag{2.93}$$

Here we know, $\mathbf{j}_\rho = -D\nabla\rho + \sigma\mathbf{E}$ where $D = \frac{k_BT}{\gamma} := diffusion\ constant$, the first term is Fick diffusion current and the second term is the Ohmic contribution due to the charges of V and A. Therefore we get

$$\dot{\rho} - D\nabla^2\rho + \sigma\nabla\cdot\mathbf{E} = 0 \tag{2.94}$$

$$or, \qquad \frac{\partial\rho(\mathbf{r},t)}{\partial t} - D\frac{\partial^2\rho(\mathbf{r},t)}{\partial\mathbf{r}^2} + \frac{\sigma}{\varepsilon}\rho(\mathbf{r},t) = 0 \tag{2.95}$$

where we have used the Maxwell's equation

$$\nabla \cdot \mathbf{E} = \frac{1}{\varepsilon}\rho(\mathbf{r}, t) \tag{2.96}$$

Now Fourier transformation of $\rho(\mathbf{r}, t)$ is

$$\hat{\rho}(p, t) = \frac{1}{\sqrt{N}} \int_{-\infty}^{\infty} d^2 r e^{i\mathbf{p}\cdot\mathbf{r}} \rho(\mathbf{r}, t) \tag{2.97}$$

and

$$\varphi_{\rho\rho}(p, t) = \langle \hat{\rho}(p, t)\hat{\rho}^*(p, 0)\rangle \tag{2.98}$$

The correlation function in the Fourier transformation is

$$\varphi_{\hat{\rho}\hat{\rho}}(p, \omega) = \int_{-\infty}^{\infty} dt e^{i\omega t} \varphi_{\hat{\rho}\hat{\rho}}(p, t) \tag{2.99}$$

Laplace transformation of the correlation function is

$$\phi_{\hat{\rho}\hat{\rho}}(p, z) = \int_{0}^{\infty} dt e^{-zt} \varphi_{\hat{\rho}\hat{\rho}}(p, t) \tag{2.100}$$

Using these we get from the continuity equation

$$\frac{\partial \hat{\rho}(p, t)}{\partial t} - D(-ip)^2 \hat{\rho}(p, t) + \frac{\sigma}{\varepsilon}\hat{\rho}(p, t) = 0 \tag{2.101}$$

Using Laplace's transformation we get

$$z\hat{\rho}_L(p, z) - \hat{\rho}(p, 0) + Dp^2 \hat{\rho}_L(p, z) + \frac{\sigma}{\varepsilon}\hat{\rho}_L(p, z) = 0 \tag{2.102}$$

Here we have used the initialization condition: at $t = 0$, $\hat{\rho}_L(p, t = 0) = \hat{\rho}(p, 0)$.

Now we use Einstein's diffusion relation $D = \frac{k_B T}{\gamma}$ where γ = frictional constant which is the inverse of the vortex mobility at finite temperature T. Here $\frac{\sigma}{\varepsilon} = Dp_0^2$ where we know $p_0^2 = \frac{2\pi n e^2}{k_B T}$. Considering the value of dielectric constant $\varepsilon = 1$ we get

$$\hat{\rho}_L(p, z) = \frac{\hat{\rho}(p, 0)}{z + \frac{k_B T}{\gamma}(p^2 + p_0^2)} \tag{2.103}$$

Using the above expressions we get

$$\begin{aligned} \phi_{\rho\rho}(p, z) \quad &= \int_{0}^{\infty} dt e^{-zt} \langle \hat{\rho}(p, t)\hat{\rho}^*(p, 0)\rangle \\ &= \langle \hat{\rho}_L(p, z)\hat{\rho}^*(p, 0)\rangle \\ &= \frac{\langle \hat{\rho}(p, 0)\hat{\rho}^*(p, 0)\rangle}{z + \frac{k_B T}{\gamma}(p^2 + p_0^2)} \\ &= \frac{S_{\rho\rho}(p)}{z + \frac{k_B T}{\gamma}(p^2 + p_0^2)} \end{aligned} \tag{2.104}$$

where we have defined $\langle\hat{\rho}(p,0)\hat{\rho}^*(p,0)\rangle = S_{\rho\rho}(p)$ as the static charge structure factor.

Applying successive transformation (Laplace first and then Fourier) on $\varphi_{\rho\rho}(k_{||},t)$ and replacing $k_{||}$ by p, we get

$$\begin{aligned}\phi_{\hat{\rho}\hat{\rho}}(\mathbf{p},z) &= \int_0^\infty \langle\hat{\rho}(\mathbf{p},t)\hat{\rho}^*(\mathbf{p},0)e^{-zt}dt = \frac{1}{2\pi}\int_0^\infty dt\int_{-\infty}^{+\infty} d\omega^{'}\varphi_{\rho\rho}(\mathbf{p},\omega^{'})e^{-zt}e^{-i\omega^{'}t} \\ &= \frac{1}{2\pi}\int_{-\infty}^{+\infty} d\omega^{'}\frac{\varphi_{\rho\rho}(\mathbf{p},\omega^{'})}{i\omega^{'}+z} \qquad (2.105)\end{aligned}$$

Replacing z by $-i\omega+\varepsilon$ we get

$$\begin{aligned}\phi_{\hat{\rho}\hat{\rho}}(\mathbf{p},-i\omega+\varepsilon) &= \frac{1}{2\pi i}\int_{-\infty}^{+\infty} d\omega^{'}\frac{\varphi_{\rho\rho}(\mathbf{p},\omega^{'})}{\omega^{'}-\omega-i\varepsilon} \\ &= \frac{1}{2\pi i}\int_{-\infty}^{+\infty} d\omega^{'}\varphi_{\rho\rho}(\mathbf{p},\omega^{'})(\mathbf{P}(\frac{1}{\omega^{'}-\omega})+i\pi\delta(\omega^{'}-\omega)) \qquad (2.106)\end{aligned}$$

where the symbol $\mathbf{P}$ means taking the principal Cauchy value. The last equality holds because ε is a small real frequency.

From the above relation we get the following relation

$$\lim_{\varepsilon\to 0^+} Re[\phi_{\rho\rho}(\mathbf{p},-i\omega+\varepsilon)] = \frac{1}{2}\varphi_{\rho\rho}(\mathbf{p},\omega)$$

Using this relation and replacing $k_{||}$ by q in the Fourier transformed form of eqn.(2.92) we get

$$\begin{aligned}\hat{S}_\phi(\omega) &= \int_{-\infty}^{\infty} dt e^{i\omega t}\langle\delta\phi(t)\delta\phi(0)\rangle \\ &= 32\pi^5 R^2\phi_0^2\int_0^\infty \frac{dq}{q}\frac{|J_1(qR)|^2}{(1+\lambda_{||}q)^2}e^{-2qd}2Re[\phi_{\rho\rho}(|\mathbf{q}|,-i\omega)] \qquad (2.107)\end{aligned}$$

Using equation (2.104) for $\phi_{\rho\rho}$ the final expression for the flux noise $S_\phi(\omega)$ is given by

$$S_\phi(\omega) = 64\pi^5\frac{R^2}{\omega_a}\phi_0^2\int_0^\infty\frac{dk}{k}\frac{|J_1(k\hat{R})|^2}{(1+\hat{\lambda}k)^2}e^{-2k\hat{d}}Re[\frac{S_{\rho\rho}(k)}{-i\omega+\frac{k_BT}{\gamma(\omega)}\frac{k^2}{S_{\rho\rho}(k)}}] \qquad (2.108)$$

Here $S_{\rho\rho}(k)$ is the structure factor (explained in details in the next chapter). ω is the same scaled frequency as used and explained in section 2.1.1. In place of constant friction γ we have used here a frequency dependent friction $\gamma(\omega)$.

In the case of coexistence of paired and free vortices and antivortices above T_{BKT} the proposed mobility which is the inverse of the friction function $\gamma(\omega)$ in the above equation is replaced by a linear combination of the weighted mobilities for bound pairs $\mu_b(\omega)$ (inverse of the friction function, $\frac{1}{\gamma_b(\omega)} = \mu_b(\omega)$) and mobility for the free vortices and antivortices $\mu_f(\omega) = \frac{1}{\gamma_f(\omega)}$ that is the total mobility is

$$\mu(\omega) = (1-\nu_f)\mu_b(\omega) + \nu_f\mu_f(\omega) \qquad (2.109)$$

$\gamma_b(\omega)$ is defined through the average pair polarizability $\bar{\chi}_b$ by the following relation

$$\gamma_b(\omega) = \frac{1}{-i\omega_a\omega}\left(\frac{1}{\frac{1}{2}\bar{\chi}_b(\omega)} - \frac{1}{\frac{1}{2}\bar{\chi}_b(\omega=0)}\right) \tag{2.110}$$

where $\bar{\chi}_b(\omega)$(or $\hat{\chi}_b(\omega)$ if we consider the pair life time) is the average polarisability of a VA pair which follows from sebsection 2.1.1.

$\gamma_f(\omega)$ is derived using Mori's technique of calculating the dynamics correlation function [30,35,36] and takes the following expression

$$\begin{aligned}\gamma_f(\omega) \quad &= \Gamma(1 + \frac{g_c}{8}\frac{1}{1-2s\nu_f\times -i\omega}\{\ln(\frac{1}{2s\nu_f\times -i\omega}) + \frac{1-4s\times -i\omega}{(1-2s\nu_f\times -i\omega)^2}\ln(2s\times -i\omega) \\ &+\frac{\frac{2}{\nu_f^2}-1}{(\frac{1}{\nu_f^2}-1)^2}\ln(\frac{1}{\nu_f})^2 - \frac{1}{1-2s\times -i\omega} - \frac{1}{\frac{1}{\nu_f^2}-1}\})\end{aligned} \tag{2.111}$$

Here $\nu_f = \frac{n_f}{n}$ $(0 \leq \nu_f \leq 1)$ and $n_f = \frac{1}{\xi^2}$ is the free vortex density. $g_c = \frac{2\pi J}{k_B T}$ and takes a constant value of 7 (for $k_B T_{BKT} \approx 0.9$) or 4 (for $k_B T_{BKT} \approx \frac{\pi}{2}$). $s = \frac{1}{2\pi g_c \nu_f \bar{n}}$ where $\bar{n} = na^2$ is the average vortex density per unit cell [37,38].

2.2 Results

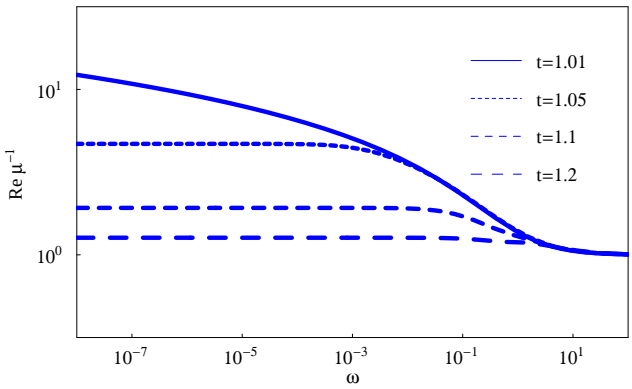

Figure 2.1: $Re\mu_f^{-1}$ vs ω (using equation 2.111) for free vortex dynamics. $\omega = \frac{\Omega}{\omega_a}$.

In the case of free vortex dynamics three frequency regimes emerge, separated by the scale frequencies $\omega_a = \frac{k_B T}{\Gamma a^2}$ and $\omega_\xi = \frac{k_B T}{\Gamma \xi^2}$. Here the inverse of the friction function (equation 2.111 and figure 2.1) $Re[\mu_f(\omega)^{-1}]$ is flat for $\omega < \omega_\xi/\omega_a$ with a value increasing as the temperature dependent correlation length ξ^2 that is depending on temperature. It coincides with the bare friction parameter Γ for $\omega > \omega_\xi/\omega_a$ whereas $Re[\mu_f(\omega)^{-1}] \propto \ln|\omega|$ in between [30]. The resulting dielectric function, shown in figure 2.2, indeed follows MP (Minnhagen phenomenology) behavior [32] that is $Re[\epsilon(\omega)^{-1}] \propto \omega$ for $\omega_\xi/\omega_a < \omega < 1$ a frequency range that increases when T_{BKT} is approached. The

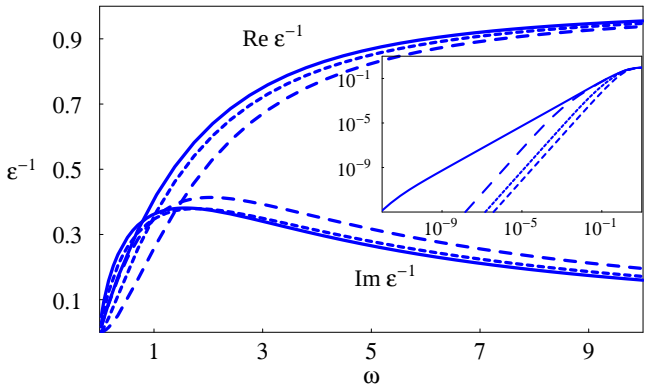

Figure 2.2: Dielectric function ϵ vs ω for free vortex dynamics. Solid, short-dashed and long-dashed lines are for $t = T/T_{BKT} = 1.01, 1.10, 1.20$. The inset represents the log-log plot for $Re\epsilon^{-1}$ with $t = 1.05$ (double dashed line) in addition to the other three temperatures.

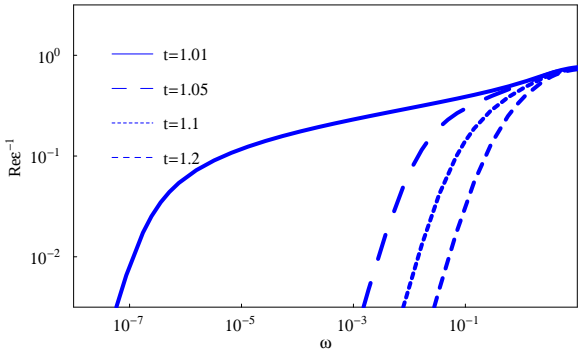

Figure 2.3: $Re\epsilon^{-1}$ vs ω (using equation 2.17 with equation 2.39 for the susceptibility) for vortex antivortex pair dynamics in the case of screened Coulomb interaction (including pair life time).

values of the peak ratio [30] $r = \frac{Im[1/\epsilon(\omega_m)]}{Re[1/\epsilon(\omega_m)]}$ varies between 0.67 and 0.73 for the three temperatures shown in figure 2.2, closer to MP ($r = 2/\pi$) than to Drude behavior ($r = 1$) where the dielectric function at low frequencies follows $Re[\epsilon_D(\omega)^{-1}] \propto \omega^2$ relation. We can memorise here the Drude form: $Re[\frac{1}{\epsilon}] = \frac{\omega^2\epsilon_b}{\omega^2\epsilon_b^2+\sigma_v^2}$ and $Im[\frac{1}{\epsilon}] = \frac{\omega\sigma_v}{\omega^2\epsilon_b^2+\sigma_v^2}$ where ϵ_b is the contribution from bound pairs and σ_v is the zero frequency vortex conductivity. Here ω_m is the frequency at which $Im[1/\epsilon(\omega_m)]$ is maximal. Thus, insofar the contribution of free vortices is concerned, anomalous MP dynamics is explained by the increasing influence of the long range Coulomb force, which makes motion more and more *sluggish*. Whereas at high temperatures the potential is (metalically) screened for all relevant length scales, screening becomes less and less efficient on approaching T_{BKT}, where the screening length ξ diverges. However, contrary to MP, we obtain a response which always crosses over to Drude-like when $\omega < \omega_\xi/\omega_a$; if this were not the

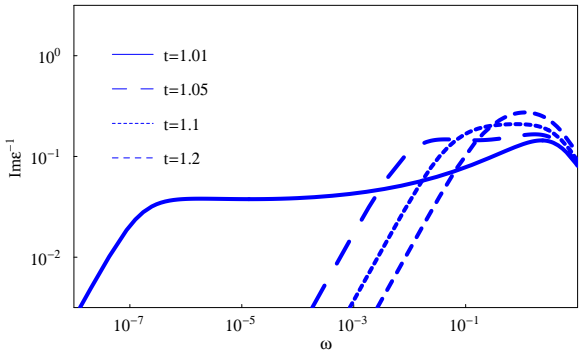

Figure 2.4: $Im\epsilon^{-1}$ vs ω (using equation 2.17 with equation 2.39 for the susceptibility) for vortex antivortex pair dynamics in the case of screened Coulomb interaction (including pair life time).

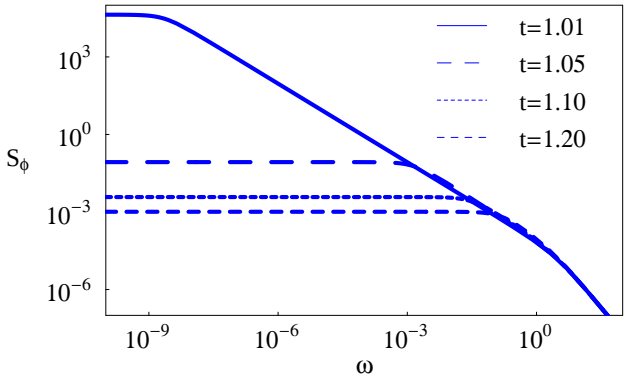

Figure 2.5: S_ϕ vs ω (using equation 2.108 with equations 2.109 and 2.41) with T-dependent $k_0^2 = \pi^2/\langle r^2 \rangle$ for vortex antivortex pair dynamics in the case of unscreened Coulomb interaction (including pair life time).

case, the array would still be superconducting above T_{BKT} [39], whereas in reality a finite flux-flow resistance yields a finite conductance at zero frequency. The flux noise spectrum we obtain considering only free vortices, however, does not show any extended $1/\omega$ region. Notably enough, both resulting $1/\epsilon(\omega)$ and $S_\phi(\omega)$ compare satisfactorily with Minnhagen's simulations [38]. One may thus draw the conclusion that anomalous MP behaviour for the dielectric function does not yield the - equally anomalous - $1/\omega$ noise, which should thus have a different origin.

For the *paired vortex* mobility $\mu_b(\omega)$, following [28], we average the dynamic polarizability of a single pair over a suitable probability distribution function (equation 2.24) for the pair size r [28,35]. The Boltzmann factor $\propto e^{-\beta \frac{q_0^2 \ln(r/a)}{\epsilon(r)}} \theta(\xi - r)$ is cut-off at the BKT correlation length, where the scaled potential ceases to be attractive. We have also introduced a finite pair life time [equation 2.38 and 2.40] which represents the time up to which the pair can survive. After this time a VA pair breaks and becomes

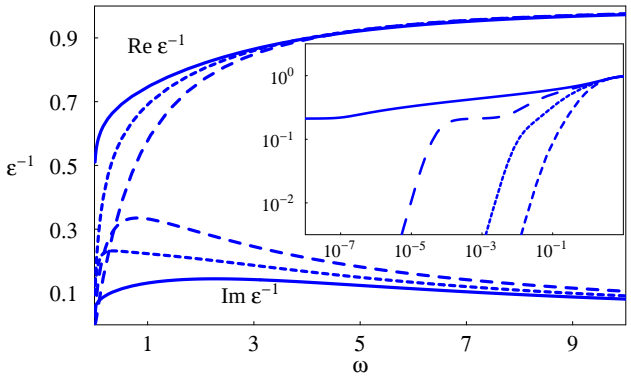

Figure 2.6: ϵ vs ω (using equation 2.17) using the combined mobility (equation 2.110) pair (including pair life time) and free dynamics. Solid, short-dashed and long-dashed lines are for $t = T/T_{BKT} = 1.01, 1.10, 1.20$. The inset represents the log-log plot for $Re\epsilon^{-1}$ with $t = 1.05$ (double dashed line) in addition to the other three temperatures.

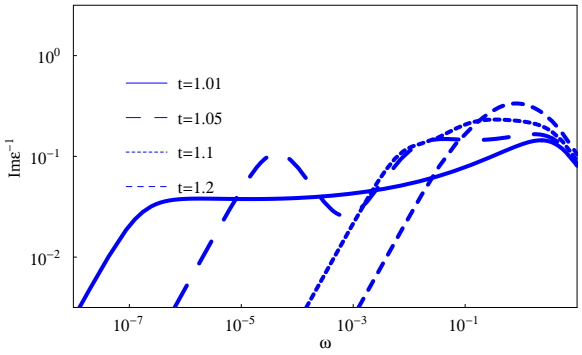

Figure 2.7: $Im\epsilon^{-1}$ vs ω using the combined mobility pair (including pair life time) and free dynamics.

free. From the polarizability, as explained earlier, by the usual relations for Coulomb systems [40], one obtains the corresponding pair mobility μ_b, the corresponding charge correlator (in equation 2.108) and the pair dielectric function $\epsilon_b(\omega)$. Three frequency regimes can be distinguished (see figure 2.3).

(i) Drude behaviour $Re[1/\epsilon_b(\omega)] \propto \omega^2$ extends up to a critical frequency $\omega_\xi \sim \xi^{-2}$.

(ii) In the window $\omega_\xi/\omega_a < \omega < 1$, $Re[1/\epsilon_b(\omega)] \propto \omega^{s(T)}$, where the T-dependent exponent $s(T) \approx 1/3$ near T_{BKT} and decreases with increasing T; its value is determined by the detailed r-dependence of the Boltzmann factor, force constant and pair life time in determining the dynamical polarizability as is explained earlier.

(iii) Finally, for $\omega > 1$, the high-frequency Drude form is recovered.

The two cross over frequencies namely ω_ξ and ω_a are both also clear in $Im[1/\epsilon_b(\omega)]$ vs ω plot (figure 2.4). Beyond ω_a all curves fall on the same line and then $Im[1/\epsilon_b(\omega)]$

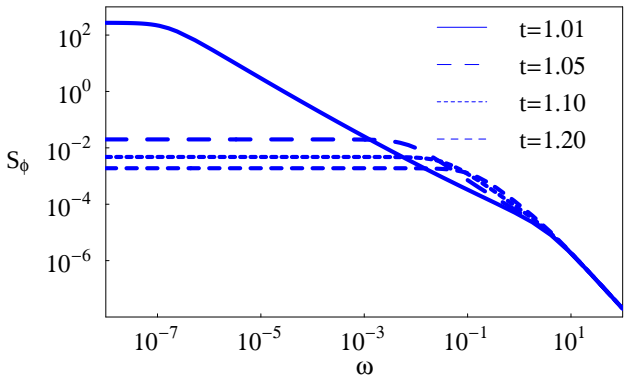

Figure 2.8: S_ϕ vs ω for the combined mobility (equation 2.110) pair (including pair life time) and free dynamics with constant $k_0^2(= 2\pi q_0^2 n/k_B T) = 1.0$ in the case of screened Coulomb interaction.

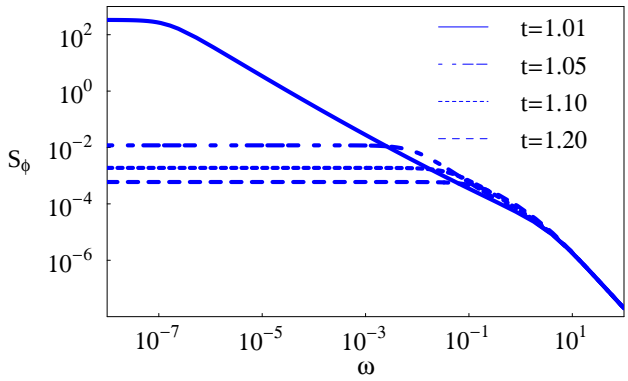

Figure 2.9: S_ϕ vs ω for the combined mobility pair (including pair life time) and free dynamics with T dependent $k_0^2(= 2\pi q_0^2 n/k_B T)$ in the case of screened Coulomb interaction.

decreases as $1/\omega$.

We have also compared our results (explained above) with the dielectric function plot (not shown here) using equation (2.45) and equation (2.48) proposed by Dierk Bormann and using our modification as explained in section 2.1.2. We see in $Re[1/\epsilon_b(\omega)]$ vs ω plot (using equation 2.45) all the curves finally fall on each other with a value of 1 at high frequency and $Re[1/\epsilon_b(\omega)] \propto \omega^2$ at low frequency region while $Re[1/\epsilon_b(\omega)] \propto \omega$ is seen for a very short mid frequency regime at higher temperatures like at $T/T_{BKT} = 1.05, 1.10$ etc. In $Re[1/\epsilon_b(\omega)]$ vs ω plot (using equation 2.48) we have got $Re[1/\epsilon_b(\omega)] \propto \omega$ for an extended mid frequency region and the Drude type behavior ($Re[1/\epsilon_b(\omega)] \propto \omega^2$) is shifted towards very low frequency region. But here we have got a strong discrepancy in the values of $Re[1/\epsilon_b(\omega)]$'s in the high frequency region where all curves ($Re[1/\epsilon_b(\omega)]$) end with a value of 0.1 which is much less (1/10th) than the value 1 which we have got for all $Re[1/\epsilon_b(\omega)]$'s in the high frequency region using our approach for the dielectric

function whose final expression is shown in equation 2.37.

The flux noise resulting from paired motion is shown in figure 2.5 where $S_{\rho\rho}(k) = \frac{k^2}{k^2+k_0^2}$ with $k_0^2 = \pi^2/\langle r^2\rangle$. If we choose a fixed value for $k_0^2 (= \frac{k_B T}{2\pi q_0^2 n})$, n being taken from [37,38], i.e. a length proportional to the mean distance between particles yields $S_\phi(\omega) \propto \omega^{-a(T)}$, with $a(T) = 1$ at T_{BKT} and increasing above (figures 2.8, 2.9). We notice that the curves for different temperatures cross each other (there is a hint that this also happens in the experimental data of [39]). On the other hand, having taken into account only the response of single pairs, it seems more appropriate using the mean structure factor for an ensemble of independent pairs; then, $k_0^2 = \frac{\pi^2}{\langle r^2\rangle}$, where $\langle r^2\rangle$ is the T-dependent mean square of the pair size calculated using Boltzmann factor $\phi(r)$. The resulting flux noise spectrum (figure 2.5) varies as $1/\omega$, and all the curves for different temperatures fall on top of each other for $\omega > \omega_\xi/\omega_a$, as it is seen in the experiments [39,41]. The white noise level showing up for $\omega < \omega_\xi/\omega_a$ is also strongly T-dependent and is given by $S_\phi(0) = \frac{1}{(2\pi)^4}\frac{\mu_b(0)^{-1}}{k_B T n}(\frac{k_B T}{J})^2$.

The KT correlation length shows up in $\mu_b(0) \sim \xi^{-2}$ and thus $S_\phi(0) \sim \xi^2$. However, when ξ reaches the sample size, $\mu_b(0)$ saturates and the T-dependence of $S_\phi(0)$ is dominated by the total density n of vortex excitations. This "masking" of the true critical slowing down has been observed in Ref.[39].

As a final step we combine the two contributions to obtain the total mobility $\mu(\omega)$. The contribution of pairs is still dominant up to $T = 1.1 T_{BKT}$, since its weight is larger, although the free vortices mobility itself exceeds the one of bound pairs. Combining the two contributions (figure 2.6 and 2.7) yields a rather extended flat region of $Im[1/\epsilon(\omega)]$ for intermediate frequencies, which is another signature of anomalous vortex dynamics, also emerging from numerical simulations [38]. The behavior of the corresponding flux noise (shown in figures 2.8 and 2.9) does not differ much from that of pair dynamics only at low temperature region. But for higher temperature region free dynamics dominates over the paired motion and thus the $1/\omega$ noise regime reduces and finally at very high temperature completely vanishes.

2.3 Conclusions

Our analytical calculations, combining *free* and *pair* motions, give the following insight into vortex dynamics in JJAs above the BKT transition temperature:

(*i*) The anomalous Minnhagen phenomenology (MP) is a consequence of the motion of (unbound) vortices in a Coulomb potential which is screened by other *free* particles. The more this screening decreases upon approaching transition temperature, the more anomalous behavior is pronounced. However, MP does not lead to $1/\omega$ flux noise.

(*ii*) Vortices and antivortices moving as *pair*, at short enough distances and up to some finite life time, yield an even more anomalous vortex dielectric constant with temperature-dependent frequency exponents. This effect, combined with a T-dependent pair structure factor indeed gives $1/\omega$ flux noise in an intermediate frequency range. That is the $1/\omega$ flux noise arises due to the vortex antivortex pair dynamics and $1/\omega$

part reduces with the increase of temperature and finally is lost at very high temperature when almost all pairs break and screened interactions dominate.

Chapter 3

Partial structure Factors in a binary mixture of vortices and antivortices in two-dimensional Josephson junction arrays

The structure factor of a vortex antivortex system in a Josephson junction array (JJA) at finite temperature is an important quantity. In this chapter we shall try to derive a concrete form of charge structure factor and some related probability distribution functions. For this we shall use the Monte Carlo simulation of XY model for the temperature dependent vortex density and position in a periodic array in two dimension (2D). We have performed the simulations [37] for periodic arrays of different sizes and temperatures. With the results of the monte Carlo simulation we have investigated the wave number and temperature dependence of the structure factor.

3.1 Basic definitions

In a two dimensional Josephson junction array at finite temperature every site of a lattice is represented by some spin angle θ_i. Now summing the successive differences of the spin angles $\triangle\theta_{ij}$ modulo 2π around one unit cell we get the following relation

$$\sum_{mode\ 2\pi} \triangle\theta_{ij} = 2\pi n \tag{3.1}$$

where n is an integer. If $n = +1$ the site is occupied by a vortex (V) and if $n = -1$ the site is occupied by an antivortex (A).

When some cells follow the above relation (eqn 3.1) with $n = \pm 1$ we consider that the cells are occupied by a vortices or antivortices. Most of the researchers consider that the vortices or antivortices are coordinated at the centers of the cells (for example see [38] and the references there in). We have given another method of choosing coordinates

of the vortices and antivortices inside the cells here. In our model we have taken the coordinates of a vortex or antivortex in a point where the lines representing the spin angles at each four corners (for square array) of a cell meet or if they don't meet at a single point each spin line will meet its neighboring two spin lines and that is how we get four crossing points which make a square. We then take the center of mass of this square to be the coordinate of the vortex or antivortex in the cell. Therefore the coordinates of vortices and antivortices can be anywhere inside the cells and are of course not always at the centers of the cells. The resultant of the Coulomb interactions on a particle (V or A) due to the surrounding particles forces the vortex or antivortex to choose the appropriate coordinate inside the lattice site and doesn't allow it to be always at the center of the cell. This is how we have calculated the positions of individual vortices and antivortices in our Monte Carlo simulation in 2D XY model.

In a two dimensional Josephson junction array (JJA) the charge density of a vortex gas is expressed in real space as

$$\rho_v(\mathbf{r}) = \frac{1}{\sqrt{N}} \sum_l q_l \delta(\mathbf{r} - \mathbf{R}_l) \tag{3.2}$$

where N is the total number of charges that is the total number of vortices and antivortices in the array, q_l and $\mathbf{R}_l$ are the charge and position of lth vortex (V) or antivortex (A) in the array. Here the charge $q_l = +1$ for vortex and $q_l = -1$ for antivortex are considered. If the temperature $T = 0$ the charge density in the array is also 0 because in our model the vortices and antivortices (so the charge density) arise due to the thermal excitations of the array at finite temperature T. This temperature effect on charge density will be explained in the results section.

The charge structure factor is defined as

$$S_{\rho\rho}(k) = \frac{1}{N} \sum_{ll'} q_l q_{l'} \langle e^{i\mathbf{k}\cdot(\mathbf{R}_l - \mathbf{R}_{l'})} \rangle \tag{3.3}$$

which is the equal time limit of expression (2.85).

We now define some functions of such a system of particles (V and A) where we shall not include the charges of V and A which we shall call the number functions. The number pair distribution function is defined as

$$D(\mathbf{r}, \mathbf{r}') = \frac{1}{N} \sum_{l \neq l'} \langle \delta(\mathbf{r} - \mathbf{R}_l) \delta(\mathbf{r}' - \mathbf{R}_{l'}) \rangle \tag{3.4}$$

The number radial distribution function

$$g(\mathbf{x}) = \frac{1}{N} \sum_{l \neq l'} \langle \delta(\mathbf{x} - (\mathbf{R}_l - \mathbf{R}_{l'}) \rangle \tag{3.5}$$

The number structure factor is defined as

$$S_{nn}(\mathbf{k}) = \frac{1}{N} \sum_{ll'} \langle e^{i\mathbf{k}\cdot(\mathbf{R}_l - \mathbf{R}_{l'})} \rangle \tag{3.6}$$

Using the functions defined above it is easy to prove the following relations

$$\int d^2x e^{i\mathbf{k}\cdot\mathbf{x}}[g(\mathbf{x})-1] = S_{nn}(\mathbf{k}) - 1 - (2\pi)^2\delta(\mathbf{k}) \tag{3.7}$$

$$\frac{1}{(2\pi)^2}\int d^2k e^{-i\mathbf{k}\cdot\mathbf{x}}[S_{nn}(\mathbf{k}) - 1 - (2\pi)^2\delta(\mathbf{k})] = g(\mathbf{x}) - 1 \tag{3.8}$$

$$where\ in\ 2D \qquad \int d^2k e^{i\mathbf{k}\cdot\mathbf{x}} = (2\pi)^2\delta(\mathbf{x}) \tag{3.9}$$

In 2D we can now evaluate the angular averaged number structure factor $\bar{S}_{nn}(k)$ and charge structure factor $\bar{S}_{\rho\rho}(k)$ averaging $S_{nn}(\mathbf{k})$ and $S_{\rho\rho}(\mathbf{k})$ respectively over $\theta \in [0, 2\pi]$.

$$\bar{S}_{nn}(k) = \frac{1}{2\pi}\int d\Omega_k S_{nn}(\mathbf{k}) = \frac{1}{N}\sum_{ll'}\langle J_0(k|\mathbf{R}_l - \mathbf{R}_{l'})\rangle \tag{3.10a}$$

$$\bar{S}_{\rho\rho}(k) = \frac{1}{2\pi}\int d\Omega_k S_{\rho\rho}(\mathbf{k}) = \frac{1}{N}\sum_{ll'}^{N} q_l q_{l'}\langle J_0(k|\mathbf{R}_l - \mathbf{R}_{l'})\rangle \tag{3.10b}$$

We now define the averaged partial structure factors $\bar{S}_{++}(k)$ for vortex vortex, $\bar{S}_{--}(k)$ for antivortex antivortex and $\bar{S}_{+-}(k)$ for vortex antivortex in a two component (vortex and antivortex) fluid in the following ways

$$\bar{S}_{++}(k) = \frac{1}{N/2}\sum_{ll'}\langle J_0(k|\mathbf{R}_l - \mathbf{R}_{l'})\rangle \tag{3.10c}$$

where $R_l, R_{l'}$ represent the coordinates of vortices only.

$$\bar{S}_{--}(k) = \frac{1}{N/2}\sum_{ll'}\langle J_0(k|\mathbf{R}_l - \mathbf{R}_{l'})\rangle \tag{3.10d}$$

where $R_l, R_{l'}$ represent the coordinates of antivortices only.

$$\bar{S}_{+-}(k) = \frac{1}{N}\sum_{ll'}\langle J_0(k|\mathbf{R}_l - \mathbf{R}_{l'})\rangle \tag{3.10e}$$

where $R_l, R_{l'}$ represent the coordinates of both vortices and antivortices but the correlation is restricted between opposite type of charges (vortices and antivortices) excluding the correlation between similar type of charges.

If we consider (excluding self-correlation $l = l'$)

$$\bar{S}'_{nn}(k) = \frac{1}{N}\sum_{l\neq l'}\langle J_0(k|\mathbf{R}_l - \mathbf{R}_{l'})\rangle \tag{3.11}$$

we get

$$As \qquad \frac{1}{(2\pi)^2}\int d^2q e^{-i\mathbf{q}\cdot\mathbf{x}}\bar{S}'_{nn}(\mathbf{q}) = g(\mathbf{x}) \tag{3.12a}$$

$$g(x) = \frac{1}{(2\pi)^2}\frac{1}{N}\sum_{l\neq l'}\int_0^\infty qdqJ_0(qx)\langle J_0(q|\mathbf{R}_l - \mathbf{R}_{l'}|)\rangle$$

$$= \frac{1}{(2\pi)^2}\int_0^\infty qdq\int_0^\infty dyJ_0(qx)J_0(qy)\frac{1}{N}\sum_{l\neq l'}\langle\delta(y - |\mathbf{R}_l - \mathbf{R}_{l'}|)\rangle \quad (3.12b)$$

Now

$$\int_0^\infty qdqJ_0(qx)J_0(qy) = \delta(x-y)A(x) \quad (3.13)$$

Therefore for isotropic system

$$g(x) = \frac{1}{(2\pi)^2}\int dy\delta(x-y)A(x)\frac{1}{N}\sum_{l\neq l'}\langle\delta(y - |\mathbf{R}_l - \mathbf{R}_{l'}|)\rangle \quad (3.14)$$

Here $A(x) = \frac{2\pi}{x}$ which follows from any integral book (e.g. hints are given in Table of Integrals Series and Products by I. S. Gradshteyn, I. M. Ryzhik; chapter 6.521, p 672) or can be achieved through the following normalisation procedure

$$\int d^2xg(x) = \frac{1}{N}\sum_{l\neq l'}\int d^2x\langle\delta(\mathbf{x} - (\mathbf{R}_l - \mathbf{R}_{l'}))\rangle = N-1$$

$$= \frac{1}{(2\pi)^2}\int dxx2\pi\frac{1}{N}\sum_{l\neq l'}A(x)\langle\delta(x - |\mathbf{R}_l - \mathbf{R}_{l'}|)\rangle$$

$$= \frac{1}{N}\sum_{l\neq l'}A(|\mathbf{R}_l - \mathbf{R}_{l'}|)|\mathbf{R}_l - \mathbf{R}_{l'}|\frac{1}{2\pi} \quad (3.15)$$

$$with \quad A(y) = \frac{2\pi}{y} \quad (3.16)$$

$$as \quad A(|\mathbf{R}_l - \mathbf{R}_{l'}|)|\mathbf{R}_l - \mathbf{R}_{l'}|\frac{1}{2\pi} = 1 \quad (3.17)$$

So we can define the distance distribution function as

$$\phi(x) = \frac{1}{N}\sum_{l\neq l'}\langle\delta(x - |\mathbf{R}_l - \mathbf{R}_{l'}|)\rangle \quad (3.18)$$

and the angular averaged radial distribution function as

$$\bar{g}(x) = \frac{1}{2\pi}\int d\Omega_x g(\mathbf{x}) \quad (3.19)$$

The relation betwen the average radial distribution function $\bar{g}(x)$ and the distance distribution function $\phi(x)$ then becomes

$$\bar{g}(x) = \frac{1}{2\pi x}\phi(x) \quad (3.20)$$

For isotropic system we get

$$\begin{aligned}\int d^2x e^{i\mathbf{q}\cdot\mathbf{x}} g(x) = & \int_0^\infty dx x J_0(qx)\bar{g}(x)2\pi \\ & = \int_0^\infty dx x J_0(qx)\frac{\phi(x)}{2\pi x}2\pi \\ & = \int_0^\infty dx J_0(qx)\phi(x) \end{aligned} \tag{3.21}$$

Therefore for isotropic system the average value of the structure factor takes the following form

$$\bar{S}_{nn}(q) = 1 + \int_0^\infty dx J_0(qx)\phi(x) \tag{3.22}$$

This gives the number structure factor if we use equation (3.18) for $\phi(x)$. But if we include $q_l q_{l'}$ inside the summation in equation (3.18) the above equation defines for the charge structure factor (both are originally defined in equation (3.10)).

3.2 Results

Here we shall explain the results coming out of the Monte Carlo simulation of the XY model. For better placement of the figures we have put them at the end of this chapter.

Figures 3.1 and 3.2 represent the snap-shots of vortices and antivortices in a 50×50 array in two dimensions for two different temperatures. The vortices and antivortces do not sit only at the centers of the lattice sites rather they follow our model of choosing any coordinates inside the cells according to the phases of the spins at the four corners of individual cell. These are clear in the figures 3.1 and 3.2. We have also plotted the distance distribution function ϕ in the figures 3.3 (for $T = 1.1J$) and 3.4 (for $T = 1.5J$) for a 50×50 array and have got some Gaussian type distributions where there are a huge number of vortices existing in the medium distance ranges (as we see at this medium separation we have the highest peak which slowly falls in both short and long distance parts) whereas fewer and fewer vortices and antivortices are existing in both shorter and longer distance ranges. This is finite size (array) effect. The temperature is in unit of Josephson coupling constant (J). Here we should also mention that there should not be two particles at zero distance to avoid recombination but we also get, in our model, particles at distance smaller than a lattice constant. There are no vortices and antivortices sitting at the boundaries of the cells because of having huge barrier potential peaks at the boundaries and therefore the positions of the particles (V and A) at the boundaries should be very much unstable.

In our simulation the Berezinskii-Kosterlitz-Thouless transition temperature (T_{BKT}) has been seen to be $0.9J$ which is determined by the helicity modulus calculation [37,42]. We have done the Monte Carlo simulation for the temperature both below and above T_{BKT}. The vortex density versus temperature plot (Figure 3.5) shows how the number of the created vortices and antivortices by thermal excitations at zero frustration in the 2D JJAs changes by the change of temperature. We can recall here the simulation

performed by Anna Jonsson and Peter Minnhagen [38] and can compare our results with it. The main difference is in the low temperature behavior that is around T_{BKT} where our vortex density increases more quickly with temperature than that of Jonsson's simulation. In our simulation we also get little less vortices and antivortices in comparison with Jonsson's simulation [38] for the same temperatures. In both cases the vortex density increase rate is reduced at very high temperature region that is nearly about $2T_{BKT}$ and onwards and finally slowly move towards the saturation region.

The most important calculations we have done with these simulations are for the structure factors in such a two component fluid. We have two types of structure factors namely the number structure factor and the charge structure factor defined in equations (3.10a) and (3.10b) respectively. From the charge neutrality concept the charge structure factor starts from zero value at zero wave number k (figures 3.11 and 3.12) but the number structure factor has a delta peak at $k = 0$ (shown in figures 3.6-3.10). Both finish with constant value 1 at very high values of k. There are also small secondary peaks seen in the number structure factors at some specific values like at $k = 1, \sqrt{2}, 2$ etc. for different temperatures. The height of the peaks decreases with the decrease of temperatures and the increase of the values of k. To have a possible explanation of this type of secondary peaks we plotted the extended version of $\phi(x)$ for small range of the values of $x \in (0, 3)$ (figure 3.4(a)). Here we see an oscillatory behavior in $\phi(x)$ which may results into such secondary peaks in the number structure factor plots. We can avoid the presence of this secondary peaks by approximating the forms of $\phi(x)$ (plotted in figures 3.3 and 3.4) by some smooth function as like as e.g. $\phi(x) = 100xe^{-2(x/53)^2}$ (shown in figure 3.13) for $T = 1.5$. We can then use this form of $\phi(x)$ in equation (3.22) to calculate the structure factor of the two component fluid. The figure 3.14 shows such structure function which goes to 1 for higher values of the wave number.

The charge structure factor increases as k^2 at very low values of k ($k > 0$). The values of the charge structure factors for the same value of k in the increasing region increase slightly with the increase of temperature but at very high temperature the values decrease again. This is clear in figures 3.11 and 3.12. There can be one possible explanation of this type of change in structure factor which becomes clear if we analyze the form of the structure factor in equation (3.3) through the average length of vortex antivortex pair. We can recall here equation (3.3) and see $S_{\rho\rho}(k) = \frac{1}{N}\sum_{ll'} q_l q_{l'} \langle e^{i\mathbf{k}\cdot(\mathbf{R}_l - \mathbf{R}_{l'})}\rangle \approx -\frac{1}{N}\sum_{ll'} q_l q_{l'} \sum_{\alpha\beta} k_\alpha k_\beta \langle (R_\alpha(l) - R_\alpha(l'))(R_\beta(l) - R_\beta(l'))\rangle$. This, for a VA pair, takes the form of the type $k^2\langle (R(l) - R(l'))^2\rangle \approx k^2 d^2$ with d being the average pair length. Below or near T_{BKT} the average pair length d increases with the increase of temperature so the structure factor also increases as the structure factor of a VA pair is proportional to the average of the square of VA pair length. Whereas for higher $T (T > T_{BKT})$ the average length decreases with the increase of temperature due to the increased density of particles and so the decrease in structure factor also happens.

3.3 Conclusions

In this chapter we have obtained structure factors for the vortex antivortex gas in a 2D JJA at different temperatures. The charge structure factor is zero for $k = 0$ which follows from the charge neutrality in a two dimensional Coulomb system but the number structure factor has a delta peak at $k = 0$. Both the structure factors end with the value of unity at very high wave numbers. The main goal of this work is to get a good form of the charge structure factor for small values of the wavenumbers k's ($k > 0$) and to see their temperature dependence. In this region we see that the charge structure factor grows as k^2 with some upward smooth peak before flattening to a constant value of unity indicating the structure of the system. For the same value of k ($k > 0$) the values of the charge structure factors increase slightly with the increase of temperature but at very high temperature the values decrease again. This temperature effect of the structure factor is another important achievement in this project.

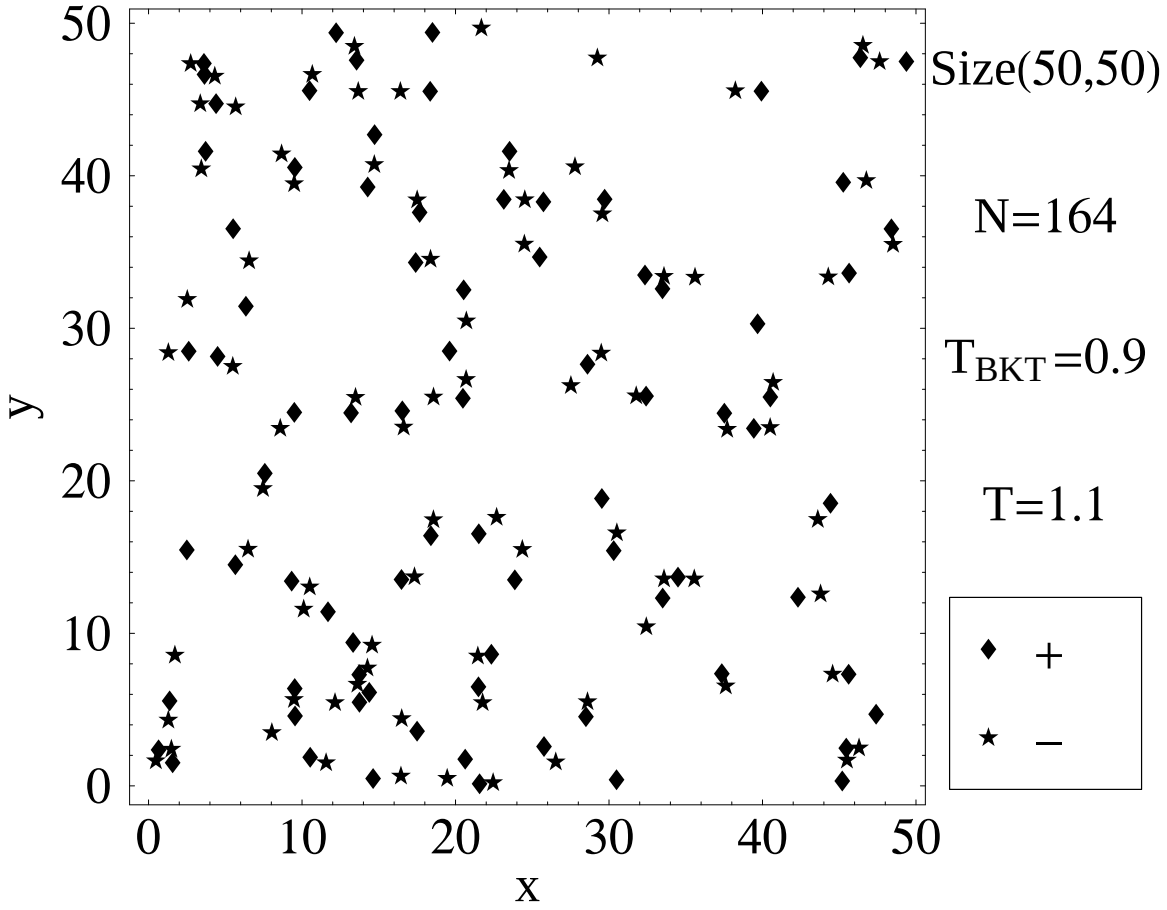

Figure 3.1: Positions of vortices and antivortices from Monte Carlo simulation in 2D XY model. In our model the particles (V and A) are not necessarily coordinated at the centers of the lattice sites which is reflected in the figure. + and - signs are indicating the vortices and antivortices. N is the total number of vortices and antivortices in the array. Here $T = 1.1$ and $N = 164$.

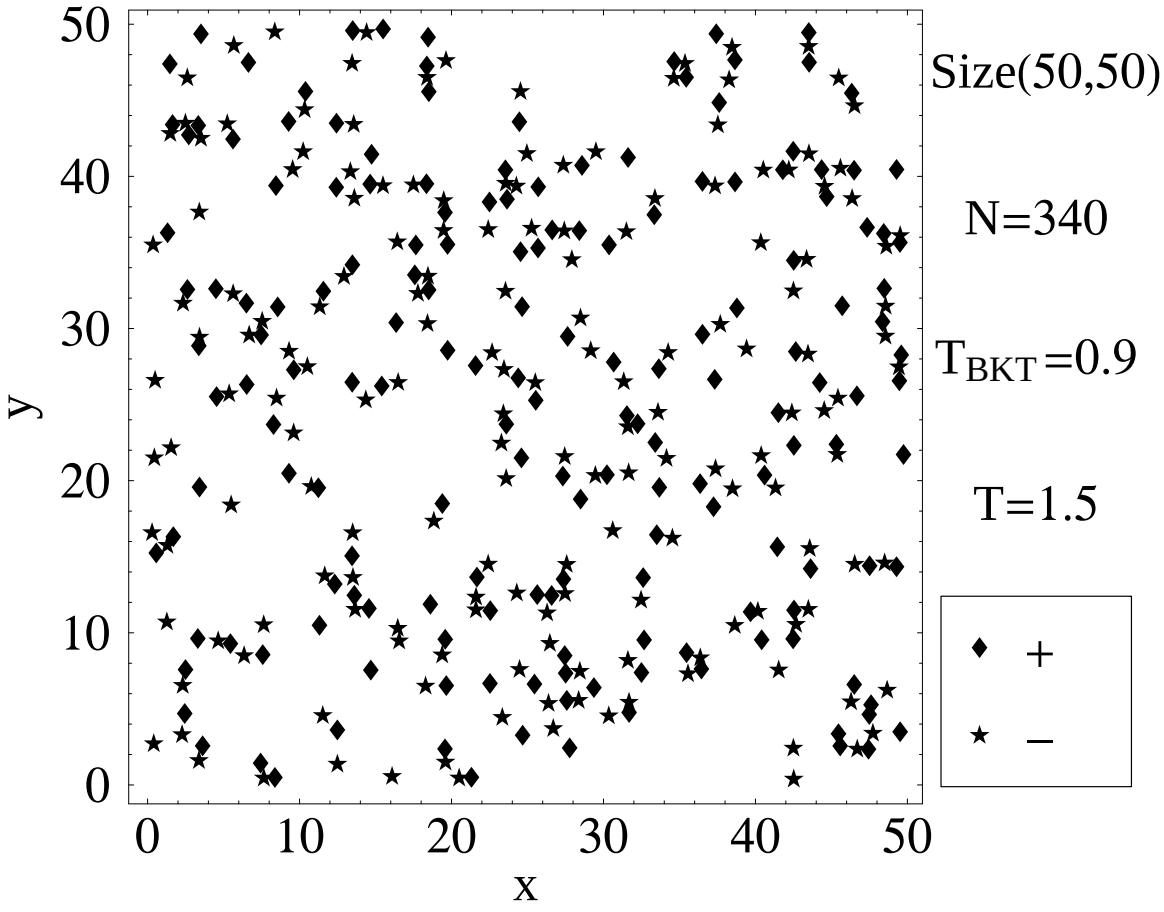

Figure 3.2: Positions of vortices and antivortices from Monte Carlo simulation in 2D XY model. In our model the particles (V and A) are not necessarily coordinated at the centers of the lattice sites which is reflected in the figure. + and - signs are indicating the vortices and antivortices. N is the total number of vortices and antivortices in the array. Here $T = 1.5$ and $N = 340$.

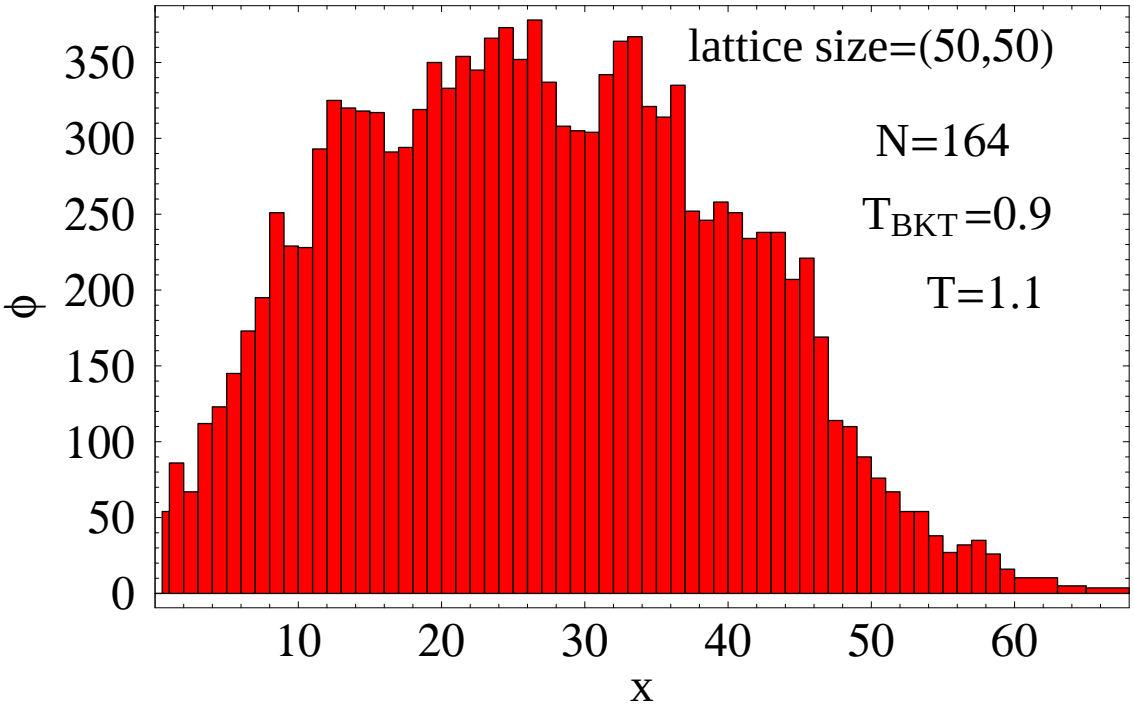

Figure 3.3: Distance distribution function $\phi(x) \times 164$ vs distance x (equation 3.18) between particles (V and A) from Monte Carlo simulation in 2D XY model. Here $T = 1.1$ and $N = 164$.

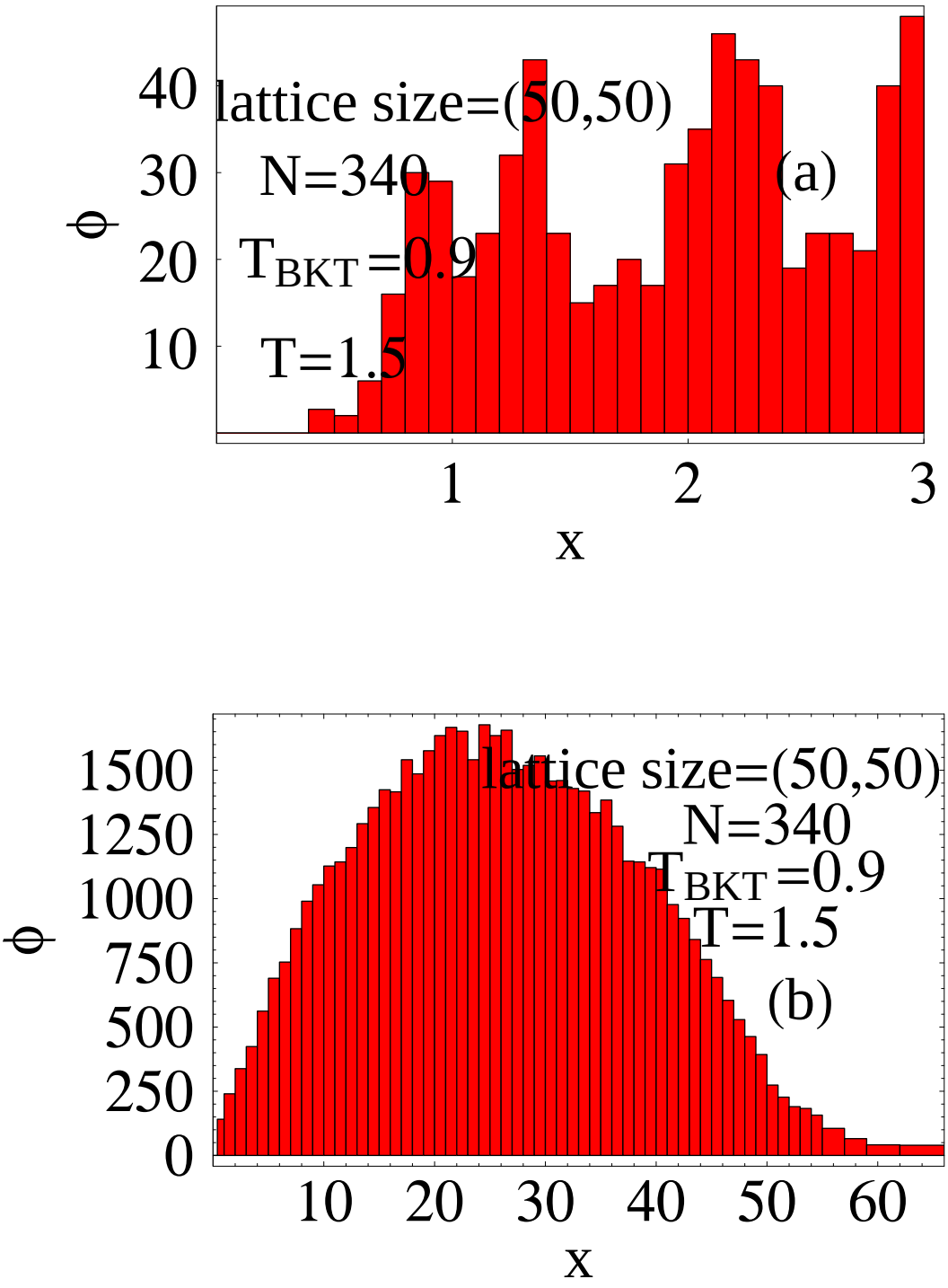

Figure 3.4: Distance distribution function $\phi(x) \times 340$ vs distance x between particles (V and A) from Monte Carlo simulation in 2D XY model. Here $T = 1.5$ and $N = 340$.

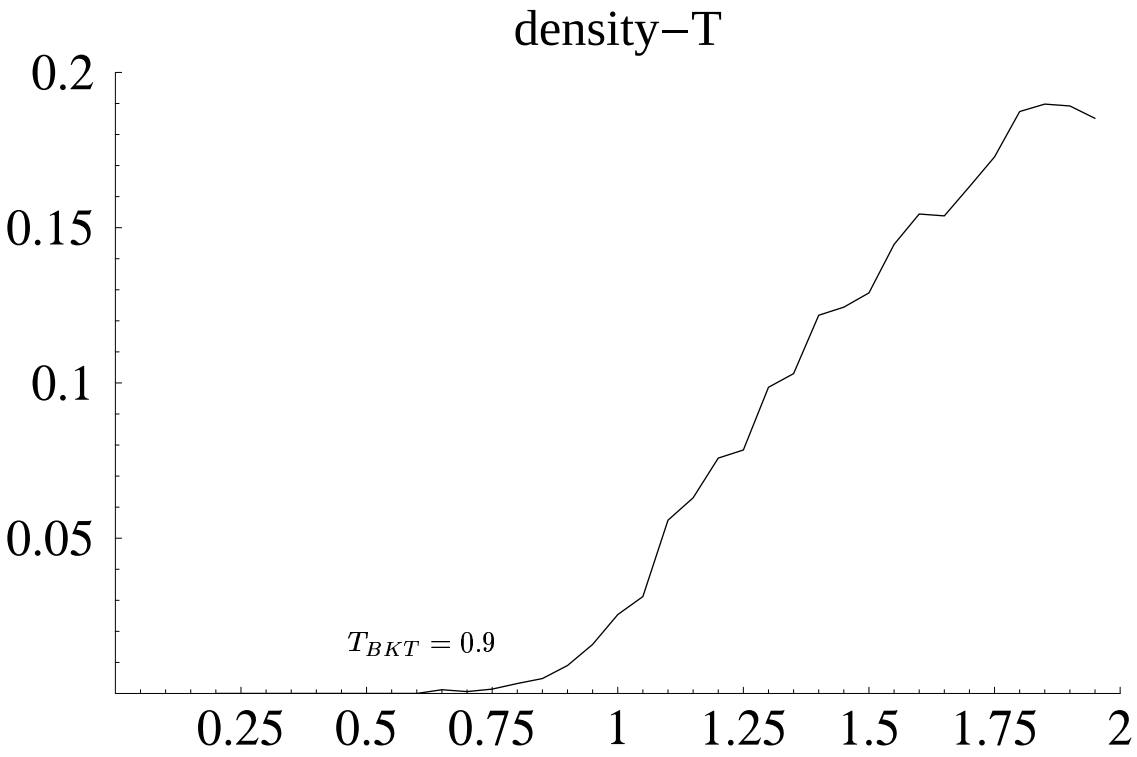

Figure 3.5: Vortex density (per site) vs temperature T from Monte Carlo simulation in 2D XY model.

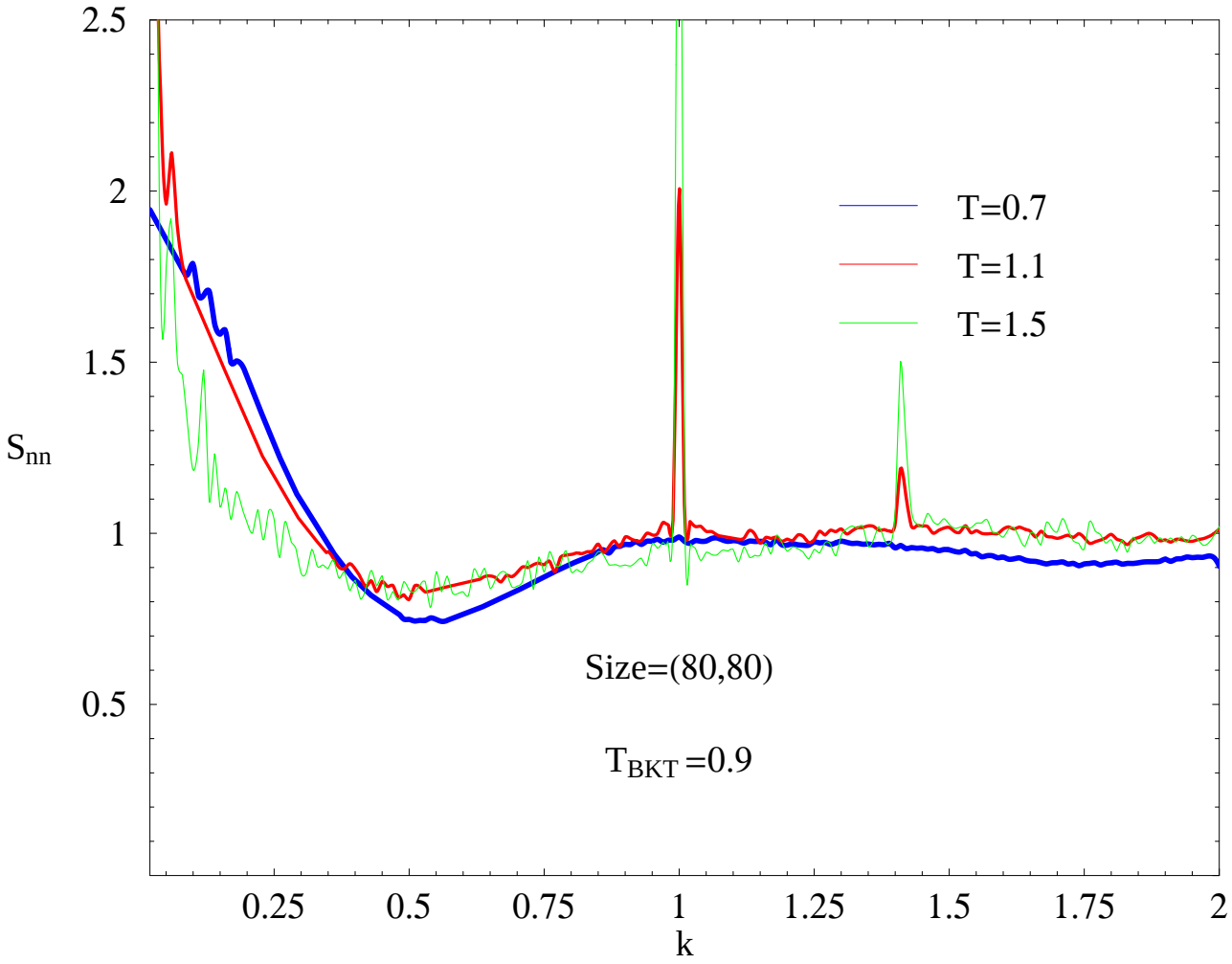

Figure 3.6: Number structure factor $\bar{S}_{nn}$ (defined in equation 3.10a) vs wave number k (in unit of $2\pi/a$, where a is the lattice constant) from Monte Carlo simulation in 2D XY model. The secondary peaks at $k = 1$ and also for some higher k's do not appear at very low temperatures like e.g., at $T = 0.7$. These peaks become sharper (high amplitudes) with the rise of T. One possible explanation for these peaks is given in the results section.

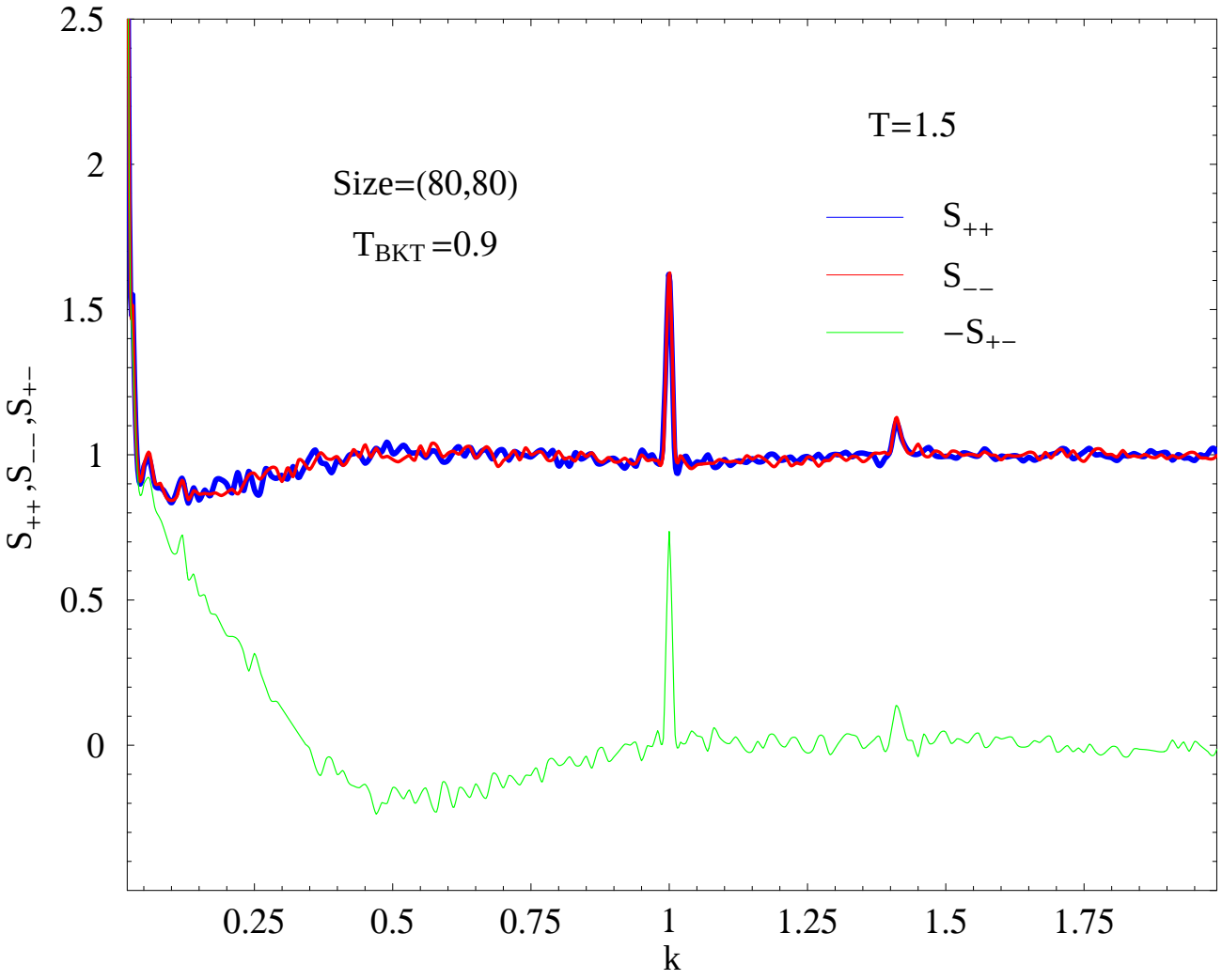

Figure 3.7: Partial structure factors (defined in equation 3.10c-3.10e) vs wave number k (in unit of $2\pi/a$) from Monte Carlo simulation in 2D XY model. S_{++}, S_{--} *and* S_{+-} are for the structure factors considering only vortex (+ for vortex) vortex, antivortex (- for antivortex) antivortex and vortex antivortex number density correlators respectively. The secondary peaks at $k = 1$ and also for some higher k's do not appear at very low temperatures like e.g., at $T = 0.7$ (shown in figure 3.9). These peaks become sharper (high amplitudes) with the rise of temperature T (figures 3.6-3.8).

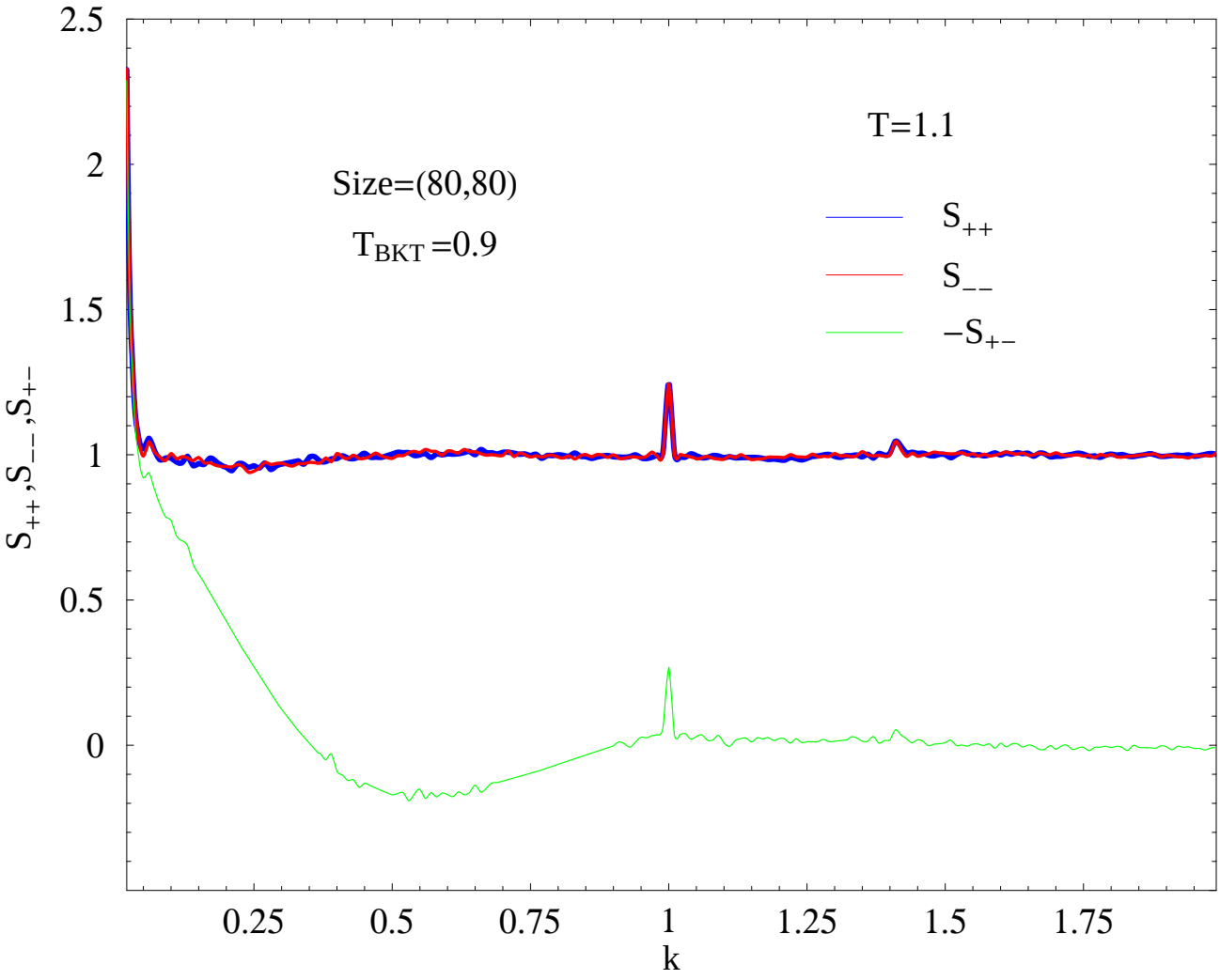

Figure 3.8: Partial structure factors (defined in equation 3.10c-3.10e) vs wave number k (in unit of $2\pi/a$) from Monte Carlo simulation in 2D XY model. S_{++}, S_{--} *and* S_{+-} are for the structure factors considering only vortex (+ for vortex) vortex, antivortex (- for antivortex) antivortex and vortex antivortex number density correlators respectively. The secondary peaks at $k = 1$ and also for some higher k's do not appear at very low temperatures like e.g., at $T = 0.7$ (shown in figure 3.6). These peaks become sharper (high amplitudes) with the rise of temperature T.

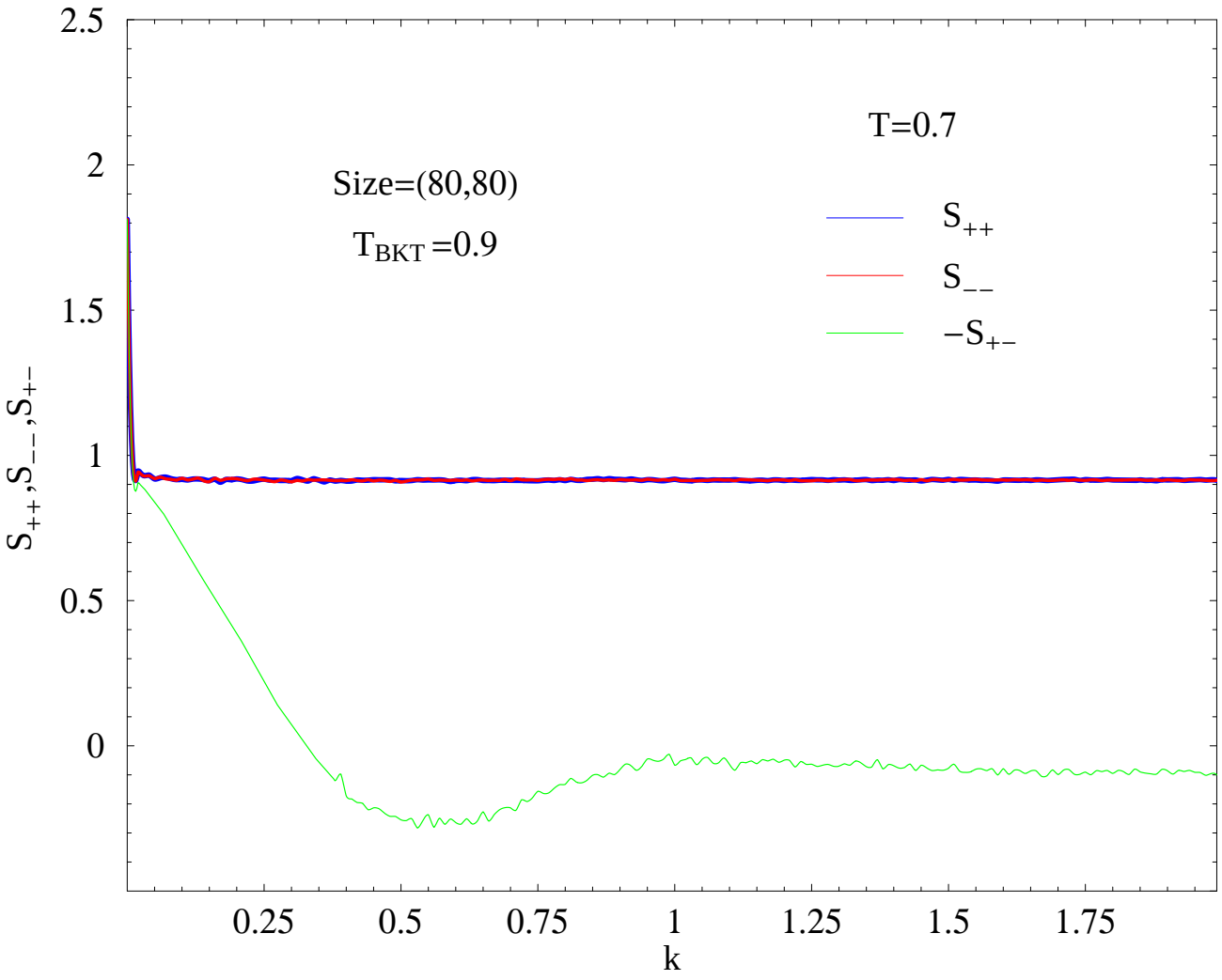

Figure 3.9: Partial structure factors (defined in equation 3.10c-3.10e) vs wave number k (in unit of $2\pi/a$) from Monte Carlo simulation in 2D XY model. S_{++}, S_{--} *and* S_{+-} are for the structure factors considering only vortex (+ for vortex) vortex, antivortex (- for antivortex) antivortex and vortex antivortex number density correlators respectively. The secondary peaks at $k = 1$ and also for some higher k's do not appear at very low temperatures like e.g., at $T = 0.7$. These peaks become sharper (high amplitudes) with the rise of temperature T.

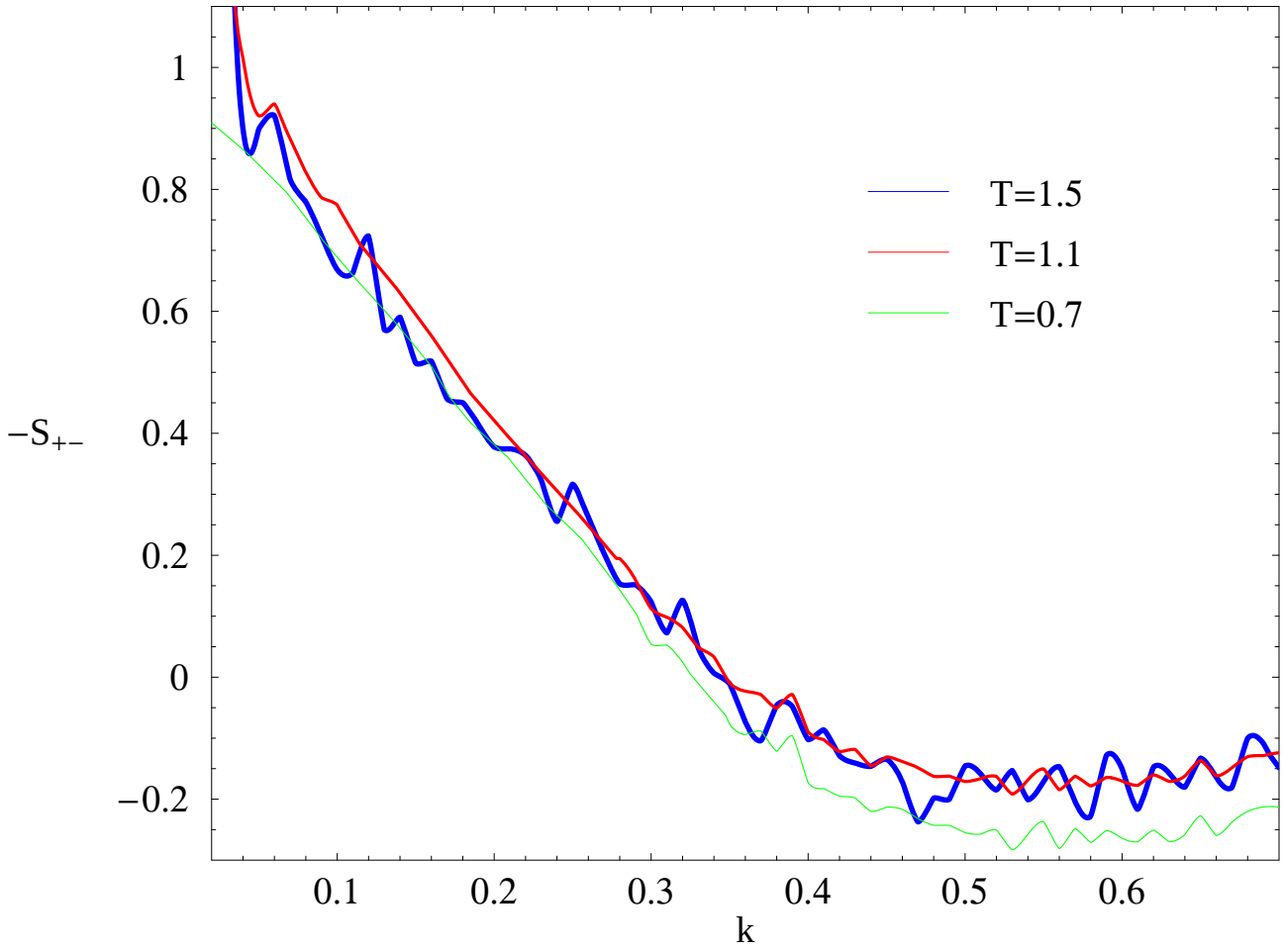

Figure 3.10: Partial structure factor S_{+-} (defined in equation 3.10e) vs wave number k (in unit of $2\pi/a$) from Monte Carlo simulation in 2D XY model.

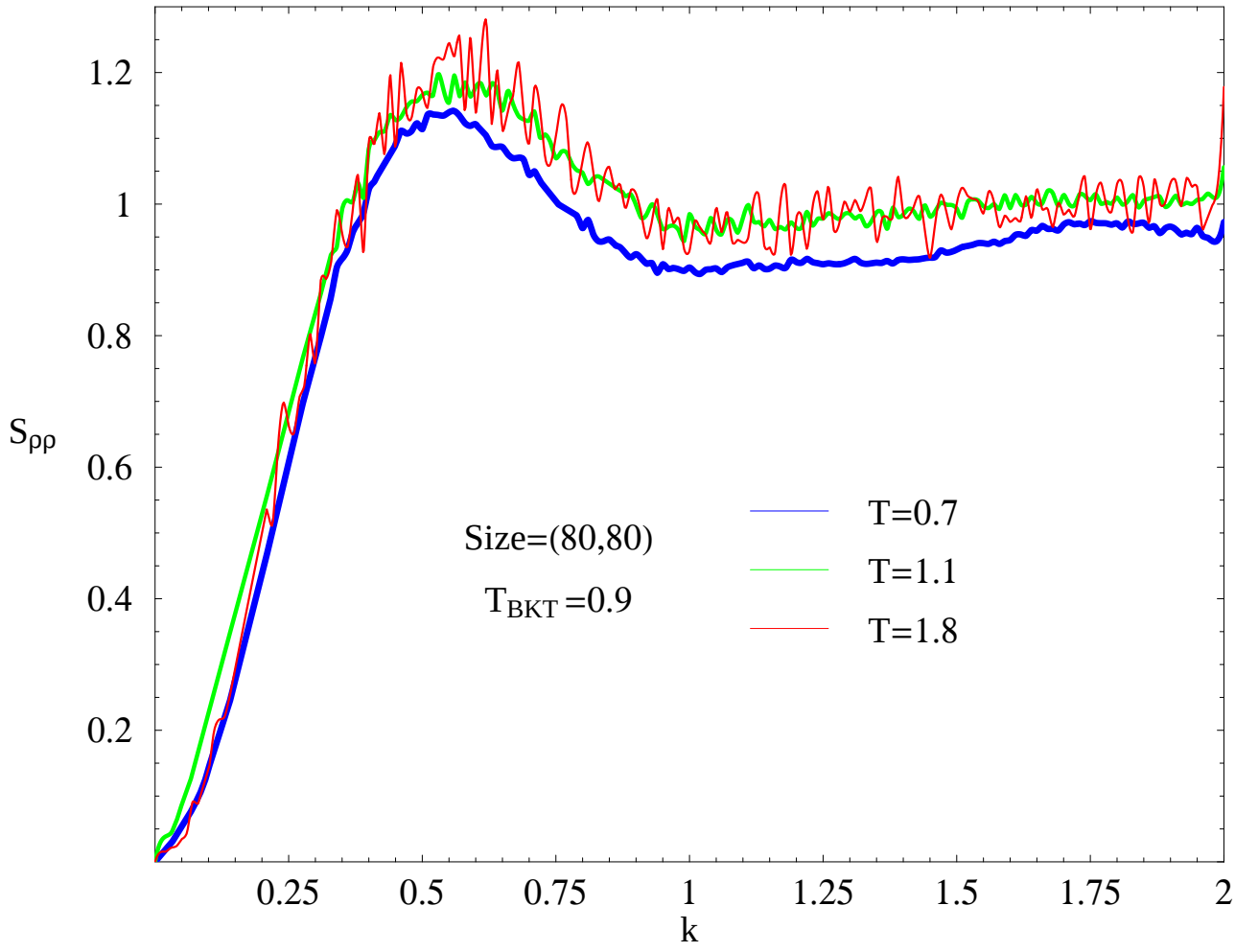

Figure 3.11: Charge structure factor (using equation 3.10b) vs wave number k (in unit of $2\pi/a$) from Monte Carlo simulation in 2D XY model. At higher temperatures structure factors have more fluctuations (e.g. at $T = 1.8$) because of having more structures due to the creation of more vortices and antivortices. The low temperature curves are relatively smooth (e.g. at $T = 0.7$) as at low temperatures there are fewer vortices and antivortices.

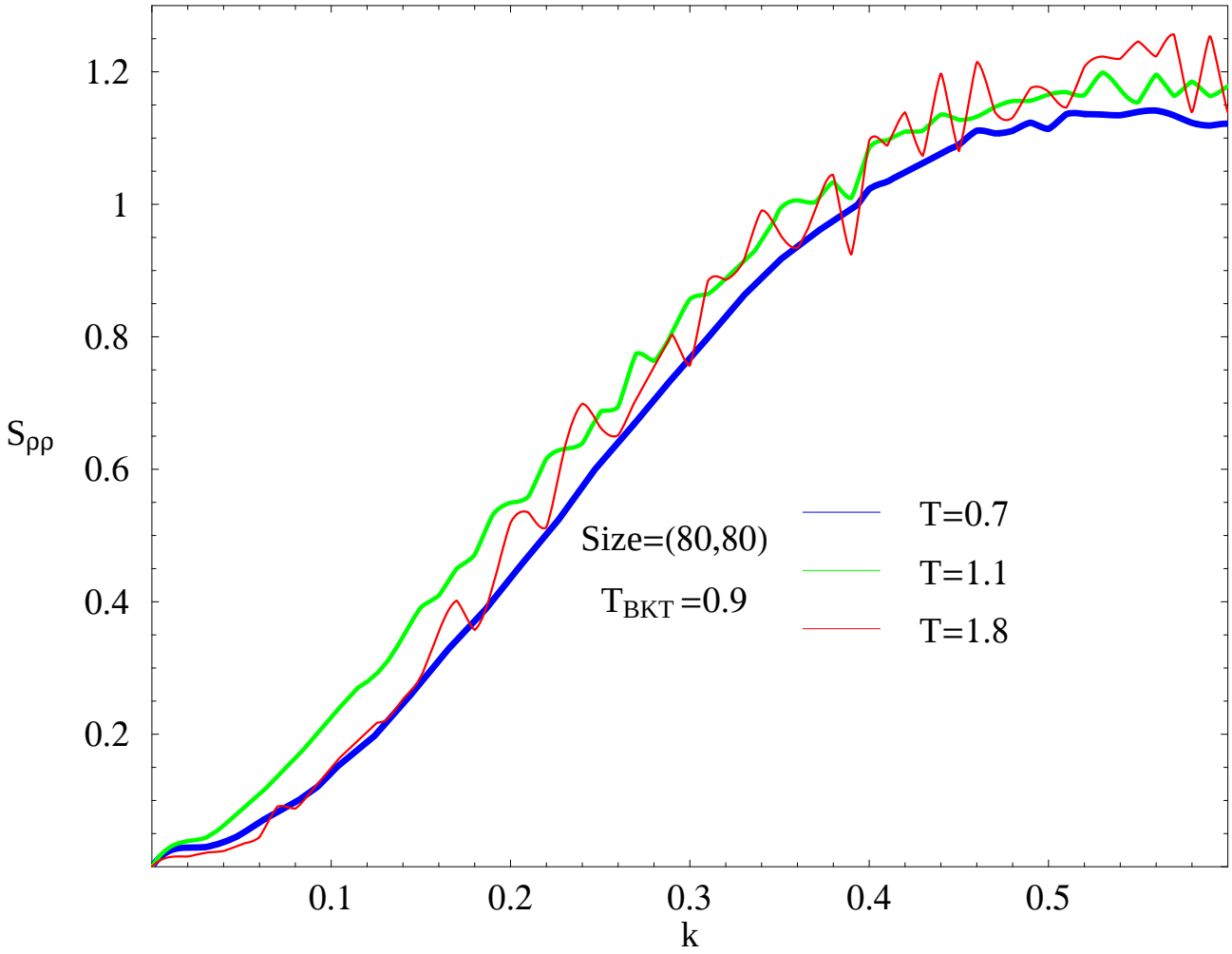

Figure 3.12: Charge structure factor (using equation 3.10b) vs wave number k (in unit of $2\pi/a$) from Monte Carlo simulation in 2D XY model for short range of values of k's. At higher temperatures structure factors have more fluctuations (e.g. at $T = 1.8$) because of having more structures due to the creation of more vortices and antivortices. The low temperature curves are relatively smooth (e.g. at $T = 0.7$) as at low temperatures there are fewer vortices and antivortices.

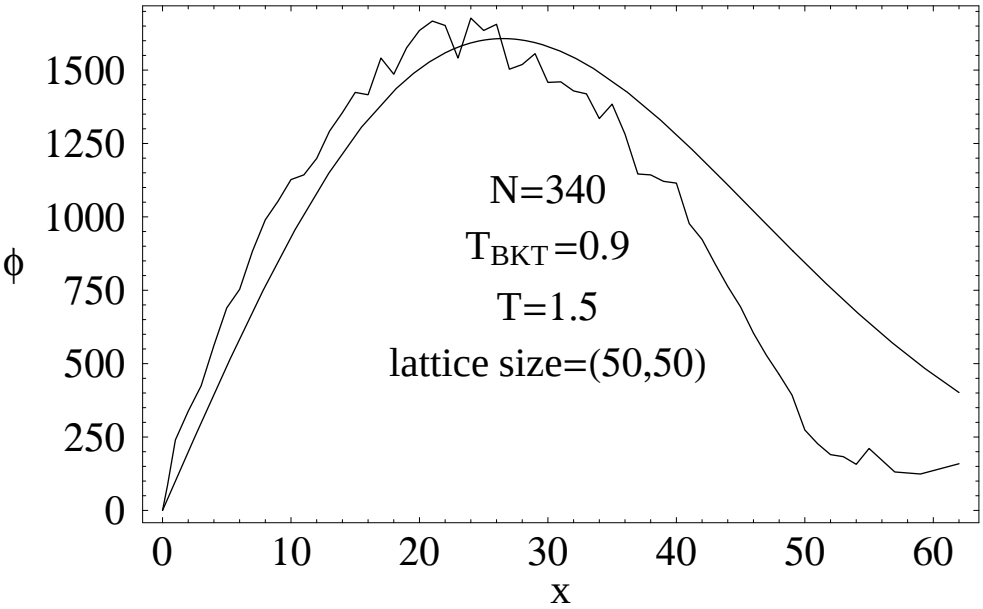

Figure 3.13: Distance distribution function $\phi(x) \times 340$ vs distance x between particles (V and A) from Monte Carlo simulation in 2D XY model. The smooth curve (for $\phi(x) \times 340 = 100xe^{-2(x/53)^2}$) is an approximation of the original non-smooth curve from simulation for $\phi(x)$ at $T = 1.5$.

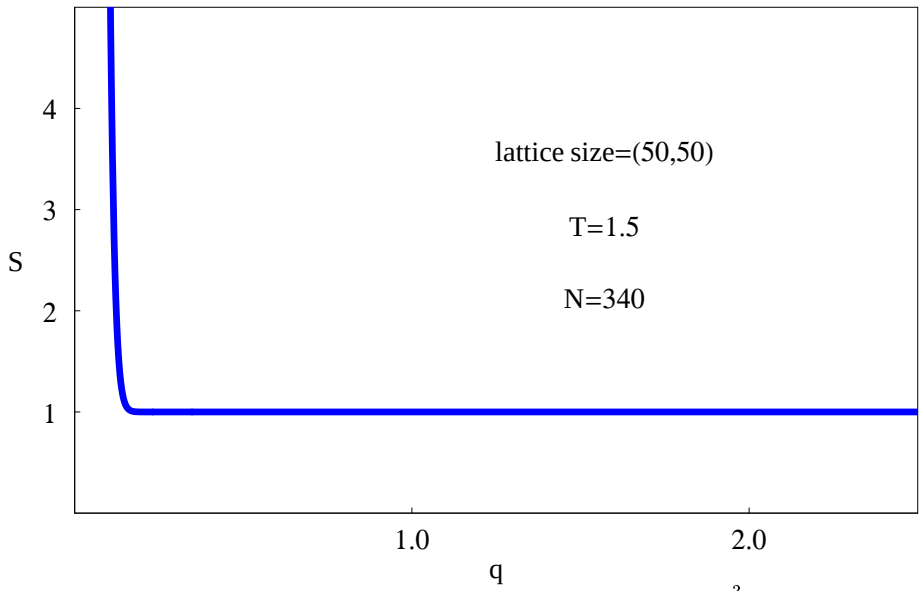

Figure 3.14: Number structure factor $S(q) = 1 + \frac{25}{340} \times 53^2 e^{-\frac{53^2}{8}q^2}$ vs q (equation 3.22) using the approximate $\phi(x) = \frac{100}{340} x e^{-2(x/53)^2}$ at $T = 1.5$. The structure factor has a delta peak at zero value of wave number and clearly ends with a value of 1 at very high wave number without making secondary peaks as were shown in figures 3.6-3.10 for different temperatures.

Chapter 4

Vortex/Antivortex free dynamics in diluted two-dimensional Josephson junction arrays

In this chapter we shall explain vortex (V) or antivortex (A) free dynamics in a diluted Josephson junction array (JJA). Here to explain the vortex dynamics and the effects of missing superconducting sites in the array on the dynamical phenomena we shall use the multiple trapping model (MTM) to calculate the vortex mobility in the array. We shall finally calculate the conductance of the array in presence of vortices and antivortices.

4.1 Introduction

Josephson junction arrays (JJA) consist of superconducting islands which are usually arranged on an ordered lattice and coupled by Josephson interaction. Two-dimensional (2D) Josephson junction arrays offer a unique opportunity for studying a variety of topics in 2D physics, such as phase transitions, non-linear dynamics, percolation, frustration and disorder, in relatively clean experimental realisation. Fabrication of arrays and their basic physical properties have been described in various articles [1,2]. The islands become superconducting below a given transition temperature T_c^o. Below this temperature each island l is characterized by its superconducting wave function

$$\psi = |\psi_l| e^{i\theta_l} \tag{4.1}$$

with its amplitude and its phase. For all practical purposes one can assume that the amplitude $|\psi_l|$ has the same value in each island, such that the phase is the only relevant variable. The islands are linked to each other by the Josephson coupling. The potential energy of the array is then given by

$$H = \sum_{\langle ll' \rangle} J_{ll'}[1 - \cos(\theta_l - \theta_{l'})] \tag{4.2}$$

The sum can usually be restricted to nearest neighbors in the array and the corresponding Josephson coupling J is related to the critical current I_c by

$$J = \frac{\hbar}{2e} I_c \tag{4.3}$$

A charging energy required when Cooper pairs move from one island to another has to be added to the expression (4.2) (details are in chapter 1). It is given by a capacitance matrix $C_{ll'}$ coupling the time derivatives of the phases (respectively their conjugate momenta) on different sites [1,2,29]. Arrays can then be divided into classical and quantum arrays depending on the ratio of the Josephson coupling energy to the relevant charging energy. The experimental work we are referring to in this article has been performed on classical arrays for which charging energies are unimportant. Dynamic phenomena for such arrays are usually described in the framework of the resistively shunted junction (RSJ) model [2,22,29]. A resistance matrix $R_{ll'}$ describes the normal currents flowing between the islands.

Research on disordered JJAs is a particularly exciting field. In an array where some sites are missing the electrical and magnetic properties of the lattice may change drastically depending on the number of missing sites relative to the whole array. This effect is related to percolation. About half a century ago this concept was introduced by Flory [43] and Stockmayer [44] in order to describe disordered structures. Later on the geometrical and statistical concepts introduced by Broadbend and Hammersley [45] in connection with the study of diffusion of fluids in random media, introduction of fractal concepts [46] and the development of computers and simulation techniques as well as theoretical and experimental analysis have contributed to deepening our understanding of the phenomenon of percolation.

We consider an infinite triangular or square lattice, where each site is randomly occupied by a superconducting island with some probability p and empty with probability $1 - p$. The electrical and magnetic properties of the array depend on the value of this percolation fraction p. With a decreasing value of p the properties of the array change more and more and at a certain lower value p_c of p the superconducting properties of the array are destroyed. p_c is called critical percolation limit below which the array has no superconductivity. At high concentration of missing sites, the occupied sites are either isolated or form small clusters of nearest-neighbors, and no path connecting opposite edges of the lattice exists. With increasing p, the mean cluster size of the occupied sites increases up to the appearance of an infinite cluster which connects opposite edges of the whole lattice. The existence of an infinite percolating cluster of occupied sites is connected with the criticality of the percolation (p_c). When p is further increased, more and more sites become part of the infinite cluster of occupied sites, and finally at $p = 1$, all sites belong to the infinite cluster. The percolation threshold depends on different aspects of the lattice structure like its form (triangular, square or others), dimensionality, and on the type of percolation (bond, site, etc.). For example, in a triangular 2D array, for site percolation, one can analytically [47] show that $p_c = 0.5$, but this value can be different for other dimensions of the array and other types of disorder.

Different types of disorder can be considered:

a. For **bond disorder** the parameters characterizing the individual junctions, namely the Josphson couplings $J_{ll'}$, the junction resistances $R_{ll'}$ and the mutual capacities $C_{ll'}$, are random. This type of disorder is realized when the positions of the individual superconducting islands deviate in a random way from their ideal lattice positions or if they have random size, since $J_{ll'}$, $R_{ll'}$ and $C_{ll'}$ depend on the distance between the adjacent superconductors and on their geometry.

b. For **site disorder** the properties of the superconducting islands, i.e. their resistance and capacitance to ground, are random. More simply, in a dilute array certain islands are totally missing.

Dynamic measurements [48,49] have been done on dilute, or percolative , arrays for p-values somewhat larger than the percolation threshold $p_c = 0.5$, where the disorder has a marked influence on the properties of the array. At temperatures that are low compared to the Berezinskii-Kosterlitz-Thouless (BKT) transition temperature, T_{BKT} (which in a dilute array is lower than for the regular counterpart, due to the absence of certain bonds, see below) the equations of motion can be linearized, taking into account only small amplitude spin wave excitations. The problem at hand is then the same as determining the vibrational modes of a disordered harmonic solid, which is a well studied field [50]. In reference [51] the impedance $Z(\omega)$ of such a dilute JJA has been determined by evaluating the dynamic voltage correlation function by different methods. The coherent potential approximation (CPA) has proven to be a useful approach for treating dynamic disorder problems. The inverse of the impedance is expressed by an effective coupling function $K(\omega, p)$ depending on frequency and on the dilution fraction p :

$$Z(\omega) = (\eta + \frac{K(\omega, p)}{i\omega})^{-1} \tag{4.4}$$

corresponding to the effective inductance L and resistance R of the array.

As a main result for the BKT transition these calculations reveal the existence of an effective Josephson coupling constant, J_{eff}. For bonds where one or both of the superconducting islands is missing, the coupling energy vanishes, i.e. $J_{ll'} = 0$. Thermodynamics is then governed by an effective coupling constant J_{eff} given by the relation [51]

$$J_{eff} = \frac{p - p_c}{1 - p_c} J \tag{4.5}$$

and thus the transition temperature T_{BKT} ($k_B T_{BKT} = \frac{\pi}{2} J_{eff}$ or $0.9 J_{eff}$ for triangular or tetrangular array respectively) also decreases. Close to and above T_{BKT} the dynamic response is then dominated by the motion of thermally created vortices.

An equation of motion for vortices can be obtained starting from the RSJ equations for the supeconducting phases [29]. Much analytical and numerical efforts have been devoted [29] to describing the dynamic behaviour of the vortices in regular JJAs. One of the key quantities is the frequency and temperature dependent vortex mobility $\mu(\omega, T)$. For calculating this quantity the Coulomb interaction between the vortices has to be taken into account, which makes the problem difficult.

For disordered JJAs this is an even more complex problem, since one should now describe the motion of interacting particles in a random potential landscape. We will treat the vortex response mainly above T_{BKT} where the interaction between vortices should not be too important and will thus be neglected. The influence of the random potential on the vortex dynamics will be treated in the multiple trapping model , that has been developed for handling the motion of electrons in disordered semiconductors. This model will be presented in section 4.2. It allows to calculate the average vortex mobility $\mu(\omega, T)$ in the dilute array as a function of frequency ω and temperature T. In section 4.3 the measured electrodynamic response, expressed by the complex impedance of the array, will be related to μ. In section 4.4 our results for μ will be presented and analised, and our theoretical data for the complex impedance will be compared to experimental data [49]. We shall also show theoretically calculated flux noise spectra for in disordered arrays. Finally in chapter V we shall give some conclusions.

4.2 The multiple trapping model

4.2.1 The multiple trapping equations

In this chapter we discuss our model for the vortex dynamics in dilute 2D JJAs (missing sites or bonds). Deviations from a regular lattice structure will have an influence on the vortices of an array through the Peierls force or pinning potential. The equilibrium arrangement of the (thermal or field induced) vortices and antivortices will correspond to a minimum of the free energy in the given random pinning potential landscape. It is generally accepted that weak disorder results in some sort of glassy vortex state [52,53]. At sufficiently low temperatures such a vortex configuration would then be trapped by the underlying potential, and the system should have a vanishing linear resistance, i.e. it would be truly superconducting. This should be valid for dilute JJAs, as they have been described in the preceding subsection, as well as for ultrathin superconducting films [54] that are intrinsically disordered. At higher T, in particular above T_{BKT}, vortices will move around in the dilute array thus giving rise to interesting power law behaviour in the dynamic impedance $Z(\omega)$ [54].

Our main goal is therefore to calculate the frequency dependent resistance (R) and inductance (L) of a dilute array. In calculating R and L we have to first find the mobility (μ) of the vortex (V) and antivortex (A) in the disordered array. For this we use the so called multiple trapping model (MTM), developed for electronic transport in amorphous semiconductors [55]. In this model the regions where sites of the array are missing are regrouped into holes of different shapes and sizes. The motion of a given particle (we will not distinguish between V and A, since in the absence of interaction they undergo the same influence by the random potential) is then described in probabilistic terms. At a given position $\mathbf{r}$ in the array one can either be in one of the holes of the array or in a regular region, occupied by superconducting islands. Thus the state of a particle sitting at $\mathbf{r}$ is determined by the following probabilities:

$p(\mathbf{r}, \tau) \equiv$ probability that a given particle is free at position $\mathbf{r}$ and time τ, i.e. it is sitting between holes, in a

regular region.

$p_n(\mathbf{r},\tau) \equiv$ probability that the particle is trapped in one of the holes which is indexed by n.

In the multiple trapping model the time evolution of these probabilities is governed by two rate equations:

$$\frac{\partial p(\mathbf{r},\tau)}{\partial \tau} + \sum_n \frac{\partial p_n(\mathbf{r},\tau)}{\partial \tau} = -\nabla \cdot \mathbf{j} \tag{4.6}$$

$$with \qquad \frac{\partial p_n(\mathbf{r},\tau)}{\partial \tau} = -\gamma_{r,n} p_n(\mathbf{r},\tau) + \gamma_{t,n} p(\mathbf{r},\tau) \tag{4.7}$$

Here $\gamma_{t,n}$ is the probability per unit time (transition rate) for a particle to get trapped inside the hole n and $\gamma_{r,n}$ is the release rate out of the hole n.

If the particle remains in a regular area it contributes to the current density $\mathbf{j} = \mathbf{v}p(\mathbf{r},\tau)$ with its velocity $\mathbf{v} = \mu_0\mathbf{E}$ determined by the mobility μ_0 for a regular array of the same structure, and the effective field $\mathbf{E}$ which will be assumed here as unidirectional (in X direction). Thus the first of the two rate equations can be written as

$$\frac{\partial p(\mathbf{r},\tau)}{\partial \tau} + \mu_0 E \frac{\partial p(\mathbf{r},\tau)}{\partial x} = \sum_n \gamma_{r,n} p_n(\mathbf{r},\tau) - \sum_n \gamma_{t,n} p(\mathbf{r},\tau) \tag{4.8}$$

Now we use Laplace transformation

$$\begin{aligned} \hat{f}(z) &= \textstyle\int_0^\infty d\tau e^{-z\tau} f(\tau) \\ \tfrac{\partial f(\tau)}{\partial \tau} &\to z\hat{f}(z) - f(0) \end{aligned} \tag{4.9}$$

$f(0)$ being the initial condition.

For (4.8) this yields (in the case of unidirection)

$$z\hat{p}(z) - p(0) + \mu_0 E \frac{\partial \hat{p}(\mathbf{r},z)}{\partial x} = \sum_n \gamma_{r,n}\hat{p}_n(z) - \sum_n \gamma_{t,n}\hat{p}(z) \tag{4.10}$$

and for (4.7)

$$z\hat{p}_n(z) = \gamma_{t,n}\hat{p}(z) - \gamma_{r,n}\hat{p}_n(z) + p_n(0) \tag{4.11}$$

Imposing the initial condition $p(0) = 1$ and $p_n(0) = 0$ we get from the previous equation

$$\hat{p}_n(z) = \frac{\gamma_{t,n}}{z + \gamma_{r,n}}\hat{p}(z) \tag{4.12}$$

Now we define

$$\pi_n(z) = \frac{\gamma_{t,n}}{z + \gamma_{r,n}} \tag{4.13}$$

and equation (4.10) becomes

$$z\hat{p}(z)(1 + \pi(z)) = 1 - \mu_0 E \frac{\partial \hat{p}(\mathbf{r},z)}{\partial x} \tag{4.14}$$

The quantity

$$\pi(z) = \sum_n \pi_n(z) \tag{4.15}$$

will turn out to play a central part for the frequency and temperature dependence of the electrodynamic response of the array through the mobility changes due to the trapping and releasing of vortices by the holes.

In order to get concrete expressions for our transition rates we consider thermal equilibrium in zero external field where the probabilities, $p(\mathbf{r},\tau) = p_0$ and $p_n(\mathbf{r},\tau) = p_n$, are independent of space and time. The former is simply proportional to the total regular area $p.(La)^2$, a being the lattice constant, L^2 the total number of sites :

$$p_0 = A.p.(La)^2 \tag{4.16}$$

The probabilities p_n are given by a Boltzmann factor, involving the binding energy E_n of a particle trapped in hole number n, and the surface S_n of the corresponding hole

$$p_n = AS_n e^{\beta E_n} \tag{4.17}$$

The thermally activated release rate is given by

$$\gamma_{r,n} \doteq r_a e^{-\beta E_n} \tag{4.18}$$

with r_a being the attempt frequency and $\beta = \frac{1}{k_B T}$.

In the case of detailed balance all terms in equation (4.7) vanish, therefore

$$p_0 \gamma_{t,n} = p_n \gamma_{r,n} \tag{4.19}$$

and $\gamma_{t,n} = \frac{p_n}{p_0}\gamma_{r,n} = r_a \frac{S_n}{p(La)^2}$.

For the circular holes, considered here, the area is given by $S_n = S(N) = Na^2$, N being the number of missing sites.

Combining these relations we find the following expression for the trapping rate $\gamma_{t,n} = \gamma_t(N)$

$$\gamma_t(N) = r_a \frac{N}{pL^2} = r_a \frac{N}{pN_{tot}} \tag{4.20}$$

where $N_{tot} = L^2 \equiv$ is the total number of sites.

4.2.2 The vortex mobility

The mean velocity $\bar{v}$ of a V is related to its mean position $\bar{x}$ by

$$\bar{v} = \frac{\partial \bar{x}}{\partial \tau} = \int d^2 r x \frac{\partial p(\mathbf{r},\tau)}{\partial \tau} \tag{4.21}$$

Through Laplace transformation (4.9) we get

$$\hat{\bar{v}} = z\hat{\bar{x}} = \int d^2 r x z \hat{p}(\mathbf{r}, z) \tag{4.22}$$

taking, for simplicity, $\bar{x}(0) = 0$, i.e. the vortex started ($t = 0$) its motion from the origin of the lattice. Now using equation (4.14) the previous equation, through partial integration, becomes

$$\hat{\bar{v}} = \int d^2rx \frac{1 - \mu_0 E \frac{\partial \hat{p}(\mathbf{r},z)}{\partial x}}{1 + \pi(z)} = \frac{-\mu_0 E}{1 + \pi(z)} \int d^2rx \frac{\partial \hat{p}(\mathbf{r},z)}{\partial x} + \int d^2r \frac{x}{1 + \pi(z)}$$
$$= \frac{\mu_0 E}{1 + \pi(z)} \tag{4.23}$$

The last term of the first part in the previous equation represents the initial condition of the velocity and contributes zero by our assumption.

The effective mobility μ of a V is given by $\hat{\bar{v}} = \mu E$. We get from the previous equation

$$\mu(z) = \frac{\mu_0}{1 + \pi(z)} \tag{4.24}$$

and $\pi(z)$ is given by equation (4.15). The purpose of our calculations is to exhibit, through the mobility μ, the influence of disorder on the dynamic response of the vortex system. In order not to mix these effects with the intrinsic frequency dependence of μ in regular arrays and for computational simplicity we take μ_0, the vortex mobility in the regular array, to be constant, setting the scale for μ (see expression (4.38)).

Taking $D(N)$ to be the number of holes having N missing sites and considering (4.20) for $\gamma_t(N)$, the key quantity $\pi(z = i\Omega) = \pi(\Omega)$, for real frequencies Ω, can be expressed by

$$\begin{aligned} \pi(\Omega) &= \textstyle\sum_N D(N)\pi(z = i\Omega, N) \\ &= \textstyle\sum_N \gamma_t(N) \frac{D(N)}{i\Omega + r_a e^{-\beta E(N)}} \\ &= \textstyle\int_1^{N_{max}} dN \frac{\hat{D}(N)N}{i\frac{\Omega}{r_a} + e^{-\beta E(N)}} \end{aligned} \tag{4.25a}$$

In the above expression, $\hat{D}(N) = \frac{D(N)}{pN_{tot}}$ is a normalized number density of holes. In equation (4.25b) we have introduced the dimensionless frequency $\omega = \frac{\Omega}{\omega_a}$, with $\omega_a = \frac{k_B T_{BKT} \mu_0}{a^2}$ being a characteristic frequency which includes the lattice constant a of the array and the bare vortex mobility μ_0 of the ordered array. Introducing the vortex diffusion constant by $D_0 \equiv k_B T_{BKT} \mu_0$, for temperature T_{BKT}, the frequency ω_a is given by $\omega_a = \frac{D_0}{a^2}$. Its inverse is thus the average time for a vortex to diffuse across one lattice constant a. A very sensitive step in our entire procedure is represented by the choice of the attempt frequency r_a. We will write the latter as $r_a = \omega_a f(t)$ where $t = \frac{T}{T_{BKT}}$ represents the scaled temperature. Here we consider either $f(t) = t$, if the attempt frequency is considered to increase linearly with temperature - i.e. $r_a = \omega_a t$ -, or $f(t) = 1$, in the case where r_a is assumed to be constant. At first glance, the former case probably appears to be more sound and intuitive from a physical point of view. However, choosing a constant r_a may be understood as arising from the fact that our system is considered to be overdamped; hence, kinetic energy - which is indeed

proportional to temperature - is an ill-defined quantity and one may consequently be led to assume, that r_a does not depend on temperature and simply represents a characteristic frequency of the vortex system. We end up with

$$\pi(\omega) = \int_1^{N_{max}} dN \frac{\hat{D}(N)N}{i\frac{\omega}{f(t)} + e^{-\beta E(N)}} \tag{4.25b}$$

The value of N_{max} has to guarantee the correct total number of missing sites:

$$N_{tot}(1-p) = \sum_1^{N_{max}} D(N)N \tag{4.26}$$

Therefore N_{max} depends on the value of p, the sample size N_{tot} and of course the choice of a hole distribution function $D(N)$.

4.2.3 Binding energy for circular holes

In the XY model the energy is expressed by (4.2). In the case of percolative arrays

$$J_{ll'} = \begin{cases} J & \text{with probability } p \\ 0 & \text{with probability } 1-p \end{cases} \tag{4.27}$$

where J is the Josephson coupling constant between two islands.

Now when phase field $\theta(r)$ varies slowly we can write $1-\cos(\theta_l - \theta_{l'}) \approx \frac{(\theta_l - \theta_{l'})^2}{2}$ so we get, converting the summation to the integration for slowly varying phase fields,

$$E \approx J \int d^2r \frac{(\nabla\theta)^2}{2} \tag{4.28}$$

Now if a V exists at the origin, the phase field $\theta(r)$ for the V is given by $\theta(r) = arc\tan\frac{y}{x}$ where x and y are cartesian coordinates in the array. So we get $|\nabla\theta|^2 = \frac{1}{r^2}$ and the total energy of a vortex in the array is

$$E_V = \frac{J}{2}\int_{r_1}^{L} d^2r \frac{1}{r^2} \tag{4.29}$$

where L is the size of array and r_1 is a lower cut-off corresponding to lattice constant. Now the binding energy of the V or A inside a hole (approximated to be circular) of radius r_2 with $\pi r_2^2 = (N+1)\pi r_1^2$ (the area of the hole is equal to $N+1$ times the area of a unit cell) is

$$\begin{aligned} E(N) &= \frac{J}{2}\int_{r_1}^{L} d^2\frac{1}{r^2} - \frac{J}{2}\int_{r_2}^{L} d^2\frac{1}{r^2} \\ &= \frac{J}{2}\int_{r_1}^{L} drr\frac{1}{r^2}\int_0^{2\pi} d\theta - \frac{J}{2}\int_{r_2}^{L} drr\frac{1}{r^2}\int_0^{2\pi} d\theta \\ &= \pi J \ln\frac{r_2}{r_1} = \pi J \ln\sqrt{N+1} \end{aligned} \tag{4.30}$$

because $\pi(r_2^2 - r_1^2) = N\pi r_1^2$ or $\frac{r_2}{r_1} = \sqrt{N+1}$.

Using (4.5)

$$k_B T_{BKT} = \frac{\pi}{2} J_{eff} = \frac{\pi}{2} \frac{p - p_c}{1 - p_c} J \tag{4.31}$$

the exponent of the Boltzmann factor in (4.25) can be rewritten as

$$\beta E(N) = \frac{1 - p_c}{p - p_c} \frac{2}{t} \ln \sqrt{N+1} \tag{4.32}$$

Thus we obtain from equation (4.25)

$$\pi(\omega) = \frac{1}{N_{tot} p} \int_1^{N_{max}} dN \frac{N D(N)}{i\frac{\omega}{t} + (1+N)^{-a(t)}} \tag{4.33}$$

with a temperature dependent exponent

$$a(t) = \frac{1}{t} \frac{1 - p_c}{p - p_c} \tag{4.34}$$

4.3 Electrodynamic response of the array

4.3.1 Resistance and Inductance

Generally, the response of the array to an external electromagnetic excitation can be characterized taking the contributions of the superfluid, normal electrons and vortices into account. This corresponds to a two-fluid model, where the medium is described by an inductive superfluid channel in parallel with a dissipative channel.

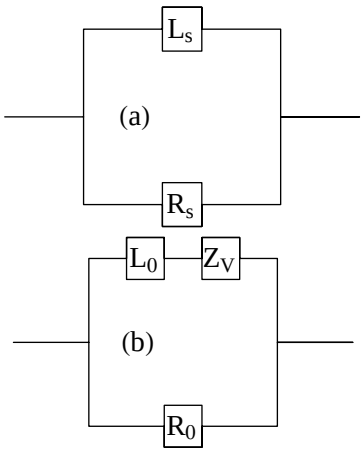

Figure 4.1: Circuit diagram for a 2D superconductor. (a) in terms of an inductive and resistive component, (b) in the presence of vortices.

The measured quantity in the array is the sheet conductance G. The effect due to the vortices can be incorporated in this conductance of the array. In the presence of a current, the vortices experience a Lorentz force which will set them in motion perpendicular to the current flow. Associated with the vortex motion, there is an electric field which adds to the electric field of the accelerated superfluid background. This phenomenon therefore leads to an increase in the sheet impedance by an amount Z_V, which comes in series with the impedance of the superfluid background, as shown in figures 4.1(a) and 4.1(b) schematically.

G is the sheet conductance which is the inverse of the sheet impedance Z

$$\begin{aligned} G &= \frac{1}{R_s} + \frac{1}{i\Omega L_s} = Z^{-1} \\ &= \frac{1}{R_0} + G_{sup} \end{aligned} \tag{4.35}$$

where G_{sup} is the superconducting part of the conductance, the resistance R_0 is due to the dissipative processes (Ohmic contribution of the conductance) resulting from the currents flowing in the junction in absence of vortices and antivortices, whereas L_s is the sheet inductance and R_s is the sheet resistance when there are vortices and antivortices present in the array.

We shall now relate the resistive (R_s) and inductive (L_s) parts of the sheet conductance G with the resistive (R_V) and inductive (L_V) parts of the vortex impedance Z_V through the following relations : $Z_V = Z_{sup} - i\Omega L_0 = G_{sup}^{-1} - i\Omega L_0$ and $G_{sup} = G - \frac{1}{R_0} = \frac{1}{R_s} - \frac{1}{R_0} + \frac{1}{i\Omega L_s}$ so $Z_V = \frac{1}{R_s^{-1} - R_0^{-1} + (i\Omega L_s)^{-1}} - i\Omega L_0 = R_V + i\Omega L_V$ which gives

$$R_V = \frac{R_s^{-1} - R_0^{-1}}{(R_s^{-1} - R_0^{-1})^2 + (\Omega L_s)^{-2}} \tag{4.36}$$

$$L_V = \frac{1}{\Omega} \frac{(\Omega L_s)^{-1}}{(R_s^{-1} - R_0^{-1})^2 + (\Omega L_s)^{-2}} - L_0 \tag{4.37}$$

Here L_0, the inductive part, arises from the currents flowing in the junction in absence of vortices and antivortices.

The frequency dependent dielectric function of the vortex system $\epsilon_V(\Omega) = 1 - iZ_V/(\Omega L_0)$ is related to the vortex mobility $\mu(\Omega)$ by the following expression

$$\begin{aligned} i\Omega L_0 \epsilon_V(\Omega) &= i\Omega L_0 (1 + 2\pi q_0^2 n \mu(\Omega) \frac{1}{i\Omega}) \\ &= i\Omega L_0 + L_0 2\pi q_0^2 n \mu_0 (\nu'(\Omega) + i\nu''(\Omega)) \\ &= i\Omega L_0 + Z_V = i\Omega L_0 + R_V + i\Omega L_V \end{aligned} \tag{4.38}$$

where q_0 ($q_0^2 = 2\pi J$) is the charge of a vortex, n is the vortex density and $\nu(\Omega) = \frac{\mu(\Omega)}{\mu_0} = \nu'(\Omega) + i\nu''(\Omega)$ is our dimensionless mobility.

Solving for the real and imaginary parts from the previous equation through the use of equation (4.5) for the triangular array we get

$$R_V = 2\pi q_0^2 n \mu_0 \nu' L_0 = 8\pi \omega_a L_0 \frac{1 - p_c}{p - p_c} \bar{n} \nu'(\omega) \tag{4.39}$$

$$L_V = 2\pi q_0^2 n\mu_0 \frac{\nu''}{\Omega} L_0 = 8\pi L_0 \frac{1-p_c}{p-p_c}\bar{n}\frac{\nu''(\omega)}{\omega} \tag{4.40}$$

where we have used $\bar{n} = na^2$ which is the density of V per unit cell.

As $Z_V + i\Omega L_0 = i\Omega L_0 + 2\pi q_0^2 n L_0\mu_0(\nu'(\Omega) + i\nu''(\Omega))$ we get

$$\begin{aligned}\frac{1}{R_s} - \frac{1}{R_0} + \frac{1}{i\Omega L_s} &= \frac{1}{Z_V + i\Omega L_0} \\ &= \frac{1}{L_0}\frac{1}{i(\Omega + 2\pi q_0^2 n\mu_0\nu''(\Omega)) + 2\pi q_0^2 n\mu_0\nu'(\Omega)} \\ &= \frac{1}{L_0}\frac{\sigma_V' - i(\Omega + \sigma_V'')}{(\Omega + \sigma_V'')^2 + \sigma_V'^2}\end{aligned} \tag{4.41}$$

where we have used

$$\begin{aligned}\sigma_V' = \quad & 2\pi q_0^2 n\mu_0\nu'(\Omega) = (2\pi)^2 Jn\mu_0\nu'(\Omega) \\ & = 8\pi\omega_a\bar{n}\frac{1-p_c}{p-p_c}\nu'(\Omega)\end{aligned} \tag{4.42}$$

$$\begin{aligned}\sigma_V'' = \quad & 2\pi q_0^2 n\mu_0\nu''(\Omega) = (2\pi)^2 Jn\mu_0\nu''(\Omega) \\ & = 8\pi\omega_a\bar{n}\frac{1-p_c}{p-p_c}\nu''(\Omega)\end{aligned} \tag{4.43}$$

where σ_V' and σ_V'' are the real and imaginary parts of the vortex conductance σ_V which is related to vortex dielectric function through $\epsilon_V(\Omega) = 1 + \frac{\sigma_V(\Omega)}{i\Omega}$.

Separating the real and imaginary parts from both sides of equation (4.41) we get the following results [56]

$$\begin{aligned}\frac{1}{R_s} &= \frac{1}{R_0} + \frac{\sigma_V'}{L_0((\Omega + \sigma_V'')^2 + \sigma_V'^2)} \\ &= \frac{1}{R_0} + \frac{8\pi}{L_0\omega_a}\frac{\frac{1-p_c}{p-p_c}\bar{n}\nu'(\omega)}{(\omega + 8\pi\frac{1-p_c}{p-p_c}\bar{n}\nu''(\omega))^2 + (8\pi\frac{1-p_c}{p-p_c}\bar{n}\nu'(\omega))^2}\end{aligned} \tag{4.44}$$

$$\begin{aligned}\frac{1}{L_s} &= \frac{1}{L_0}\frac{\Omega(\Omega + \sigma_V'')}{(\Omega + \sigma_V'')^2 + \sigma_V'^2} \\ &= \frac{1}{L_0}\frac{\omega(\omega + 8\pi\frac{1-p_c}{p-p_c}\bar{n}\nu''(\omega))}{(\omega + 8\pi\frac{1-p_c}{p-p_c}\bar{n}\nu''(\omega))^2 + (8\pi\frac{1-p_c}{p-p_c}\bar{n}\nu'(\omega))^2}\end{aligned} \tag{4.45}$$

The scale quantities R_0 and L_0 are expressed as follows:

$$R_0 = 4.5R_J \tag{4.46}$$

where R_J is the junction resistance and the prefactor 4.5 is an estimate deduced by setting the energy barrier for vortex motion to its theoretical value (for details see Ref [49]).

The temperature dependent expression for L_0, the sheet inductance of a single junction, is given by (for details see Ref. [49])

$$\begin{aligned} \frac{1}{L_0(T)} &= \sqrt{3}\frac{2e}{\hbar} b^{-\zeta} I_c(0)(1-\frac{T}{T_c^o})^2 e^{-c\sqrt{T}} \\ &= 3.5\times 10^{14}(1-\frac{T}{T_c^o})^2 e^{-c\sqrt{T}} \end{aligned} \tag{4.47}$$

Here ζ is a critical exponent in two dimensions, $b^{-\zeta}$ is some constant deduced experimentally by setting the energy barrier for vortex motion to its theoretical value [48], $I_c(0)$ is the critical current of a single junction, c is some constant in unit of $K^{-1/2}$ and T_c^o is the transition temperature for the superconducting islands.

4.3.2 Flux noise

Flux noise measurements give interesting information about time correlations in the vortex dynamics. The Fourier transform $S_\phi(\omega)$ of the dynamic correlation function of the magnetic flux threading through a closed loop above the array is given by (details are given in chapter 2.1.3 of this thesis)

$$S_\phi(\omega) = S_0 \int_0^\infty dk \frac{J_1(kR)^2 e^{-2kd}}{k(1+\lambda k)^2} Re\left[\phi_{\rho\rho}(k,-i\omega)\right] \tag{4.48}$$

where $J_1(x)$ is the first order Bessel function and λ represents the magnetic penetration depth of the JJA and $\phi(k,z)$ is the Fourier-Laplace transform of the dynamic correlator of the vortex charge density $\rho_v(r,\tau)$

$$\phi(k,z) = \int d^2r \int_0^\infty d\tau e^{-z\tau} e^{i\mathbf{k}\cdot\mathbf{r}} \langle \rho_v(\mathbf{r},\tau)\rho_v(\mathbf{0},0)\rangle \tag{4.49}$$

It can be evaluated, for example, by Mori's procedure for calculating dynamic correlation functions, which yields the following form

$$\phi(k,z) = \frac{S_{\rho\rho}(k)}{z + \frac{k_B T k^2 \mu(z)}{S_{\rho\rho}(k)}} \tag{4.50}$$

involving the static charge structure factor $S_{\rho\rho}(k)$ and the dynamic vortex mobility $\mu(z)$. Neglecting again the effect of vortex interaction we use the mobility resulting from the multiple trapping model for the flux noise calculation. The structure factor should, in principle, be calculated by taking into account the effect of the random potential landscape due to the holes on the vortex configuration. We instead take the simple form [30]

$$S_{\rho\rho}(k) = \frac{k^2}{k^2 + k_0^2} \tag{4.51}$$

with

$$k_0^2 = \frac{2\pi q_0^2 n}{k_B T} \tag{4.52}$$

which has the correct behaviour for $k \to 0$ (charge neutrality of the V-A-system) and for $k \to \infty$.

4.4 Results

In this chapter we present our theoretical results for the frequency dependent mobility of vortices or antivortices in a diluted superconducting array using the multiple trapping model, the conductance of the array and the vortex resistance. Affolter [49] has measured the properties of such a disordered array near the critical percolation limit p_c below which the superconductivity of the array is destroyed.

In order to compare our theoretical results with these experimental data we have to determine the values of the parameters characterizing the array.

The measurements [49] have been performed on a triangular JJA of lead islands at $p = 0.515$ with the following characteristics (for the expressions in equations 4.46 and 4.47): $R_J \approx 5.2m\Omega$, $\zeta \approx 1$, $a \approx 15 \times 10^{-6}m$, $I_c(0) \approx 14mA$, $c \approx 3K^{1/2}$, $T_c^o = 7K$, $T_{BKT} = 3.7K$, $b \approx 0.22$.

From this we find (diffusion relation) : $D_0 \equiv k_B T_{BKT} \mu_0 \approx 2 \times 10^{-5} \frac{m^2}{s}$ and $\omega_a \approx 10^6$Hz.

In reference [49] a different reduced temperature $\hat{\tau} = k_B T / J(T)$ is used, based on an effective, temperature dependent Josephson coupling J. The link between $\hat{\tau}$ and T is approximately given by $\hat{\tau} = e^{1.8(T-6.04)}$. This relation allows to evaluate the quantity $L_0(T)$ given by expression (4.47). The link between $\hat{\tau}$ and t are given by the fact that at $T = T_{BKT}$ we have: $t = 1$ and $\hat{\tau}_c = 0.055$ (the relation follows from $T = 6.04 + \frac{1}{1.8} \ln(0.055t)$). This information will be needed in order to compare our theoretical results with the measured data in the following figures.

The main goal consists in elucidating the way in which the disorder of the dilute array influences vortex motion. The key quantity for this is $\pi(\omega)(= \pi'(\omega) + i\pi''(\omega))$ given by expression (4.33). Given the limits of the integral over N three frequency regimes can be distinguished, namely

$$\begin{aligned} &(a)\ \omega < \omega_1 \equiv (1 + N_{max})^{-a(t)} \\ &(b)\ \omega > \omega_2 \equiv 2^{-a(t)} \\ &(c)\ \omega_1 < \omega < \omega_2 \end{aligned} \tag{4.53}$$

In regions a and b the frequency dependence of the real and imaginary parts, $\pi'(\omega)$ and $\pi''(\omega)$, does not depend on the details of the hole distribution $D(N)$. It is given by

$$\begin{aligned} &\textit{Region } a: \quad \pi'(\omega) = \pi_0, \quad \pi''(\omega) \propto \omega \\ &\textit{Region } b: \quad \pi'(\omega) \propto \tfrac{1}{\omega^2}, \quad \pi''(\omega) \propto \tfrac{1}{\omega} \end{aligned} \tag{4.54}$$

In the intermediate region, however, the form of $D(N)$ will be reflected in temperature dependent frequency exponents for $\pi'(\omega)$ and $\pi''(\omega)$. A simple estimate can be made by assuming a power law distribution of hole sizes:

$$D(N) = D_0 N^{-s} \tag{4.55}$$

which turns out to correspond quantitatively with the arrays, studied in Ref.[49], the experimental data of which will be compared with our theoretical predictions. There the exponent $s \approx 1.8$. For frequencies lying well inside the interval $[\omega_1, \omega_2]$ the power law of π can be simply calculated:

$$\pi(\omega) \propto \int_1^{N_{max}} dN \frac{ND(N)}{i\omega + (1+N)^{-a(t)}} \approx I_0 (i\omega)^{-u(t)} \tag{4.56}$$

$$I_0 = \int_0^{\infty} dy \frac{y^{1-s}}{1+y^{-a}} \tag{4.57}$$

$$u = 1 + \frac{2-s}{a} \tag{4.58}$$

t	$a(t)$	ω_1	ω_2	$u(t)(s=1.8)$	$u(t)(s=0.3)$
0.9	37	$10^{-53} \approx 0$	7.10^{-12}	1	1.05
2	17	9.10^{-25}	8.10^{-6}	1.01	1.1
6	5.5	2.10^{-8}	0.02	1.04	1.3
10	3.3	2.10^{-5}	0.1	1.06	1.5

Table 4.1: Some parameters for $p = 0.515$ and $N_{max} = 25$; $a(t) = \frac{1}{t}\frac{1-p_c}{p-p_c} = \frac{1}{t}\frac{0.5}{0.015} = \frac{33}{t}$, $\omega_1 = (1+25)^{-a}$ and $\omega_2 = (1+1)^{-a}$.

We summarize in Table 4.1 the values of ω_1, ω_2 and u using the parameters corresponding to the experimental data of Ref.[49], namely $p = 0.515$, $0.9 < t < 10$ and $N_{max} = 25$. For the given parameter values it turns out that the exponent $u \approx 1$ is almost T-independent. The resulting frequency dependence the real part of π, $\pi' \sim 1/\omega$, is unusual, since one expects π' to be an even function of ω, as it is indeed the case in regions a and b, see relations (4.54). The power law behaviour ($\pi \sim \omega^{-u}$) is the result of the integration over a contiuous spectrum of relaxation rates in (4.56). For comparison we give another form of $D(N)$ which gives more weight to large holes ($s = 0.3$). The corresponding exponent has a more pronounced T-dependence.

The vortex mobility resulting from π through (4.24) will determine the electrodynamic response in (4.44) and (4.45), as well as flux noise (4.48). Its behaviour, in units of the free vortex mobility μ_0, is shown in figure 4.2 for different temperatures and for different defect concentrations $1 - p$. The three frequency regimes are again visible, although the curves have more structure than the ones for π since $\pi'(\omega)$ and $\pi''(\omega)$ are combine with each other in the expression (4.24) for $\nu'(\omega)$ and $\nu''(\omega)$.

At very high frequencies, namely $\omega > 1$ the real part of the mobility is constant with the bare value μ_0; In this regime we are investigating the short-time response of the

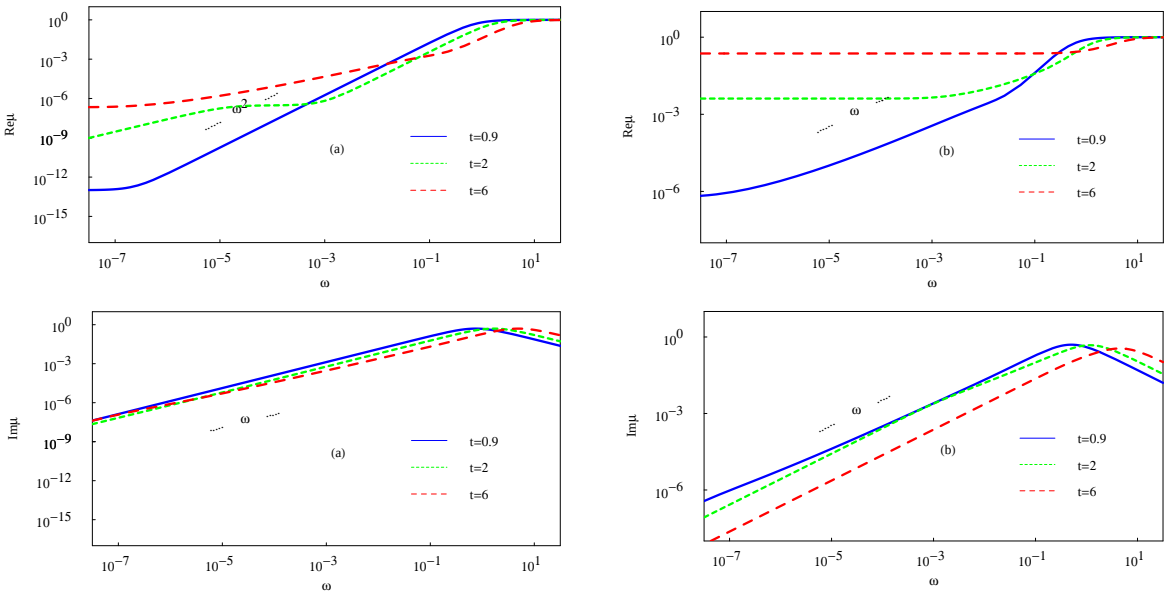

Figure 4.2: μ **vs** ω **for (a)** $p = 0.515$ **(**$N_{max} = 25$**) and (b)** $p = 0.6$ **(**$N_{max} = 22$**).** $s = 1.8$**.**

array: the vortices lying outside the holes do not have a significant probability of being trapped and their mobility is just the bare one. At the other extremity of the frequency spectrum, the vortex mobility is also constant but the bare value μ_0 is renormalized by $1 + \pi_0$ leading to a reduction by several orders of magnitudes, strongly depending on p. Over very long time spans the vortices get trapped and released many times and, as they do not contribute to mobility as long as they stay in a hole, the overall mobility dramatically diminishes upon increasing the number and size of the holes.

The imaginary part of the vortex mobility displays a maximum near $\omega = 1$. For lower frequencies $Im[\mu(\omega)] \propto \omega$, although at $p = 0.6$ and below T_{BKT} a small kink appears around $\omega \sim 10^{-7}$ (especially for $s = 0.3$).

The intermediate-frequency behaviour of the real part of the vortex mobility can be understood by looking carefully at the interplay of the real and imaginary parts of $\pi(\omega)$ going into $\mu'(\omega) = \frac{1+\pi'(\omega)}{(1+\pi'(\omega)^2)+\pi''(\omega)^2}$.

Two frequency domains show up: In a range below $\omega = 1$, extending as far down as 10^{-7} for $t = 0.9$, $\pi''(\omega) \propto \omega^{-1}$ for all interesting frequencies, while $\pi'(\omega)$ becomes significantly lower than unity. Thus the real part of the mobility increases quadratically with frequency, which is in some sense a surprisingly normal behaviour. Conversely, at smaller frequencies, $\pi'(\omega)$ becomes constant, while $\pi''(\omega) \propto \omega$ (i.e. it reaches a maximum at some frequency, below the quadratic-behaviour window), giving rise to a constant vortex mobility with a value intermediate between μ_0 and the low frequency limit. The two frequency regimes get shifted towards lower ω-values when temperature is reduced, as it can be seen in figure 4.2. The curves in figure 4.2 have been calculated

for the choice $f(t) = t$ in equation (4.25b). We have verified that the result for $f(t) = 1$ is almost identical if we don't go to very high temperature.

In addition to the intermediate-frequency regime, where the real part of the mobility becomes constant, we see on Fig. 2, that at $t = 2$ yet another anomalous regime shows up at very low frequencies, where $\mu'(\omega) \propto \omega$, approximately. At high temperature $t = 6$ and at frequencies below the tiny $\mu \propto \omega^2$ window centered around $\omega \approx 1$, the mobility plateau gets replaced by a regime where $\mu'(\omega) \propto \omega^{0.8}$, down to $\omega \approx 10^{-6}$. The non-integer exponent arises from the fact that, in accordance with the Table 4.1, $\pi''(\omega) \propto \omega^{-1.04}$ in this frequency window, while $\pi'(\omega) \propto \omega^{-1}$ and $\pi'(\omega) >> 1$ still. Obviously, this non-integer power-law behaviour of the real part of the mobility also arises at lower temperatures, but it becomes less pronounced as the exponent $u(T)$ is extremely close to unity at $t = 2$. In order to confirm this behaviour, we have computed the vortex mobility at $s = 0.3$, a choice for which the exponen $u(T)$ has a much more marked temperature-dependence than at $s = 1.8$. see Table 4.1. In the former case, we find that, at $t = 0.9$, no relevant changes occur, with respect to the resuls obtained at $s = 1.8$. Nevertheless, at higher temperature $t = 2$, the intermediate-frequency plateau discussed above gets substantially reduced and covers at most only one frequency decade. At even higher temperature $t = 6$, the plateau is replaced by an anomalous regime extending roughly from $\omega \approx 10^{-7}$ to $\omega \approx 10^{-2}$, in which the real part of the mobility behaves as a power-law $\omega \propto \omega^{-0.7}$ again with a non integer exponent. For both choices of the parameter s, the real part of the mobility eventually turns to a constant at extremely low frequencies. Therefore, in conclusion, for temperatures above T_{BKT}, the mobility displays four distinct frequency regimes, which collapse into three regimes below the transition temperature.

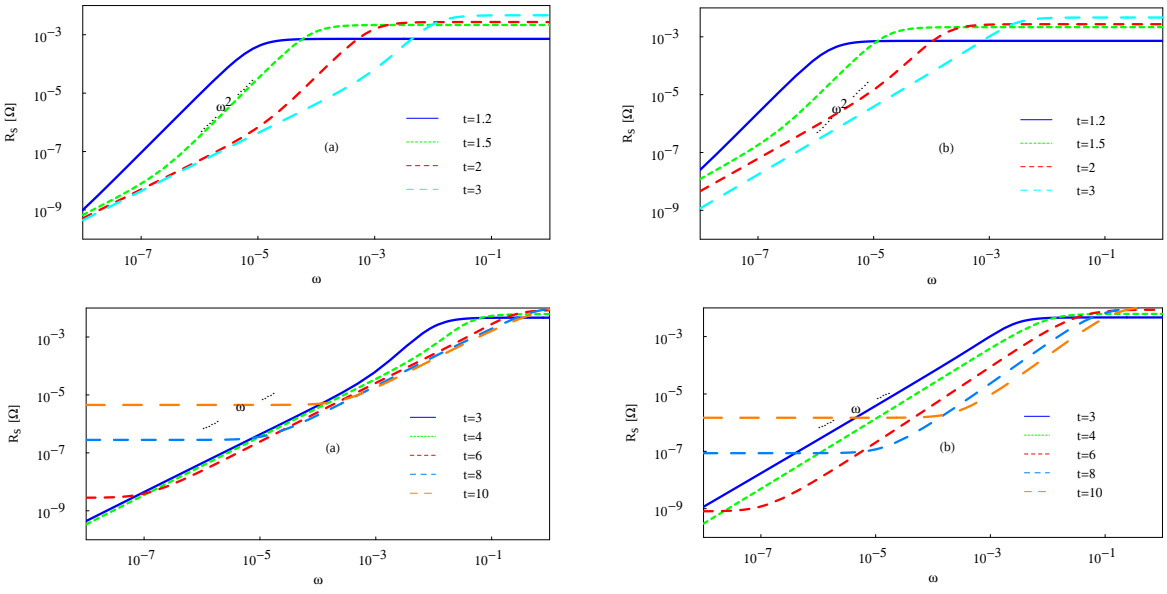

Figure 4.3: R_s **vs** ω **for** $p = 0.515$. **(a)** $s = 1.8$ **and (b)** $s = 0.3$.

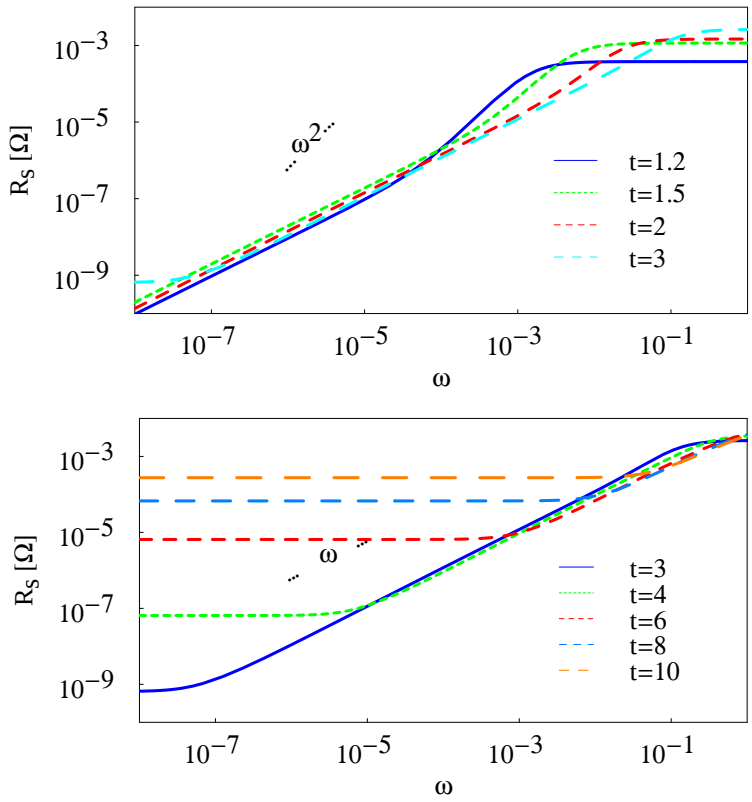

Figure 4.4: R_s **vs** ω **plot for** $p = 0.53$ $(N_{max} = 25)$ **and** $s = 1.8$**.**

We now turn to the electrodynamic response for which experimental data are available in Ref.[49]. For the vortex density n showing up in (4.44) and (4.45) we have used the values obtained in the References [37,38] through Monte Carlo simulations of the regular arrays. In order to have a consistent treatment one should, of course, know the vortex density of a dilute array. The presence of holes indeed makes the formation of phase singularities more easy, since, in particular, vortices centered in a hole cost less energy than in a regular array. However, for temperatures above T_{BKT}, where even in a regular array the number of vortices grows rather rapidly, the difference should not be too important. Our sheet resistance curves for $p = 0.515$ are shown in figures 4.3a and 4.3b for two different exponents s in $D(N)$, see equation (4.55). For the sake of comparison figure 4.4 shows the same curves as are shown in the measured R_s curves [49] for a slightly larger value of p. The following observations can be made:

- The same three frequency regimes determining the quantity $\pi(\omega)$ and the vortex mobility can be identified in $R_s(\omega)$: at very low and at very high frequencies R_s is constant, whereas in the intermediate regime it increases as a power of ω: $R_s \sim \omega^{x(T)}$. This temperature dependent exponent x is a fine detail of the MT model which is in good agreement with the experimental data. For higher temperature $x = 1$, which is again an interesting signature of the disorder of the array. For lower T the sheet

resistance undergoes an upturn to ω^2-behaviour, which is clearly visible in Fig. 3. The latter behaviour is intimately linked to the real part of the vortex mobility (discussed above) going through an intermediate plateau in some frequency window. Indeed, within the latter, we notice that $\mu'_V(\omega) \ll \mu''_V(\omega)$, trivially implying $\sigma'_V(\omega) \ll \sigma''_V(\omega)$. Upon considering Eqns. (4.42) and (4.43) for p close to p_c, we furthermore deduce that $\sigma''_V(\omega)$ is larger than that for the frequency in the "plateau" ω-window. Consequently, inserting this into expression (4.44), we obtain $R_S^1 = \frac{L_0\sigma''_V(\omega)^2 + R_0\sigma'_V(\omega)}{R_0 L_0 \sigma''_V(\omega)^2}$. Hence, bearing in mind that for all the frequencies that we are considering here, $\mu''_V(\omega) \propto \omega$, there exists a frequency window in which $\mu'_V(\omega) = const.$ implies $R_S \propto \omega^2$, especially for temperatures close to and above T_{BKT}, where $L_0(T)$ is small. In turn, at higher frequencies, we fall in the ω-window where $\mu'_V(\omega) \propto \omega^2$, in which the sheet resistance turns to a constant. In conclusion, the anomalous vortex mobility plateau which arises from the balance between the real and imaginary parts of $\pi(\omega)$ is at the root of the ω^2-upturn of the sheet resistance in our model.

- In experiment [49] R_s approaches a square root frequency dependence for ω larger than ω_c, rather than becoming constant. This may point to a new dynamic regime that is not fully covered by our model calculations. There is however a growing tendency in the theoretical curves to such a further increase of R_S at the highest frequencies shown for larger p-values (see figure 4.4).

- The temperature variation of the low frequency level of R_s, as well as the difference between the low and high frequency limits are larger in the MTM results than in experiment. This may be a hint that the model, at least for the p- value used, attributes too much value to the disorder of the array.

- For $\tau > 0.173$ the measured data show universality: when the curves have reached a linear slope they lie on top of each other. In the model results this universality is rather well reproduced for a higher value of the exponent s of the hole distribution function $D(N)$ (figures 4.3a and 4.4), which corresponds to the effective hole hierarchy of the experimental array [49], giving thus less weight to large holes than the lower values of s.

The inverse of the inductive response, $1/L_s$, for our MT model is presented in figures 4.5a and 4.5b for the same parameters as in figure 4.3 for R_s and for a large p in figure 4.6. Comparing the two leads to the following observations:

- The three frequency regimes are again visible: for small and for large ω, $1/L_s$ varies as ω^2, whereas in between it is constant. The experimental data in ref.[49] show this behaviour for low frequency. However, except for the lowest temperature, there is no real constant part, but relatively smooth cross-over to a square root like behaviour when ω increases. This again points to a high frequency dynamics that is not covered by our MT model for $p = 0.515$. However the experimentally obtained $\sqrt{\omega}$ type behaviour is almost achieved in our theoretical model for higher values of p and T.

On the whole our MTM results are in good agreement with the measured data. Certain experimental features (in particular the low frequency and low temperature behaviour of R_s) are better reproduced for the value $p = 0.515$ of the percolation parameter, which corresponds to the experimental array. Other details of the data are

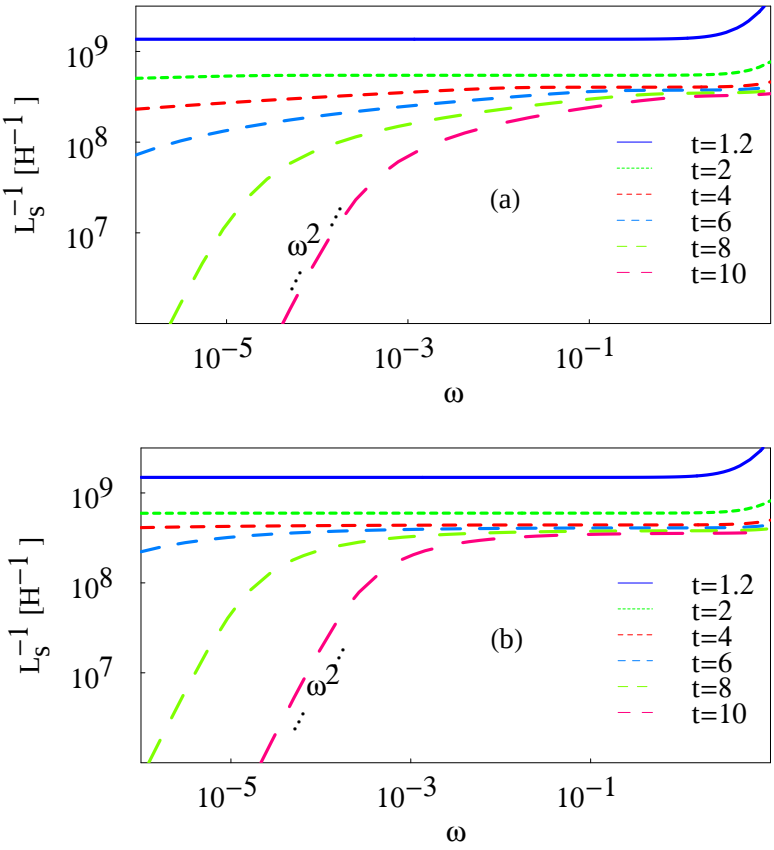

Figure 4.5: L_s **vs** ω **for** $p = 0.515$. **(a)** $s = 1.8$, **(b)** $s = 0.3$.

closer to the theoretical curves for $p = 0.53$. This may be due to the oversimplification of the true, ramified structure of the regions of missing sites, which in the model are approximated by circular holes. On the other hand, concerning the probability distribution $D(N)$ of these holes the exponent $s = 1.8$, corresponding to the experimental situation, is more satisfactory than a form for D which would give more weight to large holes.

In section 4.3.1, equations (4.36) and (4.37), we have introduced the notion of a vortex impedance $Z_V = R_V + i\Omega L_V$. At low frequencies its real part is thermally activated as shown in figure 4.7. This behaviour is confirmed by the measurements presented in ref.[49]. The slope of the theoretical curves at high enough temperature (e.g., around $t = 5$) yields activation energies of about 4 and 2.6 in unit of J for $p = 0.515$ and $p = 0.53$ respectively, in good agreement with the experimental data. For very low temperatures the curves become flat. The activation energies for different

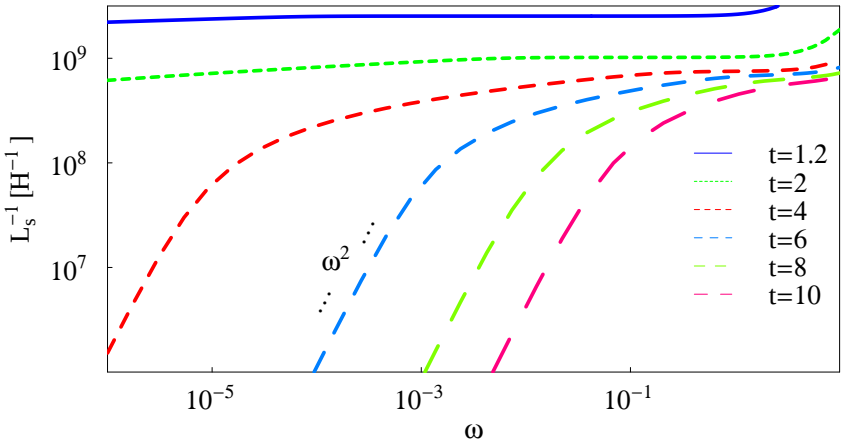

Figure 4.6: L_s **vs** ω **plot for** $p = 0.53$**.** $s = 1.8$**.**

p's also show little different values depending on the values of t's at which we draw the slopes. However, in between the two limiting regimes, there are other common slopes in the R_V vs $1/t$ plot at about $1/t = 0.6$ for $p = 0.515$ and $1/t = 1.1$ for $p = 0.53$, for example, in our theoretical plots. The measurements do not really exhibit our second common slope but the experimental curves in ref.[49] for 317 Hz and lower frequencies do indeed show a tendency to a steeper slope before they approach the constant value in the low temperature limit. In this respect the experimental data look more similar to our curves for a larger percolation fraction ($p = 0.53$ in figure 4.7).

Finally we present, in figure 4.8, the flux noise spectrum resulting from our multiple trapping approach, for different temperatures and p. Flux noise is an interesting observable even for regular arrays [29,30]. It is white (frequency independent) for sufficiently low ω with a value that depends on T. For intermediate frequencies the curves for different T are identical, having a $1/\omega$ slope. This universality has been explained in different ways, for example by invoking the dynamic response of bound vortex-antivortex pairs which exist below T_{BKT}, but also above, with a finite life-time. It is interesting to note that disorder seems to produce a similar behaviour, although the intermediate regime has structure superposed on a simple $1/\omega$ dependence, specially for p close to p_c. In particular, there is another white noise region for higher frequency, before the behaviour crosses over to $1/\omega^2$ at high frequencies. This structure is again a consequence of the frequency dependence of the vortex mobility. Moreover, the universality in this regime is not perfect: even for $p = 0.6$ the curves are not on top of each other. Unfortunately there are, at least for the time being, no experimental data to compare with.

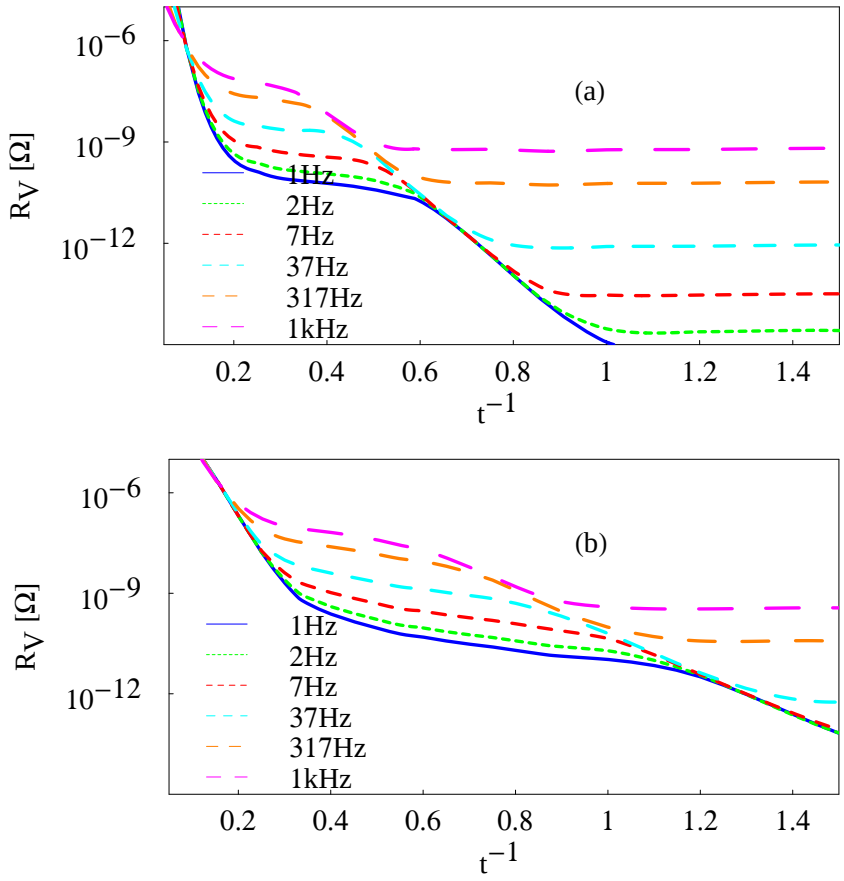

Figure 4.7: R_V **vs** $1/t$ **for different** Ω. **(a)** $p = 0.515$, **(b)** $p = 0.53$. $s = 1.8$.

4.5 Summary and conclusions

In this chapter we have aimed at explaining the electrodynamic response of a Josephson junction array in which a substantial fraction of the superconducting sites is missing. For the motion of thermally excited vortices and antivortices in this type of strongly disordered array we have used a multiple trapping model. The regions of missing sites are grouped into holes which we take to be of ciruclar shape. When a vortex or antivortex reaches a hole it has some probility of being trapped into the hole (pinning effect). It can later on be released due to the thermal excitation. The effect of this disorder is phrased in terms of a frequency dependent vortex mobility which determines observable quantities, such as the electrical conductance, composed by the sheet resistance R_s and the inductance L_s of the array, or the flux noise. We compare our theoretical results with measurements obtained on such a percolative array [49].

We find the following results :

(i) R_s exhibits three frequency regimes. At very low and high frequency ω a white

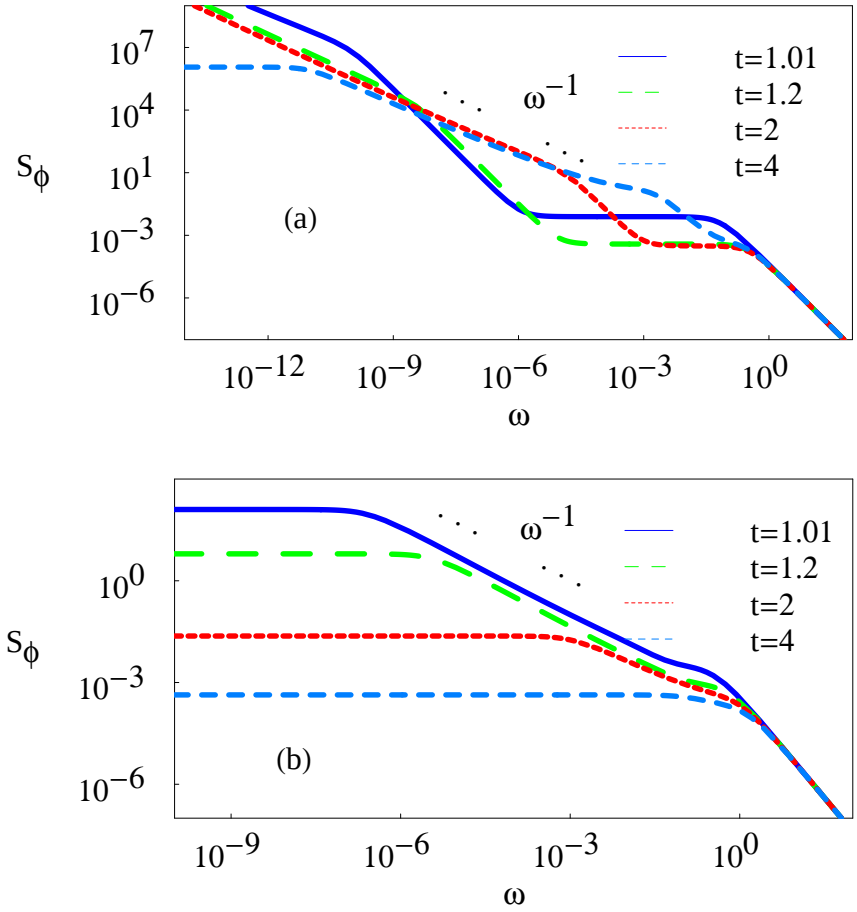

Figure 4.8: S_ϕ **vs** ω. **(a)** $p = 0.515$, **(b)** $p = 0.60$. $s = 1.8$.

spectrum is observed with a much lower value for low ω than for large ω. For the time scale corresponding to the latter regime vortices remain either trapped in a hole or free outside any hole. Thus the mobility, and the corresponding response is given by the one of a regular array. At the opposite end, for very low frequencies, vortices get trapped many times during one excitation cycle, which strongly reduces their mobility. For intermediate frequency regime $R_s \propto \omega^x$ with x varying between $x = 1$ and $x = 2$. For higher temperatures the $R_s \propto \omega$ almost coincide, signalling some kind of universality. These features are in good agreement with the experimental data in [49].

(ii) For the inductive part we find $L_s^{-1} \propto \omega^2$ at low ω while for intermediate frequency regime L_s^{-1} is independent of ω. For large frequencies a tendency of L_s^{-1} to grow with frequency with some new exponent is also seen for higher values of p. The critical frequency for crossover from $L_s^{-1} \propto \omega^2$ to constant L_s^{-1} decreases with the decrease of temperature T and percolation fraction p. These results also reproduce well

the experimental data of reference [49].

(iii) For a given frequency the vortex resistance is thermally activated at sufficiently high temperatures. The activation energy on the order of 4 times the Josephson coupling between the existing superconducting sites corresponds to the measured value [49]. For lower temperatures a tendency towards having slightly different values for the activation energies is visible from the R_V versus $1/T$ curves, which also slightly appear in the measured data.

(iv) We have also evaluated the frequency dependent flux noise. $1/\omega$ noise is achieved for the intermediate frequencies separating the white noise part for small ω and $1/\omega^2$ noise for very high frequencies. thus the presence of disorder leads to similar results as seen in regular arrays [30]. However at very close to p_c the flux noise data has some unexpected flatenning before turning to $1/\omega^2$ part which is a consequence of the frequency dependence of the vortex mobility. Unfortunately there are no experimental flux noise data for the disordered arrays to compare with our theoretical investigations.

Chapter 5

Vortex Dynamics in two-dimensional Josephson junction arrays : Fokker-Planck Approach

In this chapter we shall focus on calculating the vortex density correlator using a Fokker Planck equation for the time-dependent probability distribution function of vortices (V) and antivortices (A). Some collective effects, namely screening of the long range Coulomb interaction, modification of purely diffusive dynamics and generalization of the friction function etc. are explained in the framework of Fokker-Planck approach. We apply this technique in order to treat the vortex dynamics above the Berezinskii-Kosterlitz-Thouless (BKT) transition temperature T_{BKT} where bound pairs and free vortices contribute to the dynamic response. We shall, for simplicity, first treat the problem of one component plasma where we consider all the particles (vortices and antivortices) are identical in order to show many body effects like friction, screening of Coulomb interaction etc. used in Mori approach in a better way. We shall then extend our analysis into treating vortex antivortex single pair dynamics. Here we shall show our own calculations and will compare our results with other existing approaches (and results) available to describe the vortex antivortex pair dynamics in JJAs.

5.1 Theoretical approach and basic definitions

The Fokker-Planck equation [57,58] describes the time evolution of the probability density function of position and velocity of particles (for detailed picture see [59]). The first use of the Fokker-Planck equation for particles in a fluid was the statistical description of the Brownian motion that follows from the Langevin equation. If we consider $P(\{x\},t)$ to be the probability density function of the particles in such a stochastic system we can write the general form of the Fokker-Planck equation as

follows

$$\frac{\partial P}{\partial t} = [-\sum_{i=1}^{N} \frac{\partial}{\partial x_i} D_i^{(1)}(\{x\}) + \sum_{i=1}^{N}\sum_{j=1}^{N} \frac{\partial^2}{\partial x_i \partial x_j} D_{ij}^{(2)}(\{x\})]P \tag{5.1}$$

where $D^{(1)}$ is the drift vector and $D^{(2)}$ is the diffusion tensor resulting from the presence of the stochastic force. $\{x\}$ represents the positions and/or velocities of N particles.

5.1.1 Fokker-Planck equation for vortex dynamics in JJAs when vortices and antivortices are considered to be massless particles - overdamped limit

In our vortex antivortex system in a two-dimensional Josephson junction array we are interested to see the time dependent evolution of the positions and velocities of the particles (V and A). We shall first consider the vortices and antivortices to be massless identical particles (so the velocity effects are negligible). The expression of the force in the vortex antivortex system arises from the Coulomb interaction between the charged particles and this takes the following form

$$F_i(l) = -\nabla_i \sum_{l'} V(\mathbf{R}_l - \mathbf{R}_{l'}) \tag{5.2}$$

where the Coulomb interaction between the charged particles in 2D is given by

$$V(\mathbf{R}_l - \mathbf{R}_{l'}) \approx \ln(|\mathbf{R}_l - \mathbf{R}_{l'}|) \tag{5.3}$$

Here the charges of vortex and antivortex are, for simplicity, considered to be identical and unity in a one component plasma.

In this case we consider $P(\{\mathbf{R}\};\{\mathbf{R}'\};t)$ to be the conditional probability density function multiplied by the initial distribution function for the vortex antivortex system in a 2D JJA and this function describes that the particles occupy the positions $\{\mathbf{R}\} = \{\mathbf{R}_1, \mathbf{R}_2, ..., \mathbf{R}_N\}$ at time t while they occupied the positions $\{\mathbf{R}'\} = \{\mathbf{R}'_1, \mathbf{R}'_2, ..., \mathbf{R}'_N\}$ at time $t = 0$ [60]. So we get the Fokker-Planck equation for the vortex antivortex system in a 2D JJA as follows

$$\frac{\partial}{\partial t} P(\{\mathbf{R}\};\{\mathbf{R}'\};t) = -\sum_{il} \frac{\partial}{\partial R_i(l)} (F_i(l) P(\{\mathbf{R}\};\{\mathbf{R}'\};t)) + D\sum_{il} \frac{\partial^2}{\partial R_i(l)^2} P(\{\mathbf{R}\};\{\mathbf{R}'\};t)$$

$$= -\sum_{ill'} \frac{\partial}{\partial R_i(l)} (-\nabla_i V(\mathbf{R}_l - \mathbf{R}_{l'}) P(\{\mathbf{R}\};\{\mathbf{R}'\};t)) + D\sum_{il} \frac{\partial^2}{\partial R_i(l)^2} P(\{\mathbf{R}\};\{\mathbf{R}'\};t) \tag{5.4}$$

where $D = \frac{k_B T}{\Gamma}$ is the Einstein's diffusion constant and Γ is the bare friction function of the particles in the array.

We now apply the following Fourier transformations

$$P(\{\mathbf{k}\};\{\mathbf{k}'\};t) = \int d^2R_1 ... d^2R_N \int d^2R'_1 ... d^2R'_N e^{-i\sum_l \mathbf{k}_l \cdot \mathbf{R}_l - i\sum_s \mathbf{k}'_s \cdot \mathbf{R}'_s} P(\{\mathbf{R}\};\{\mathbf{R}'\};t) \tag{5.5}$$

$$V(\mathbf{R}) = \int d^2 p e^{-i\mathbf{p}\cdot\mathbf{R}} \hat{V}(\mathbf{p}) \tag{5.6}$$

The diffusion term

$$\sum_{il} \frac{\partial^2}{\partial R_i(l)^2} P(\{\mathbf{R}\};\{\mathbf{R}'\};t) \to -\sum_{l} \mathbf{k}_l^2 P(\{\mathbf{k}\};\{\mathbf{k}'\};t) \tag{5.7}$$

From now on we shall sometimes write $P(\{\mathbf{k}\};t)$ in place of $P(\{\mathbf{k}\};\{\mathbf{k}'\};t)$ for simplicity and in that case we must remember that $\{\mathbf{k}'\}$ is always there. We now use the Laplace transformation

$$\hat{P}(\{\mathbf{k}\};z) = \int dt e^{-zt} P(\{\mathbf{k}\};t) \tag{5.8}$$

$$\frac{\partial}{\partial t} P(\{\mathbf{k}\};t) \to z\hat{P}(\{\mathbf{k}\};z) - \hat{P}(\{\mathbf{k}\};0) \tag{5.9}$$

where z is the frequency and $\hat{P}(\{\mathbf{k}\};0)$ is the Fokker-Planck distribution function at $t = 0$.

Now the Fokker-Planck equation takes the following form

$$(z + A\sum_l \mathbf{k}_l^2)\hat{P}(\{\mathbf{k}\};\{\mathbf{k}'\};z) = \hat{P}(\{\mathbf{k}\};\{\mathbf{k}'\};0)$$
$$+ \int B d^2 p_0 \sum_{nn'} \mathbf{p}_0 \cdot (\mathbf{p}_0 + \mathbf{k}_n)\hat{V}(\mathbf{p}_0) \int d^N p \chi_{nn'}(\{\mathbf{k}\},\{\mathbf{p}\})\hat{P}(\{\mathbf{p}\};\{\mathbf{k}'\};z) \tag{5.10}$$

where $A = \frac{k_B T}{\Gamma}$, $B = -\frac{1}{2\pi\Gamma}$ and $\hat{P}(\{\mathbf{k}\};\{\mathbf{k}'\};0)$ is the intial equilibrium distribution that is the probability density function in Fourier space at time $t = 0$.

At $t = 0 \quad P(\{\mathbf{R}\};\{\mathbf{R}'\};0) = \prod_l \delta(\mathbf{R} - \mathbf{R}')\phi(\{\mathbf{R}'\})$

Here $\phi(\{\mathbf{R}'\})$ is the initial equilibrium distribution. So at $t = 0$

$$P(\{\mathbf{k}\};\{\mathbf{k}'\};t) = \int d^N R e^{-i\sum_l \mathbf{k}_l\cdot\mathbf{R}_l} \int d^N R' e^{-i\sum_s \mathbf{k}'_s\cdot\mathbf{R}'_s} P(\{\mathbf{R}\};\{\mathbf{R}'\};t)$$

becomes

$$P(\{\mathbf{k}\};\{\mathbf{k}'\};0) = \int d^N R \int d^N R' e^{-i\sum_l \mathbf{k}_l\cdot\mathbf{R}_l - i\sum_s \mathbf{k}'_s\cdot\mathbf{R}'_s} \prod \delta(\mathbf{R}_t - \mathbf{R}'_t)\phi(\{\mathbf{R}'_t\})$$

which can be rewritten as

$$P(\{\mathbf{k}\};\{\mathbf{k}'\};0) = \int d^N R' e^{-i\sum_l (\mathbf{k}_l + \mathbf{k}'_l)\cdot\mathbf{R}'_s} \phi(\{\mathbf{R}'\}) = \phi(\{\mathbf{k} + \mathbf{k}'\}) \tag{5.11}$$

We have also

$$\chi_{nn'}(\{\mathbf{k}\},\{\mathbf{p}\}) = \prod_{l\neq(n,n')} \delta(\mathbf{p}_n - (\mathbf{k}_n - \mathbf{p}_0))\delta(\mathbf{p}_{n'} - (\mathbf{k}_{n'} + \mathbf{p}_0))\delta(\mathbf{p}_l - \mathbf{k}_l) \tag{5.12}$$

At this point we now relate the distribution function $\hat{P}(\{\mathbf{k}\};\{\mathbf{k'}\};z)$ with the particles charge density correlator $\phi_{\rho\rho}(\mathbf{p},t)$ which gives the correlation between the charge of a particle at position R_l at time t and the charge of a particle at position $R_{l'}$ at time $t=0$ (complete analysis and definition of charge density correlator are given in chapter 2.1.3) and can mathematically be defined [29,30] as

$$\begin{aligned}\phi_{\rho\rho}(\mathbf{p},t) &= \frac{1}{N}\sum_{ll'}\langle e^{i\mathbf{p}\cdot(\mathbf{R}_l(t)-\mathbf{R}'_{l'}(0))}\rangle \\ &= \frac{1}{N}\sum_{ll'}\int d^N R d^N R' e^{i\mathbf{p}\cdot\mathbf{R}_l}e^{-i\mathbf{p}\cdot\mathbf{R}'_{l'}}P(\{\mathbf{R}\};\{\mathbf{R'}\};t) \qquad (5.13)\end{aligned}$$

Using the above definitions we get the charge density correlator, in the case where we consider that all charges are of the same sign, through the Laplace transformations as follows

$$\phi_{\rho\rho}(\mathbf{p},z) = (N-1)\hat{P}(\mathbf{p},\mathbf{0},..;\mathbf{0},-\mathbf{p},..;z) + \hat{P}(\mathbf{p},\mathbf{0},..;-\mathbf{p},\mathbf{0},..;z) \qquad (5.14)$$

where $\hat{P}(\mathbf{p},\mathbf{0},..;\mathbf{0},-\mathbf{p},..;z)$ and $\hat{P}(\mathbf{p},\mathbf{0},..;-\mathbf{p},\mathbf{0},..;z)$ are so called hetero and auto correlators respectively. Using the previous Fokker-Planck equation (5.10) where we let $\{\mathbf{k}\}=\{\mathbf{p},\mathbf{0},\mathbf{0},...\}$ and $\{\mathbf{k'}\}=\{\mathbf{0},-\mathbf{p},\mathbf{0},...\}$ the correlators follow the following equations

$$\begin{aligned}(z+A\mathbf{p}^2)\hat{P}(\mathbf{p},\mathbf{0},...;\mathbf{0},-\mathbf{p},...;z) &= \hat{P}(\mathbf{p},\mathbf{0},...;\mathbf{0},-\mathbf{p},...;0) \\ +\int Bd^2p_0\sum_{nn'}\mathbf{p}_0\cdot(\mathbf{p}_0+\mathbf{k}_n)\hat{V}(\mathbf{p}_0)\int d^N p\chi_{nn'}(\{\mathbf{k}\},\{\mathbf{p}\})\hat{P}(\{\mathbf{p}\};\mathbf{0},-\mathbf{p},...;z) \qquad (5.15)\end{aligned}$$

$$\begin{aligned}(z+A\mathbf{p}^2)\hat{P}(\mathbf{p},\mathbf{0},...;-\mathbf{p},\mathbf{0},...;z) &= \hat{P}(\mathbf{p},\mathbf{0},...;-\mathbf{p},\mathbf{0},...;0) \\ +\int Bd^2p_0\sum_{nn'}\mathbf{p}_0\cdot(\mathbf{p}_0+\mathbf{k}_n)\hat{V}(\mathbf{p}_0)\int d^N p\chi_{nn'}(\{\mathbf{k}\},\{\mathbf{p}\})\hat{P}(\{\mathbf{p}\};\mathbf{0},-\mathbf{p},...;z) \qquad (5.16)\end{aligned}$$

Here

$$\hat{P}(\mathbf{p},\mathbf{0},...;\mathbf{0},-\mathbf{p},...;0) = S_{\rho\rho}(\mathbf{p}) \qquad (5.17)$$

is the charge structure factor (detailed explanations of structure factor are given in chapter 2 and 3). $\hat{P}(\mathbf{p},\mathbf{0},...;-\mathbf{p},\mathbf{0},...;0)=\phi(\mathbf{0},\mathbf{0};0)$, a constant, is the auto correlator at the initial time ($t=0$).

Here we have introduced two types of correlators which are namely: hetero correlator and auto correlator for one component fluid. For hetero correlator we consider the correlation between one particle in position R_1 at time t and another particle in position R'_2 at time $t=0$. The correlation between a particle in position R_1 at time t and another particle in any other position e.g., in R_2 at the same time is a differently considered hetero type correlation.

In the case of one component fluid that is when we consider all charges (vortex or antivortex) to be of the same sign (sign of $q_l q_{l'}$ is positive for all values of l,l', q's are

charges of vortex or antivortex) we have $N-1$ hetero correlators which dominate over the only one auto correlator for a fluid with N particles.

We shall now consider different types of arrangements and interactions of particles. They are explained here in details. For simplicity we shall consider here only the cases for the hetero correlator $\hat{P}(\mathbf{p},\mathbf{0},...;\mathbf{0},-\mathbf{p},...;z)$ because it is the main contributor to the vortex density correlator $\phi_{\rho\rho}(\mathbf{p},z)$.

The Coulomb interaction between a vortex and an antivortex, considered in the previous Fokker-Planck equations (5.15 and 5.16), in Fourier two-dimensional space, is taken to be of the following form

$$\hat{V}(\mathbf{p}_0)=\frac{1}{\mathbf{p}_0^2} \tag{5.18}$$

Free vortex dynamics

In the case where there is no interaction between particles we get the two particle (particles 1 and 2) correlator $\hat{P}(\mathbf{p},\mathbf{0},..;\mathbf{0},-\mathbf{p},..;z)$, using the Fokker-Planck equation (equation 5.15), which follows the free diffusive relation

$$\hat{P}(\mathbf{p},\mathbf{0},..;\mathbf{0},-\mathbf{p},..;z)=\frac{S_{\rho\rho}(\mathbf{p})}{z+\frac{k_BT}{\Gamma}\mathbf{p}^2} \tag{5.19}$$

Contribution from the Coulomb interaction between two particles - Pair dynamics

We want to calculate the two particle (particles 1 and 2) correlator $\hat{P}^{(2)}(\mathbf{p},\mathbf{0};\mathbf{0},-\mathbf{p};z)$, using the Fokker-Planck equation (5.15), where particles 1 and 2 are in direct Coulomb interaction. Here $\hat{P}^{(2)}$ represents the correlator between say the particle number 1 with coordinate $\mathbf{R_1}$ at time t in real space and particle number 2 with coordinate $\mathbf{R_2}'$ at time $t=0$ and at time t they are in direct Coulomb interaction. So we use $n=1,\ n'=2$ in equation (5.15) which then takes the following form

$$\begin{aligned}&(z+\frac{k_BT}{\Gamma}\mathbf{p}^2)\hat{P}^{(2)}(\mathbf{p},\mathbf{0};\mathbf{0},-\mathbf{p};z)=\hat{P}^{(2)}(\mathbf{p},\mathbf{0};\mathbf{0},-\mathbf{p};0)\\&+(-\frac{1}{2\pi\Gamma})\int d^2k_1'\int d^2k_2'\int d^2p_1\mathbf{p}_1\cdot(\mathbf{p}+\mathbf{p}_1)\hat{V}(\mathbf{p}_1)\\&\delta(\mathbf{k}_1'-\mathbf{p}+\mathbf{p}_1)\delta(\mathbf{k}_2'-\mathbf{0}-\mathbf{p}_1)\hat{P}^{(2)}(\mathbf{k}_1',\mathbf{k}_2';\mathbf{0},-\mathbf{p};z)\end{aligned} \tag{5.20a}$$

As $\hat{P}^{(2)}(\mathbf{p},\mathbf{0};\mathbf{0},-\mathbf{p};0)=S_{\rho\rho}(\mathbf{p})$ (equation 5.17) we get

$$\begin{aligned}&(z+\frac{k_BT}{\Gamma}\mathbf{p}^2)\hat{P}^{(2)}(\mathbf{p},\mathbf{0};\mathbf{0},-\mathbf{p};z)\\&=S_{\rho\rho}(\mathbf{p})+(-\frac{1}{2\pi\Gamma})\int d^2p_1\mathbf{p}_1\cdot(\mathbf{p}+\mathbf{p}_1)\hat{V}(\mathbf{p}_1)\hat{P}^{(2)}(\mathbf{p}-\mathbf{p}_1,\mathbf{p}_1;\mathbf{0},-\mathbf{p};z)\end{aligned} \tag{5.20b}$$

The two particle distribution function, defined as $P^{(2)}(\mathbf{R}_1,\mathbf{R}_2;\mathbf{R}'_1,\mathbf{R}'_2;z) \equiv \int d\mathbf{R}_3 d\mathbf{R}_4.. \int d\mathbf{R}'_3 d\mathbf{R}'_4..P(\mathbf{R}_1,\mathbf{R}_2,\mathbf{R}_3..;\mathbf{R}'_1,\mathbf{R}'_2,\mathbf{R}'_3..;z)$, in real space, satisfies the following Fokker-Planck equation

$$(z+\frac{k_BT}{\Gamma}(\triangle_{\mathbf{R}_1}+\triangle_{\mathbf{R}_2}))P^{(2)}(\mathbf{R}_1,\mathbf{R}_2;\mathbf{R}'_1,\mathbf{R}'_2;z) = P^{(2)}(\mathbf{R}_1,\mathbf{R}_2;\mathbf{R}'_1,\mathbf{R}'_2;0)$$
$$+(-\frac{1}{2\pi\Gamma})\sum_{j=1}^{2}\nabla_j V(\mathbf{R}_1-\mathbf{R}_2)\cdot\nabla_j P^{(2)}(\mathbf{R}_1,\mathbf{R}_2;\mathbf{R}'_1,\mathbf{R}'_2;z) \quad (5.21)$$

Now consider the center of mass and relative coordinates of the two particles system to be $\mathbf{X}$ and $\mathbf{r}$ respectively which are defined in terms of the individual coordinates ($\mathbf{R}_1$ and $\mathbf{R}_2$) of the two paticles by the following relations

$$\mathbf{X}=\frac{1}{2}(\mathbf{R}_1+\mathbf{R}_2), \qquad \mathbf{r}=\mathbf{R}_1-\mathbf{R}_2 \quad (5.22)$$

So the two particle correlator, when they are in direct Coulomb interaction, follows the following Fokker-Planck equation in terms of the center of mass and relative coordinates

$$(z+\frac{k_BT}{\Gamma}(\frac{1}{2}\triangle_{\mathbf{X}}+2\triangle_{\mathbf{r}}))P^{(2)}(\mathbf{X},\mathbf{r};\mathbf{X}',\mathbf{r}';z) = P^{(2)}(\mathbf{X},\mathbf{r};\mathbf{X}',\mathbf{r}';0)$$
$$+(-\frac{1}{2\pi\Gamma})\sum_{j=1}^{2}\nabla_{\mathbf{r}j}V(\mathbf{r})\cdot\nabla_{\mathbf{r}j}P^{(2)}(\mathbf{X},\mathbf{r};\mathbf{X}',\mathbf{r}';z) \quad (5.23)$$

Correlator renormalisation

We show the derivation of two particle (particles 1, 2) correlator when particles 1 and 3 are in Coulomb interaction. This type of configuration adds a relaxation term in the correlator which will be clear from the following result. We use $n=1,\ n'=3$ in equation (5.15) which then takes the following form

$$(z+\frac{k_BT}{\Gamma}\mathbf{p}^2)\hat{P}(\mathbf{p},\mathbf{0},...;\mathbf{0},-\mathbf{p},...;z) = S_{\rho\rho}(\mathbf{p})$$
$$+(-\frac{1}{2\pi\Gamma})\int d^2k'_1\int d^2k'_3\int d^2p_1\mathbf{p}_1\cdot(\mathbf{p}+\mathbf{p}_1)\hat{V}(\mathbf{p}_1)\delta(\mathbf{k}'_1-\mathbf{p}+\mathbf{p}_1)\delta(\mathbf{k}'_3-\mathbf{0}-\mathbf{p}_1)$$
$$\int d^2k'_{r_1}\prod_{r_1\neq 1,3}^{N}\delta(\mathbf{k}_{r_1}-\mathbf{k}'_{r_1})\hat{P}(\{\mathbf{k}'\};\mathbf{0},-\mathbf{p},...;z)$$
$$= S_{\rho\rho}(\mathbf{p})+(-\frac{1}{2\pi\Gamma})\int d^2p_1\mathbf{p}_1\cdot(\mathbf{p}+\mathbf{p}_1)\hat{V}(\mathbf{p}_1)\hat{P}(\mathbf{p}-\mathbf{p}_1,\mathbf{0},\mathbf{p}_1,..;\mathbf{0},-\mathbf{p},..;z)$$
$$\approx S_{\rho\rho}(\mathbf{p})+(-\frac{1}{2\pi\Gamma})\int d^2p_1\mathbf{p}_1\cdot(\mathbf{p}+\mathbf{p}_1)\hat{V}(\mathbf{p}_1)\hat{P}(\mathbf{p}-\mathbf{p}_1,\mathbf{0};\mathbf{0},-\mathbf{p};z)n\delta(\mathbf{p}_1) \quad (5.24)$$

with n being the average background charge (vortex charge) density. Here we have used the following approximation

$$\hat{P}(\mathbf{p}_1,\mathbf{p}_2,\mathbf{p}_3;\mathbf{0},-\mathbf{p},...;z) \approx \hat{P}(\mathbf{p}_1,\mathbf{p}_2;\mathbf{0},-\mathbf{p};z)n\delta(\mathbf{p}_3) \quad (5.25)$$

Where from, after we have done the integration, we get for $p \to 0$

$$\hat{P}(\mathbf{p}, \mathbf{0}, ..; \mathbf{0}, -\mathbf{p}, ..; z) = \frac{S_{\rho\rho}(\mathbf{p})}{z + \frac{k_B T(\mathbf{p}^2 + \mathbf{p}_0^2)}{\Gamma}} \tag{5.26}$$

where $p_0^2 = \frac{n}{2\pi k_B T}$ is the square of the inverse Debye screening length of the Coulomb system (can be compared with equation (2.104) in chapter 2).

Screening of the Coulomb interaction

We now show the derivation of two particle (particles 1,2) correlator $\hat{P}(\mathbf{p}, \mathbf{0}, ...; \mathbf{0}, -\mathbf{p}, ...; z)$ in presence of a 3rd particle when particles 1, 3 and 3, 2 are in Coulomb interactions but there is no direct interaction between particles 1 and 2. We first consider in the interaction term the Coulomb interaction line between particles 1 and 3. We use $n = 1,\ n' = 3$ in equation (5.15) which then takes the following form

$$\begin{aligned}
&(z + \frac{k_B T}{\Gamma}\mathbf{p}^2)\hat{P}(\mathbf{p}, \mathbf{0}, ...; \mathbf{0}, -\mathbf{p}, ...; z) = S_{\rho\rho}(\mathbf{p}) \\
&+(-\frac{1}{2\pi\Gamma}) \int d^2k_1' \int d^2k_3' \int d^2p_1 \mathbf{p}_1 \cdot (\mathbf{p} + \mathbf{p}_1)\hat{V}(\mathbf{p}_1)\delta(\mathbf{k}_1' - \mathbf{p} + \mathbf{p}_1)\delta(\mathbf{k}_3' - \mathbf{0} - \mathbf{p}_1) \\
&\int d^2k_{r_1}' \prod_{r_1 \neq 1,3}^{N} \delta(\mathbf{k}_{r_1} - \mathbf{k}_{r_1}')\hat{P}(\{\mathbf{k}'\}; \mathbf{0}, -\mathbf{p}, ..; z) \\
&= S_{\rho\rho}(\mathbf{p}) + (-\frac{1}{2\pi\Gamma}) \int d^2p_1 \mathbf{p}_1 \cdot (\mathbf{p} + \mathbf{p}_1)\hat{V}(\mathbf{p}_1)\hat{P}(\mathbf{p} - \mathbf{p}_1, \mathbf{0}, \mathbf{p}_1, ..; \mathbf{0}, -\mathbf{p}, .; z)
\end{aligned} \tag{5.27}$$

Now considering the Coulomb interaction line between particles 3 and 2 for $\hat{P}(\mathbf{p} - \mathbf{p}_1, \mathbf{0}, \mathbf{p}_1, ..; \mathbf{0}, -\mathbf{p}, .; z)$ we get in the interaction term in the previous equation (use $n = 3,\ n' = 2$ and take the form in equation (5.15))

$$\begin{aligned}
&\hat{P}(\mathbf{p} - \mathbf{p}_1, \mathbf{0}, \mathbf{p}_1, ..; \mathbf{0}, -\mathbf{p}, .; z) = \frac{-\frac{1}{2\pi\Gamma}}{z + \frac{k_B T}{\Gamma}[(\mathbf{p} - \mathbf{p}_1)^2 + \mathbf{p}_1^2]} \\
&\int d^2k_3'' \int d^2k_2'' \int d^2p_2 \mathbf{p}_2 \cdot (\mathbf{p}_1 + \mathbf{p}_2)\hat{V}(\mathbf{p}_2)\delta(\mathbf{k}_3'' - \mathbf{p}_1 + \mathbf{p}_2)\delta(\mathbf{k}_2'' - \mathbf{0} - \mathbf{p}_2) \\
&\int d^2k_{r_2}'' \prod_{r_2 \neq 3,2}^{N} \delta(\mathbf{k}_{r_2} - \mathbf{k}_{r_2}'')\hat{P}(\{\mathbf{k}''\}; \mathbf{0}, -\mathbf{p}, ..; z)
\end{aligned} \tag{5.28}$$

Using the above relation (equation 5.28) in equation (5.27) we get

$$
\begin{aligned}
&(z+\frac{k_BT}{\Gamma}\mathbf{p}^2)\hat{P}(\mathbf{p},\mathbf{0},...;\mathbf{0},-\mathbf{p},...;z)\\
&=S_{\rho\rho}(\mathbf{p})+(-\frac{1}{2\pi\Gamma})\int d^2p_1\mathbf{p}_1\cdot(\mathbf{p}+\mathbf{p}_1)\hat{V}(\mathbf{p}_1)\frac{-\frac{1}{2\pi\Gamma}}{z+\frac{k_BT}{\Gamma}[(\mathbf{p}-\mathbf{p}_1)^2+\mathbf{p}_1^2]}\\
&\int d^2k_3''\int d^2k_2''\int d^2p_2\mathbf{p}_2\cdot(\mathbf{p}_1+\mathbf{p}_2)\hat{V}(\mathbf{p}_2)\delta(\mathbf{k}_3''-\mathbf{p}_1+\mathbf{p}_2)\delta(\mathbf{k}_2''-\mathbf{0}-\mathbf{p}_2)\\
&\int d^2k_{r_2}''\prod_{r_2\neq 3,2}^{N}\delta(\mathbf{k}_{r_2}-\mathbf{k}_{r_2}'')\hat{P}(\{\mathbf{k}''\};\mathbf{0},-\mathbf{p},..;z)\\
&=S_{\rho\rho}(\mathbf{p})+(-\frac{1}{2\pi\Gamma})^2\int d^2p_1d^2p_2\mathbf{p}_1\cdot(\mathbf{p}+\mathbf{p}_1)\mathbf{p}_2\cdot(\mathbf{p}_1+\mathbf{p}_2)\hat{V}(\mathbf{p}_1)\hat{V}(\mathbf{p}_2)\\
&\qquad\qquad\frac{\hat{P}(\mathbf{p}-\mathbf{p}_1,\mathbf{p}_2,\mathbf{p}_1-\mathbf{p}_2,\mathbf{0},...;\mathbf{0},-\mathbf{p},...;z)}{z+\frac{k_BT}{\Gamma}[(\mathbf{p}-\mathbf{p}_1)^2+\mathbf{p}_1^2]}
\end{aligned}
\tag{5.29}
$$

Using equation (5.25) we get from the above equation, for the limits of small $\mathbf{p}$ and z

$$
\begin{aligned}
&(z+\frac{k_BT}{\Gamma}\mathbf{p}^2)\hat{P}(\mathbf{p},\mathbf{0},...;\mathbf{0},-\mathbf{p},...;z)\\
&=S_{\rho\rho}(\mathbf{p})+(-\frac{1}{2\pi\Gamma})\int d^2p_1\mathbf{p}_1\cdot(\mathbf{p}+\mathbf{p}_1)\hat{V}(\mathbf{p}_1)(-\frac{\hat{V}(\mathbf{p}_1)}{2\pi k_BT})n\\
&\qquad\qquad\hat{P}(\mathbf{p}-\mathbf{p}_1,\mathbf{p}_1;\mathbf{0},-\mathbf{p};z)
\end{aligned}
\tag{5.30}
$$

This result is identical with the result in equation (5.20b) where particle no 1 has a direct Coulomb interaction with particle no 2. The only exception here is in the interaction term which appears as the interaction between particles 1 and 2 to be screened by the presence of 3rd particle which is the 1st order term in the expansion of the following screened potential (for the direct case of interaction in equation 5.20 the zero order term exists)

$$
\hat{V}_{sc}(\mathbf{p}_1)=\frac{\hat{V}(\mathbf{p}_1)}{1+\frac{\hat{V}(\mathbf{p}_1)}{2\pi k_BT}n}\approx\hat{V}(\mathbf{p}_1)(1-\frac{\hat{V}(\mathbf{p}_1)}{2\pi k_BT}n+...)
\tag{5.31}
$$

Similarly in place of 3rd particle if we have more particles like e.g., another 4th particle connects the 3rd and 2nd particles through Coulomb interactions their collective effect will be just to modify the interaction term in equation (5.30) which will be the 2nd order term of equation (5.31). Similarly the presence of 5th, 6th, etc. particles will replace the interaction term by 3rd, 4th, etc. order terms of equation (5.31).

Friction function

We now show the derivation of two particle (particles 1, 2) correlator $\hat{P}(\mathbf{p},\mathbf{0},...;\mathbf{0},-\mathbf{p},...;z)$ in presence of 3rd and 4th particles when particles 1, 3 and 1, 4

are in Coulomb interactions but there is no direct interaction between particles 3 and 4 (but they are correlated). This type of correlation gives us the friction function. Using the Fokker-Planck equation (equation 5.15 where we have to use $n = 1,\ n' = 3$ in the 1st interaction line and $n = 1,\ n' = 4$ in the 2nd interaction line) we get

$$\begin{aligned}
&(z + \frac{k_BT}{\Gamma}\mathbf{p}^2)\hat{P}(\mathbf{p}, \mathbf{0}, ...; \mathbf{0}, -\mathbf{p}, ...; z) \\
&= S_{\rho\rho}(\mathbf{p}) + (-\frac{1}{2\pi\Gamma}) \int d^2p_1 \mathbf{p}_1^2 \hat{V}(\mathbf{p}_1) \frac{-\frac{1}{2\pi\Gamma}}{z + \frac{k_BT}{\Gamma}[(\mathbf{p} + \mathbf{p}_1)^2 + \mathbf{p}_1^2]} \\
&\int d^2p_2 \mathbf{p}_2^2 \hat{V}(\mathbf{p}_2) \hat{P}(\mathbf{p} + \mathbf{p}_1 + \mathbf{p}_2, \mathbf{0}, -\mathbf{p}_1, -\mathbf{p}_2, \mathbf{0}, ...; \mathbf{0}, -\mathbf{p}, ...; z) \qquad (5.32)
\end{aligned}$$

We can write $\hat{P}(\mathbf{p} + \mathbf{p}_1 + \mathbf{p}_2, \mathbf{0}, -\mathbf{p}_1, -\mathbf{p}_2, ...; \mathbf{0}, -\mathbf{p}, ...; z) \approx$
$\hat{P}(\mathbf{p} + \mathbf{p}_1 + \mathbf{p}_2, \mathbf{0}, ...; \mathbf{0}, -\mathbf{p}, ...; z)\hat{P}(\mathbf{0}, \mathbf{0}, -\mathbf{p}_1, -\mathbf{p}_2, ...; \mathbf{0}, -\mathbf{p}, ...; z)$
with $\hat{P}(\mathbf{0}, \mathbf{0}, -\mathbf{p}_1, -\mathbf{p}_2, ...; \mathbf{0}, -\mathbf{p}, ...; z) \approx n\delta(\mathbf{p}_1 + \mathbf{p}_2)\hat{P}(\mathbf{0}, \mathbf{0}, -\mathbf{p}_1, \mathbf{p}_1, ...; \mathbf{0}, -\mathbf{p}, ...; z)$.
We can now easily do the integration over p_2 using the delta function in the above equation and get

$$\hat{P}(\mathbf{p}, \mathbf{0}, ...; \mathbf{0}, -\mathbf{p}, ...; z) = \frac{S_{\rho\rho}(\mathbf{p})}{z + \frac{k_BT}{\Gamma + \gamma(z)}\mathbf{p}^2} \qquad (5.33a)$$

with

$$\gamma(z) \approx \Gamma[(\frac{1}{2\pi})^2 \frac{n}{k_BT\mathbf{p}^2} \int d^2p_1 p_1^4 \hat{V}(\mathbf{p}_1)^2 \frac{\hat{P}(\mathbf{0}, \mathbf{0}, -\mathbf{p}_1, \mathbf{p}_1, ..; \mathbf{0}, -\mathbf{p}, ..; z)}{z\Gamma + k_BT[(\mathbf{p} + \mathbf{p}_1)^2 + \mathbf{p}_1^2]}] \qquad (5.33b)$$

It means the bare friction Γ is replaced by modified friction function $\Gamma + \gamma(z)$ where $\gamma(z)$, the frequency dependent friction function comes through the interaction terms in equation (5.32).

Considering both the friction function (equation 5.33) and Debye screening (equation 5.26) together the two particle correlator takes the following general form

$$\hat{P}(\mathbf{p}, \mathbf{0}, ...; \mathbf{0}, -\mathbf{p}, ...; z) = \frac{S_{\rho\rho}(\mathbf{p})}{z + \frac{k_BT}{\Gamma + \gamma(z)}(\mathbf{p}^2 + \mathbf{p}_0^2)} \qquad (5.34)$$

Resulting equation for two-particle correlator

Finally we present the general form of the two particle correlator in screened Coulomb interaction (similar like equation 5.21 but with modified friction and interaction terms), in real space, as follows

$$\begin{aligned}
&(z + \frac{k_BT}{\Gamma + \gamma(z)}(\triangle_{\mathbf{R}_1} + \triangle_{\mathbf{R}_2} + \mathbf{p}_0^2))P^{(2)}(\mathbf{R}_1, \mathbf{R}_2; \mathbf{R}_1', \mathbf{R}_2'; z) = P^{(2)}(\mathbf{R}_1, \mathbf{R}_2; \mathbf{R}_1', \mathbf{R}_2'; 0) \\
&+(-\frac{1}{2\pi\Gamma}) \sum_{j=1}^{2} \nabla_j V_{sc}(\mathbf{R}_1 - \mathbf{R}_2) \cdot \nabla_j P^{(2)}(\mathbf{R}_1, \mathbf{R}_2; \mathbf{R}_1', \mathbf{R}_2'; z) \qquad (5.35)
\end{aligned}$$

where $V_{sc}(\mathbf{R}_1 - \mathbf{R}_2)$ is the screened Coulomb interaction between particles 1 and 2. $\mathbf{p}_0^2$ is the square of the inverse Debye screening length. The initial distribution function can be expressed like

$$P^{(2)}(\mathbf{R}_1, \mathbf{R}_2; \mathbf{R}_1', \mathbf{R}_2'; t = 0) = \delta(\mathbf{R}_1 - \mathbf{R}_1')\delta(\mathbf{R}_2 - \mathbf{R}_2')g(\mathbf{R}_1 - \mathbf{R}_2) \tag{5.36}$$

with $g(\mathbf{R}_1 - \mathbf{R}_2)$ is the radial distribution function.

Two situations arises:

(a) $|\mathbf{R}_1 - \mathbf{R}_2| > \xi_{BKT}$; the vortices are *free* at $t = 0$. In this case the solution follows from equation (5.10) excluding the interaction term.

(b) $|\mathbf{R}_1 - \mathbf{R}_2| < \xi_{BKT}$; the vortices are *paired* at $t = 0$. In this case we neglect $\gamma(z)$ and Hartree type screening ($p_0^2 = \frac{n}{2\pi k_B T}$) but consider the direct screened Coulomb interaction. We shall explain further details of the vortex antivortex pair dynamics later in this chapter.

Here ξ_{BKT} is the temperature dependent correlation length of a vortex-antivortex pair which diverges ($\xi_{BKT} \to \infty$) at T_{BKT}.

5.1.2 Fokker-Planck equation for vortex dynamics in JJAs when vortices and antivortices are considered to be massive particles

Generalized Fokker-Planck probability distribution function P for vortex dynamics in JJAs when vortices and antivortices are considered to be massive particles follow [59]

$$\frac{\partial P}{\partial t} = -(\mathbf{v}\frac{\partial}{\partial \mathbf{r}} + \frac{1}{M}\frac{\partial}{\partial \mathbf{v}}\mathbf{F})P + \frac{D}{M}\frac{\partial^2 P}{\partial \mathbf{v}^2} \tag{5.37}$$

where M is the mass of a particle (vortex or antivortex), $\mathbf{v}$ is the velocity of the particle, D is the Einstein's diffusion constant and $\mathbf{F}$ is the force on the particle in a vortex gas. The expression for the force is

$$\mathbf{F} = M\frac{\partial \mathbf{v}}{\partial t} = -(\frac{\partial V}{\partial \mathbf{r}} + \Gamma\mathbf{v}) \tag{5.38a}$$

Here V is the Coulomb interaction on a particular vortex/antivortex due to other vortices and antivortices in the vicinity and Γ is the friction. The force on ith vortex or antivortex due to other l particles is [29]

$$\mathbf{F}_i(l) = M\frac{\partial \mathbf{v}_i(l)}{\partial t} = -(\nabla_i \sum_{l'} V(\mathbf{R}_l - \mathbf{R}_{l'}) + \Gamma\mathbf{v}_i(l)) \tag{5.38b}$$

The diffusion term in our system is

$$\frac{D}{M}\frac{\partial^2 P}{\partial \mathbf{v}^2} = \frac{k_B T}{\Gamma M}\frac{\partial^2 P}{\partial \mathbf{v}^2} \tag{5.39}$$

The Fokker-Planck equation, in the case of massive vortices, takes the following form

$$\begin{aligned}\frac{\partial}{\partial t}P(\{\mathbf{R}\},\{\mathbf{v}\};t) = \quad & -\sum_{il}(\mathbf{v}_i(l)\frac{\partial}{\partial \mathbf{R}_i(l)} - \frac{1}{M}\sum_{l'}\nabla V(\mathbf{R}_l - \mathbf{R}_{l'})\cdot\frac{\partial}{\partial \mathbf{v}_i(l)} \\ & -\frac{\Gamma}{M}\frac{\partial}{\partial \mathbf{v}_i(l)}\mathbf{v}_i(l) - \frac{D}{M}\frac{\partial^2}{\partial \mathbf{v}_i(l)^2})P(\{\mathbf{R}\},\{\mathbf{v}\};t)\end{aligned} \tag{5.40}$$

In Fourier space the above Fokker-Planck equation takes the following form

$$\begin{aligned}\frac{\partial}{\partial t}P(\{\mathbf{k}\},\{\mathbf{v}\};t) &= -\sum_{jn} v_j(n)(ik_{jn})P(\{\mathbf{k}\},\{\mathbf{v}\};t) \\ &+\int d^N k'' \int d^2p \frac{1}{M}\sum_{jnn'}(i\mathbf{p}_{1j})\hat{V}(\mathbf{p}_1)\chi_{nn'}(\{\mathbf{k}\},\{\mathbf{k}''\})\frac{\partial}{\partial v_j(n)}P(\{\mathbf{k}''\},\{\mathbf{v}\};t) \\ &+\frac{\Gamma}{M}\sum_{jn}\frac{\partial}{\partial v_j(n)}(v_j(n)P(\{\mathbf{k}\},\{\mathbf{v}\};t)) \\ &+\frac{D}{M}\sum_{jn}\frac{\partial^2}{\partial v_j(n)^2}P(\{\mathbf{k}\},\{\mathbf{v}\};t) \qquad (5.41)\end{aligned}$$

where $\chi_{nn'}(\{\mathbf{k}\},\{\mathbf{k}''\})$ follows from equation (5.12) and $\hat{V}(\mathbf{p})$ follows from equation (5.18).

Using the Laplace transformation the Fokker-Planck equation takes the following form

$$\begin{aligned}(z+\sum_{jn}(v_j(n)(ik_{jn}) - \frac{\Gamma}{M}\frac{\partial}{\partial v_j(n)}v_j(n) - \frac{D}{M}\frac{\partial^2}{\partial v_j(n)^2}))\hat{P}(\{\mathbf{k}\},\{\mathbf{v}\};z) &= \hat{P}(\{\mathbf{k}\},\{\mathbf{v}\};0) \\ +\int d^N k'' \int d^2p_1 \frac{1}{M}\sum_{jnn'}(i\mathbf{p}_{1j})\hat{V}(\mathbf{p}_1)\chi_{nn'}(\{\mathbf{k}\},\{\mathbf{k}''\})\frac{\partial}{\partial v_j(n)}\hat{P}(\{\mathbf{k}''\},\{\mathbf{v}\};z) \qquad (5.42)\end{aligned}$$

Using the above Fokker-Planck equation we can repeat the calculation for different interaction lines and get screening, friction etc. terms (similar to the case of overdamped limit or massless vortex) for the vortex dynamics where vortices and antivortices are considered to be massive particles.

5.1.3 Massive vortex antivortex pair dynamics

Let us now consider $P^{(2)}(\mathbf{R}_1,\mathbf{R}_2,\mathbf{v}_1,\mathbf{v}_2;t)$ to be the conditional reduced distribution function for pair dynamics. We can then define some function

$$\phi(\mathbf{R}_1,\mathbf{R}_2;t) \equiv \int dR_1' \int dR_2' \int dv_1 \int dv_2 \int dv_1' \int dv_2' P^{(2)}(\mathbf{R}_1,\mathbf{R}_2,\mathbf{v}_1,\mathbf{v}_2;t) \qquad (5.43)$$

Now the continuity equation for equal time heterocorrelator $\phi(\mathbf{R}_1,\mathbf{R}_2;t)$ is

$$\frac{\partial\phi(\mathbf{R}_1,\mathbf{R}_2;t)}{\partial t} = -\sum_{l=1}^{2}\frac{\partial}{\partial\mathbf{R}_l}\mathbf{J}(\mathbf{R}_1,\mathbf{R}_2;t) \qquad (5.44)$$

$$with \qquad \mathbf{J}(\mathbf{R}_1,\mathbf{R}_2;t) = \int dv_1 dv_2 \mathbf{v}_l P^{(2)} \qquad (5.45)$$

is the vortex current density. From this definition of $\mathbf{J}$ and using the Fokker-Planck equation (5.40) we get

$$\frac{\partial}{\partial t}\mathbf{J}(\mathbf{R}_1,\mathbf{R}_2;t) = -\sum_{l,l'=1}^{2}\int dv_1 dv_2 \mathbf{v}_l \frac{\partial}{\partial \mathbf{R}_{l'}}\mathbf{J}(\mathbf{R}_1,\mathbf{R}_2;t) - \frac{\Gamma}{M}\mathbf{J}(\mathbf{R}_1,\mathbf{R}_2;t) + \frac{1}{M}\sum_{l=1}^{2}\frac{\partial}{\partial \mathbf{R}_l}V(\mathbf{R}_1-\mathbf{R}_2)\phi(\mathbf{R}_1,\mathbf{R}_2;t) \tag{5.46}$$

We have the first term in the right hand side of the above equation as $\frac{\partial}{\partial t}\mathbf{J}(\mathbf{R}_1,\mathbf{R}_2;t)$ as follows

$$-\sum_{l,l'=1}^{2}\int dv_1 dv_2 \mathbf{v}_l \frac{\partial}{\partial \mathbf{R}_{l'}}\mathbf{J}(\mathbf{R}_1,\mathbf{R}_2;t) = -\sum_{l,l'=1}^{2}\int dv_1 dv_2 \mathbf{v}_l\mathbf{v}_{l'} \frac{\partial}{\partial \mathbf{R}_{l'}}\phi(\mathbf{R}_1,\mathbf{R}_2;t) \tag{5.47}$$

We know in a thermodynamic system

$$\langle \mathbf{v}_l \mathbf{v}_{l'}\rangle \approx \delta_{ll'}\frac{k_B T}{M} \tag{5.48}$$

Using this relation we get the full form approximate as

$$\frac{\partial}{\partial t}\mathbf{J}(\mathbf{R}_1,\mathbf{R}_2;t) = -\frac{k_B T}{M}\sum_{l=1}^{2}\frac{\partial}{\partial \mathbf{R}_l}\phi(\mathbf{R}_1,\mathbf{R}_2;t) - \frac{\Gamma}{M}\mathbf{J}(\mathbf{R}_1,\mathbf{R}_2;t) + \frac{1}{M}\sum_{l=1}^{2}\frac{\partial}{\partial \mathbf{R}_l}V(\mathbf{R}_1-\mathbf{R}_2)\phi(\mathbf{R}_1,\mathbf{R}_2;t) \tag{5.49}$$

where the diffusive term (last term in the right hand side of equation 5.40) is lost for the boundary condition consideration.

5.1.4 Vortex antivortex pair dynamics in one dimension

We shall now treat the dynamics of a single vortex antivortex pair in one dimension. In this case we impose the following condition on the interaction

$$V(\mathbf{R}_1-\mathbf{R}_2) = \begin{cases} \infty & \text{for } |\mathbf{R}_1-\mathbf{R}_2| \searrow r_0 \ (\textit{hard core}) \\ -F_0|\mathbf{R}_1-\mathbf{R}_2| & \text{for } r_0 < |\mathbf{R}_1-\mathbf{R}_2| < \xi \\ 0 & \text{for } |\mathbf{R}_1-\mathbf{R}_2| \geq \xi \end{cases} \tag{5.50}$$

where ξ is the KT correlation length of a vortex antivortex (VA) pair. Considering $\mathbf{R}_1-\mathbf{R}_2=\mathbf{r}$ and letting the force between the particles (V, A) to be $\mathbf{F}(\mathbf{r}) = -\nabla_r V(\mathbf{r})$ we get the following form for the force

$$F(\mathbf{r}) = \begin{cases} \infty & \text{for } |\mathbf{r}| < r_0 \\ F_0 & \text{for } r_0 < |\mathbf{r}| < \xi \\ 0 & \text{for } |\mathbf{r}| \geq \xi \end{cases} \tag{5.51}$$

Here F_0 is considered to be some constant value for the force at $r_0 < |\mathbf{r}| < \xi$ (inside the potential well) in our assumption. Using the above boundary conditions we get the following identities

$$\begin{aligned} J(r_0) = 0 \; at \; r = r_0 \\ \phi \; and \; J \; are \; continuous \; at \; r = \xi \\ J \to 0 \; at \; r \to \infty \end{aligned} \tag{5.52}$$

In the case of relative motion we can rewrite equations (5.45) and (5.49) in the following ways (without considering the vector notations for one dimensional motion)

$$\frac{\partial \phi(r;t)}{\partial t} = -\frac{\partial J(r;t)}{\partial r} \tag{5.53a}$$

$$\frac{\partial J(r;t)}{\partial r} = -\frac{k_B T}{M}\frac{\partial \phi(r;t)}{\partial r} - \frac{\Gamma}{M} J(r;t) + \frac{1}{M}\frac{\partial V(r)}{\partial r}\phi(r;t) \tag{5.53b}$$

which gives the following (matrix) eigen value equation (ϕ and J are eigen function with corresponding eigen value E)

$$\begin{pmatrix} 0 & -\frac{\partial}{\partial r} \\ -\frac{k_B T}{M}\frac{\partial}{\partial r} + \frac{1}{M}F(r) & -\frac{\Gamma}{M} \end{pmatrix} \begin{pmatrix} \phi \\ J \end{pmatrix} = E \begin{pmatrix} \phi \\ J \end{pmatrix} \tag{5.54}$$

where E is the eigen value.

Check

For $F = 0$ we know $\phi,\ J \sim e^{ikr}$, that is plane wave form, k is the wave number. So the eigen values follow from

$$det \begin{pmatrix} -E & -ik \\ -ik\frac{k_B T}{M} & -\frac{\Gamma}{M} - E \end{pmatrix} = 0 \tag{5.55}$$

Where from we get

$$E(E + \frac{\Gamma}{M}) - k^2 \frac{k_B T}{M} = 0 \tag{5.56}$$

For $M \to 0$; $\quad E = k^2 \frac{k_B T}{\Gamma}$.

For $M > 0$; $\quad E = \frac{1}{2}(-\frac{\Gamma}{M} \pm \sqrt{(\frac{\Gamma}{M})^2 + 4k^2\frac{k_B T}{M}})$

Adjoint operator

We now introduce the scalar product $(\psi_1, \psi_2) = \int dr \psi_1^* \psi_2$ of two wave functions

$$\psi_1 = \begin{pmatrix} \phi_1 \\ J_1 \end{pmatrix} \qquad and \qquad \psi_2 = (\phi_2, J_2) \tag{5.57}$$

L is the operator which follows

$$L\psi_1 = \begin{pmatrix} -\frac{\partial J_1}{\partial r} \\ -\frac{k_B T}{M}\frac{\partial \phi_1}{\partial r} + f(r)\phi_1 - \frac{\Gamma}{M} J_1 \end{pmatrix} \tag{5.58}$$

where $f(r) = \frac{F(r)}{M}$ is the force constant. In order to define the adjoint operator L^+ we start from

$$(\psi_2, L\psi_1) = \int_{r_0}^{\xi} dr(-\phi_2 \frac{\partial J_1}{\partial r} + J_2(-\alpha \frac{\partial \phi_1}{\partial r} + f\phi_1 - \gamma J_1)) \tag{5.59}$$

where, for simplicity, we have assumed $\alpha = \frac{k_B T}{M}$ and $\gamma = \frac{\Gamma}{M}$.

We now use the following partial integrations

$$\int_{r_0}^{\xi} dr\phi_2(r)\frac{\partial J_1}{\partial r} = \phi_2(r)J_1(r)|_{r_0}^{\xi} - \int_{r_0}^{\xi} dr\frac{\partial \phi_2}{\partial r}J_1 \tag{5.60a}$$

$$\int_{r_0}^{\xi} dr J_2(r)\frac{\partial \phi_1}{\partial r} = J_2(r)\phi_1(r)|_{r_0}^{\xi} - \int_{r_0}^{\xi} dr\frac{\partial J_2}{\partial r}\phi_1 \tag{5.60b}$$

Now consider that there are no currents across the boundaries ,i.e., $J(r_0) = 0$. This gives

$$\begin{aligned}(\psi_2, L\psi_1) &= \int_{r_0}^{\xi} dr(\alpha\frac{\partial J_2}{\partial r} + fJ_2\phi_1 - \gamma J_2 J_1 + \frac{\partial \phi_2}{\partial r}J_1) \\ &\equiv (L^+\psi_2, \psi_1) = \sum_j (L^+\psi_2)_j \psi_{1j} = (L^+\psi_2)_1\phi_1 + (L^+\psi_2)_2 J_1\end{aligned} \tag{5.61}$$

This implies that

$$(L^+\psi_2)_1 = \alpha\frac{\partial J_2}{\partial r} + fJ_2; \qquad (L^+\psi_2)_2 = -\gamma J_2 + \frac{\partial \phi_2}{\partial r} \tag{5.62}$$

Now we get

$$L^+ = \begin{pmatrix} 0 & \alpha\frac{\partial}{\partial r} + f \\ \frac{\partial}{\partial r} & -\gamma \end{pmatrix} \qquad and \qquad L = \begin{pmatrix} 0 & -\frac{\partial}{\partial r} \\ -\alpha\frac{\partial}{\partial r} + f & -\gamma \end{pmatrix} \tag{5.63}$$

We now come back to check the case for finite and constant force $F = F_0$ (the force constant $f = f_0 = \frac{F_0}{M}$ is also constant). We get (similar to equation (5.55) and (5.56))

$$(\gamma + E)E + ik(f_0 - ik\alpha) = 0; \qquad k = (k_1, k_2) \tag{5.64}$$

Which satisfies the following relation

$$k^2\alpha - ikf_0 - c = 0 \tag{5.65a}$$

with solution

$$k = \frac{1}{2\alpha}\{+if_0 \pm \sqrt{-f_0^2 + 4\alpha c}\} \tag{5.65b}$$

where $c = (\gamma + E)E$.

Limit

(a) $F_0 \to 0; \qquad k = \pm\sqrt{c/\alpha}$

(b) $M \to 0 \qquad k = \frac{M}{2\alpha_0}\{+i\frac{F_0}{M} \pm \sqrt{-\frac{F_0^2}{M^2} + \frac{4\alpha_0 E(ME+\gamma)}{M^2}}\} = \frac{1}{2\alpha_0}\{+iF_0 \pm \sqrt{-F_0^2 + 4\alpha_0 E\gamma}\}$
where $\alpha_0 = \alpha M = k_B T$.

Solution - Hard Core and with plane waves beyond hard core

We shall now develop the general forms for the space dependent part of density ϕ and current $\mathbf{J}$ which, in the case of one dimensional problem (motion), considering that beyond the hard core there is no interaction (beyond the hard core in equation 5.50 the interaction is zero) and according to our boundary conditions (equation 5.52), follow

$$\begin{pmatrix} \phi(r) \\ J(r) \end{pmatrix} = \begin{pmatrix} \alpha_1 \\ \beta_1 \end{pmatrix} e^{ik_1 r} + \begin{pmatrix} \alpha_2 \\ \beta_2 \end{pmatrix} e^{ik_2 r} \tag{5.66}$$

where in plane wave forms ($V = 0$) α_1, α_2 and β_1, β_2 follow from the boundary condition (equation 5.52) and other conditions (equations 5.50 and 5.51).

Here we mention that the full form (time dependent) for the probability density function will follow [59] the following equation

$$P(r, r'; t) = \sum_n c_n(t) y_n(r) y_n^+(r') = \sum_n c_n e^{-E_n t} y_n(r) y_n^+(r') \tag{5.67}$$

where E_n is the nth energy eigen value and $y_n(r) = \phi(r)$ is the eigen function from equation (5.66) and previously in equation (5.54).

We now use the relation in equation (5.66) in equation (5.54) and with rearrangement we get for $F = 0$

$$\begin{pmatrix} -E & -ik_{1,2} \\ -i\frac{k_B T}{M} k_{1,2} & -\frac{\Gamma}{M} - E \end{pmatrix} \begin{pmatrix} \alpha_{1,2} e^{ik_{1,2} r} \\ \beta_{1,2} e^{ik_{1,2} r} \end{pmatrix} = \begin{pmatrix} 0 \\ 0 \end{pmatrix} = C_{1,2} \begin{pmatrix} \alpha_{1,2} e^{ik_{1,2} r} \\ \beta_{1,2} e^{ik_{1,2} r} \end{pmatrix} \tag{5.68}$$

From the above equation we get the following relations

$$det\ C_{1,2} = 0 \quad => \qquad E(\frac{\Gamma}{M} + E) + k_{1,2}^2 \frac{k_B T}{M} = 0 \tag{5.69a}$$

$$E\alpha_{1,2} - ik_{1,2}\beta_{1,2} = 0 \tag{5.69b}$$

$$-i\frac{k_B T}{M} k_{1,2} \alpha_{1,2} - (\frac{\Gamma}{M} + E)\beta_{1,2} = 0 \tag{5.69c}$$

With the consideration of the boundary conditions in equation (5.52) we reach at the following relations

$$\alpha_1 = -\frac{ik_1}{E}\beta_1 \qquad and \qquad \alpha_2 = -\frac{ik_2}{E}\beta_2 = \frac{ik_1}{E}\beta_2 = -\frac{ik_1}{E} e^{2ir_0 k_1} \beta_1 \tag{5.70a}$$

where we have used $k_2 = -k_1$ and (from the consideration that below the hard core $r < r_0$ there is no current)

$$\beta_2 = -\beta_1 e^{2ir_0 k_1} \tag{5.70b}$$

Using these relations we can finally replace equation (5.66) by the following relations

$$\phi(r; t) = (-\frac{ik_1\beta_1}{E}(e^{ik_1 r} + e^{ik_1(2r_0 - r)}))e^{-Et} \tag{5.71a}$$

$$J(r;t) = \beta_1(e^{ik_1 r} - e^{ik_1(2r_0 - r)}))e^{-Et} \tag{5.71b}$$

with $k_1 = \sqrt{(\frac{\Gamma}{M} + E)(-\frac{ME}{k_B T})} = k_1(E)$.

Now the conditional probability and current distribution functions are defined in the following ways (integrating over all energy eigen values for $E \in (0, \infty)$)

$$\phi(r, r'; t) \propto \int_0^\infty dE \phi(r;t)\phi^+(r';0)$$
$$= \int_0^\infty dE C_1(E)(\alpha_1 e^{ik_1(E)r} + \alpha_2 e^{-ik_1(E)r})(\alpha_1^+ e^{-ik_1(E)r'} + \alpha_2^+ e^{ik_1(E)r'})e^{-E(t-0)} \tag{5.72a}$$

$$\phi(r, r'; 0) = (\frac{2\Gamma}{k_B T}) \int_{-\infty}^\infty dk C_2(k) \frac{1}{k} e^{ik(r+r')} + (\frac{2\Gamma}{k_B T}) \int_{-\infty}^\infty dk C_2(k) \frac{1}{k} e^{-ik(r-r')}$$
$$+(\frac{2\Gamma}{k_B T}) \int_{-\infty}^\infty dk C_2(k) \frac{1}{k} e^{ik(r+r'-2r_0)} + (\frac{2\Gamma}{k_B T}) \int_{-\infty}^\infty dk C_2(k) \frac{1}{k} e^{-ik(r+r'-2r_0)} \tag{5.72b}$$

with $C_2(k) = C_1(k)\beta_1^2(k)$ and here we have replaced the integration over the enrgy E by the wave number k as they are related linearly ($dE = 2\frac{k_B T}{\Gamma} k dk$ as $E(k_1) = \frac{k_B T}{\Gamma} k_1^2$ and $E(k_2) = \frac{k_B T}{\Gamma} k_2^2$).

Here we want the image probability density

$$\phi(r, r'; 0) = \frac{1}{2}\delta(r - r') + \frac{1}{2}\delta(r + r' - 2r_0) \tag{5.73}$$

We can at this point consider the time evolution of the density correlator by the following relation [59]

$$\phi(r, r'; t) = \int_{-\infty}^\infty dk e^{ik(r-r')} e^{-Et} C(k) \tag{5.74}$$

where

$$if \quad C(k) \text{ is some constant or } 1 \quad we\ get \quad \phi(r, r'; 0) = 2\pi\delta(r - r') \tag{5.75}$$

From the above arguments and calculations we get
$C(k) = \frac{1}{4}(\frac{k_B T}{2\Gamma})\frac{k_1}{2\pi} = \frac{k_B T}{16\pi\Gamma} k_1 = \frac{k_B T}{16\pi\Gamma}\sqrt{\frac{\Gamma E}{k_B T}} \Rightarrow C_2(E) = \sqrt{\frac{k_B T}{\Gamma}}\frac{1}{16\pi}\sqrt{E}$. So finally we get by the final form of the density correlator (derived from equation 5.76a)

$$\phi(r, r'; t) = \frac{1}{16}\sqrt{\frac{\Gamma}{k_B T \pi t}}(e^{-\frac{\Gamma(r-r')^2}{4k_B T t}} + e^{-\frac{\Gamma(r'-r)^2}{4k_B T t}} + e^{-\frac{\Gamma(r+r'-2r_0)^2}{4k_B T t}} + e^{-\frac{\Gamma(2r_0-r-r')^2}{4k_B T t}}) \tag{5.76}$$

For the current density we use the similar procedures and get

$$J(r, r'; t) \propto \int_0^\infty dE J(r;t) J^+(r';0)$$
$$= \beta_1^2 \int_0^\infty dE e^{ik_1(E)(r-r')} e^{-Et} + \beta_1^2 \int_0^\infty dE e^{-ik_1(E)(r-r')} e^{-Et}$$
$$-\beta_1^2 \int_0^\infty dE e^{ik_1(E)(r+r'-2r_0)} e^{-Et} - \beta_1^2 \int_0^\infty dE e^{-ik_1(E)(r+r'-2r_0)} e^{-Et} \tag{5.77a}$$

which results for

$$J(r,r';t) = \frac{\beta_1^2}{2}\sqrt{\frac{\pi\Gamma}{k_BTt^3}}((r-r')e^{-\frac{\Gamma(r-r')^2}{4k_BTt}} + (r'-r)e^{-\frac{\Gamma(r'-r)^2}{4k_BTt}} - (r+r'-2r_0)e^{-\frac{\Gamma(r+r'-2r_0)^2}{4k_BTt}} - (2r_0-r-r')e^{-\frac{\Gamma(2r_0-r-r')^2}{4k_BTt}}) \quad (5.77b)$$

Solution - Hard Core and screened interaction beyond hard core

We consider now the forms for the space dependent part of density ϕ and current $\mathbf{J}$ which, in the case of one dimensional problem (motion), considering that beyond the hard core there is screened Coulomb interaction (equation 5.50) between the particles and following our boundary conditions (equation 5.52) we propose the forms to be

$$\begin{pmatrix} \phi^{<\xi}(r) \\ J^{<\xi}(r) \end{pmatrix} = \begin{pmatrix} \alpha_1' \\ \beta_1' \end{pmatrix} e^{ik_1'r} + \begin{pmatrix} \alpha_2' \\ \beta_2' \end{pmatrix} e^{ik_2'r} \quad (5.78)$$

where inside the potential (equation 5.50) α_1', α_2' and β_1', β_2' follow from the boundary conditions (equations 5.50, 5.51 and 5.52, 5.54). Using the similar procedures as in the case of hard core and beyond hard core there is plane wave (V=0) we get the some relations for the case of finite force F (equation 5.51) as follows

$$\beta_2' = -\beta_1' e^{i(k_1'-k_2')r_0} = -\beta_1' e^{2ir_0\sqrt{-(\frac{F_0}{k_BT})^2 - \frac{ME}{k_BT}(\frac{\Gamma}{M}+E)}} \quad (5.79)$$

Using equation (5.78) in equation (5.54) we get

$$-i\frac{k_BT}{M}k_{1,2}'\alpha_{1,2}' - k_{1,2}'^2\frac{k_BT}{ME}\beta_{1,2}' = -i\frac{k_BT}{M}k_{1,2}'\alpha_{1,2}' + (\frac{\Gamma}{M}+E)\beta_{1,2}'$$

$$+(2(\frac{F_0}{k_BT})^2\beta_{1,2}' \pm \sqrt{-(\frac{F_0}{k_BT})^2 - (\frac{ME}{k_BT})(\frac{\Gamma}{M}+E)}\beta_{1,2}'\frac{2F_0}{k_BT})\frac{k_BT}{ME} = -\frac{2F_0}{M}\alpha_{1,2}' \quad (5.80)$$

Now $-\frac{2F_0}{M}\alpha_{1,2}' + \beta_{1,2}'ik_{1,2}'\frac{2F_0}{ME} = 0 \Rightarrow -\frac{2F_0}{M}\alpha_{1,2}' = -ik_{1,2}'\frac{2F_0}{ME}\beta_{1,2}' = \frac{2F_0i}{ME}\beta_{1,2}'(\frac{-iF_0}{k_BT} \pm \sqrt{-(\frac{F_0}{k_BT})^2 - (\frac{ME}{k_BT})(\frac{\Gamma}{M}+E)})$

or, $-\frac{2F_0}{M}\alpha_{1,2}' = (-\frac{2F_0^2}{MEk_BT} \mp \frac{2F_0i}{ME}\sqrt{-(\frac{F_0}{k_BT})^2 - (\frac{ME}{k_BT})(\frac{\Gamma}{M}+E)})\beta_{1,2}'$

So we get the relation between $\alpha_{1,2}'$ and $\beta_{1,2}'$ equivalent to that of $\alpha_{1,2}$ and $\beta_{1,2}$ that is

$$\alpha_1' = \frac{ik_1'}{E}\beta_1', \qquad \alpha_2' = \frac{ik_2'}{E}\beta_2' \qquad \Rightarrow \alpha_2' = -\frac{ik_2'}{E}\beta_1' e^{2ir_0\sqrt{-(\frac{F_0}{k_BT})^2 - (\frac{ME}{k_BT})(\frac{\Gamma}{M}+E)}} \quad (5.81)$$

Solution - beyond screened interaction region

Now beyond the interaction region where $F_0 = 0$ we consider now the forms for the space dependent part of density ϕ and current $\mathbf{J}$ to be of the following forms

$$\begin{pmatrix} \phi^{>\xi}(r) \\ J^{>\xi}(r) \end{pmatrix} = \begin{pmatrix} \alpha_1'' \\ \beta_1'' \end{pmatrix} e^{ik_1r} + \begin{pmatrix} \alpha_2'' \\ \beta_2'' \end{pmatrix} e^{ik_2r} \quad (5.82)$$

where we get

$$\alpha_1'' = \frac{ik_1}{E}\beta_1'', \qquad \alpha_2'' = \frac{ik_2}{E}\beta_2'' \tag{5.83}$$

We also consider that both the charge density ϕ and current density J are continuous at $r = \xi$ that is

$$\begin{aligned} \phi^{<\xi}(r=\xi) &= \phi^{>\xi}(r=\xi) \\ J^{<\xi}(r=\xi) &= J^{>\xi}(r=\xi) \end{aligned} \tag{5.84}$$

which implies

$$\begin{aligned} \beta_2'' &= \frac{Ee^{-ik_2\xi}}{E-ik_1}(e^{ik_1'\xi}(\beta_1' - \alpha_1'\frac{iE}{k_2}) + e^{ik_2'\xi}(\beta_2' - \alpha_2'\frac{iE}{k_2})) \\ \beta_1'' &= \frac{Ee^{-ik_1\xi}}{E-ik_2}(e^{ik_1'\xi}(-\beta_1' - \alpha_1'\frac{iE}{k_1}) + e^{ik_2'\xi}(-\beta_2' - \alpha_2'\frac{iE}{k_1})) \end{aligned} \tag{5.85}$$

Here $k_{1,2}' = -\frac{iF_0}{k_BT} \pm \sqrt{-(\frac{F_0}{k_BT})^2 - \frac{ME}{k_BT}(\frac{\Gamma}{M} + E)}$ for all $E \geq 0$.

Now we write the explicit form for the charge density correlators $\phi^{<\xi}(r, r'; t)$ and $\phi^{<\xi}(r, r'; t = 0)$

$$\begin{aligned} \phi^{<\xi}(r,r';t) &= \int_0^\infty dE\{C_1'(E)(\alpha_1'(E)e^{ik_1'(E)r} + \alpha_2'(E)e^{ik_2'(E)r}) \\ &\quad (\alpha_1'^{+}(E)e^{-ik_1'(E)r'} + \alpha_2'^{+}(E)e^{-ik_2'(E)r'})e^{-Et}\} \end{aligned} \tag{5.86a}$$

$$\begin{aligned} \phi^{<\xi}(r,r';t=0) &= \int_0^\infty dE\{C_1'(E)(\frac{k_1'(E)}{E})^2\beta_1'^2(E)e^{ik_1'(E)(r-r')} \\ &- \int_0^\infty dE\{C_1'(E)\frac{k_1'(E)k_2'^{+}(E)}{E^2}\beta_1'^2(E)e^{-2ir_0\sqrt{-(\frac{F_0}{k_BT})^2+\frac{\Gamma E}{k_BT}}}e^{i(k_1'(E)r - k_2'(E)r')} \\ &- \int_0^\infty dE\{C_1'(E)\frac{k_1'^{+}(E)k_2'(E)}{E^2}\beta_1'^2(E)e^{2ir_0\sqrt{-(\frac{F_0}{k_BT})^2+\frac{\Gamma E}{k_BT}}}e^{-i(k_1'(E)r' - k_2'(E)r)} \\ &+ \int_0^\infty dE\{C_1'(E)(\frac{k_2'(E)}{E})^2\beta_1'^2(E)e^{-ik_2'(E)(r-r')} \end{aligned} \tag{5.86b}$$

Here $C_2'(k) = C_2'(k(E))$ and $E = \frac{k_BT}{\Gamma}(-k_1'k_2'^{+} + 2(\frac{F_0}{k_BT})^2)$, $dE = \frac{2k_BT}{\Gamma}k_1'dk_1'$

$k_{1,2}'(E) = -\frac{iF_0}{k_BT} \pm \sqrt{-(\frac{F_0}{k_BT})^2 + \frac{ME}{k_BT}}$ for $M \to 0 =>$

$k_1'(E) = -k_2^{+}(E)$ if $E \geq \frac{F_0^2}{\Gamma k_BT}$ and $k_1'(E) = k_2^{+}(E) - \frac{2F_0}{k_BT}$ if $E < \frac{F_0^2}{\Gamma k_BT}$ and $E \geq 0$.

Let $\gamma_1 = \frac{F_0}{k_BT}$, $\gamma_2 = \frac{\Gamma}{k_BT}$ and $k = k_r + ik_i$, with $k_i = -\frac{F_0}{k_BT}$ and $kk^{+} = k_r^2 + k_i^2$.

So we get

$$\phi^{<\xi}(r,r';0) = 2\gamma_2\int_{-\infty}^{\infty} dk_r\{\frac{C_2'(k)k_r}{k_r^2+\gamma_1^2}e^{\gamma_1(r-r')}[e^{ik_r(r-r')} + e^{ik_r(r+r'-2r_0)}]\} + hc \tag{5.87}$$

If $E \geq \frac{F_0^2}{\Gamma k_B T} => C_2'(k_r) = \frac{k_B T}{16\pi\Gamma}\frac{k_r^2+(\frac{F_0}{k_B T})^2}{k_r} = \frac{1}{16\pi\gamma_2}\frac{k_r^2+\gamma_1^2}{k_r}$.

We can now write

$$\phi^{<\xi}(r,r';t) = \frac{1}{8\pi}\int_{-\infty}^{\infty} dk_r\{e^{\gamma_1(r-r')}[e^{ik_r(r-r')} + e^{ik_r(r+r'-2r_0)}]e^{-Ek_r t}\} + hc$$
$$= \frac{1}{8\pi}\int_{-\infty}^{\infty} dk_r\{e^{\gamma_1(r-r')}[e^{ik_r(r-r')-\frac{1}{\gamma_2}k_r^2 t} + e^{ik_r(r+r'-2r_0)-\frac{1}{\gamma_2}k_r^2 t}]e^{-\frac{1}{\gamma_2}k_i^2 t}\} + hc$$
$$= \frac{1}{4}\sqrt{\frac{\gamma_2}{\pi t}}e^{\gamma_1(r-r')-\frac{\gamma_1^2}{\gamma_2}t}\{e^{-\frac{\gamma_2(r-r')^2}{4t}} + e^{-\frac{\gamma_2(r+r'-2r_0)^2}{4t}}\} \tag{5.88}$$

We have now to conduct the case where $0 < E < \frac{F_0^2}{k_B T\Gamma}$.

Here $k_{1,2}'$ are both purely imaginary $=> E$ is real. Moreover, $k_1'(E) = -k_1'^{+}(E)$ and $k_2'(E) = -k_2'^{+}(E)$. We first have to evaluate

$\alpha_1(E)\alpha_1^+(E) = (\frac{ik_1'(E)}{E}\beta_1'(E))(\frac{ik_1'(E)}{E}\beta_1'(E))^+ = -(\beta_1'(E)\beta_1'^+(E))(k_1'(E))^+\frac{1}{E^2}$.

We can write
$\alpha_2(E)\alpha_2^+(E) = (-\frac{ik_2'(E)}{E}e^{2ir_0\sqrt{-\gamma_1^2+\gamma_2 E}}\beta_1')(-\frac{ik_2'(E)}{E}e^{2ir_0\sqrt{-\gamma_1^2+\gamma_2 E}}\beta_1')^+$
$= -k_2'(E)^2\frac{1}{E^2}\beta_1'(E)\beta_1'^+(E)$
and $\alpha_1(E)\alpha_2^+(E) = (\frac{ik_1'(E)}{E}\beta_1'(E))(-\frac{ik_2'(E)}{E}e^{2ir_0\sqrt{-\gamma_1^2+\gamma_2 E}}\beta_1'(E))^+$.
Now (i) $2ir_0\sqrt{-\gamma_1^2+\gamma_2 E} \in \Re$ if $0 < E < \frac{\gamma_1^2}{\gamma_2}$
(ii) $k_1'(E)k_2'(E) = (-i\gamma_1 + \sqrt{-\gamma_1^2+\gamma_2 E})(-i\gamma_1 - \sqrt{-\gamma_1^2+\gamma_2 E}) = -\gamma_2 E$.
Therefore $\alpha_1(E)\alpha_2^+(E) = \frac{\gamma_2}{E}(\beta_1'(E)\beta_1'^+(E))e^{-2ir_0\sqrt{-\gamma_1^2+\gamma_2 E}}$
and $\alpha_2(E)\alpha_1^+(E) = \frac{\gamma_2}{E}(\beta_1'(E)\beta_1'^+(E))e^{2ir_0\sqrt{-\gamma_1^2+\gamma_2 E}}$.

We get the expression for the density correlator at $t = 0$

$$\phi^{<\xi}(r,r';t=0) = -\int dE(C_1'(E)\beta_1'(E)\beta_1'^+(E)(\frac{k_1'(E)}{E})^2 e^{ik_1'(E)(r-r')})$$
$$-\int dE(C_1'(E)\beta_1'(E)\beta_1'^+(E)(\frac{k_2'(E)}{E})^2 e^{ik_2'(E)(r-r')})$$
$$+\gamma_2\int dE(C_1'(E)\beta_1'(E)\beta_1'^+(E)\frac{1}{E}e^{-2ir_0\sqrt{-\gamma_1^2+\gamma_2 E}}e^{i(k_1'(E)r-k_2'(E)r')})$$
$$+\gamma_2\int dE(C_1'(E)\beta_1'(E)\beta_1'^+(E)\frac{1}{E}e^{2ir_0\sqrt{-\gamma_1^2+\gamma_2 E}}e^{i(k_2'(E)r-k_1'(E)r')}) \tag{5.89a}$$

where we have
$C_2'(k'(E)) = C_1'(E)\beta_1'(E)\beta_2'^+(E)$, $k_1'(E)r - k_2'(E)r' = 2\sqrt{-\gamma_1^2+\gamma_2 E}(r+r')$
$= -k_1'(E)r' + k_2'(E)r$, $E = \frac{2ik}{\gamma_2} + \frac{1}{\gamma_2}k^2$ $=>$ $dE = \frac{2}{\gamma_2}(i\gamma_1 + k)dk$.

In principle the integral $\int_0^{\frac{\gamma_1^2}{\gamma_2}} dE => \int_{-2i\gamma_1}^{-i\gamma_1} dk_i$ *or* $\int_0^{-i\gamma_1} dk_i$. Therefore

$$\begin{aligned}
\phi^{<\xi}(r,r';t=0) &= \frac{2}{\gamma_2}\int_{-i\gamma_1}^{0} dk_1' C_2'(k_1')\frac{k_1'^2(i\gamma_1+k_1')}{k_1'^2(2i\gamma_1+k_1')^2}\gamma_2^2 e^{ik_1'(E)(r-r')} \\
&-\frac{2}{\gamma_2}\int_{-2i\gamma_1}^{-i\gamma_1} dk_2' C_2'(k_2')\frac{k_2'^2(i\gamma_1+k_2')}{k_2'^2(2i\gamma_1+k_2')^2}\gamma_2^2 e^{ik_2'(E)(r-r')} \\
&-2\gamma_2\int_{-2i\gamma_1}^{-i\gamma_1} dk_2' C_2'(k_2')\frac{i\gamma_1+k_2'}{k_2'(2i\gamma_1+k_2')}e^{i(r+r'-2r_0)(k_2'+i\gamma_1)-i\gamma_1(r-r')} \\
&-2\gamma_2\int_{0}^{-i\gamma_1} dk_1' C_2'(k_1')\frac{i\gamma_1+k_1'}{k_1'(2i\gamma_1+k_1')}e^{-i(r+r'-2r_0)(k_2'+i\gamma_1)+i\gamma_1(r-r')} \\
&= 2\gamma_2\int_0^{i\gamma_1} dk_1'^a C_2'(k_1'^a)\frac{k_1'^a}{(-i\gamma_1+k_1'^a)(i\gamma_1+k_1'^a)}e^{i(k_1'^a-i\gamma_1)(r-r')} \\
&+2\gamma_2\int_0^{i\gamma_1} dk_3'^a C_2'(k_3'^a)\frac{k_3'^a}{(-i\gamma_1+k_3'^a)(-i\gamma_1+k_3'^a)}e^{i(-k_3'^a-i\gamma_1)(r-r')} \\
&+2\gamma_2\int_0^{i\gamma_1} dk_3'^a C_2'(k_3'^a)\frac{k_3'^a}{(-i\gamma_1+k_3'^a)(-i\gamma_1+k_3'^a)}e^{-i(r+r'-2r_0)k_3'^a+\gamma_1(r-r')} \\
&+2\gamma_2\int_0^{i\gamma_1} dk_1'^a C_2'(k_1'^a)\frac{k_1'^a}{(-i\gamma_1+k_1'^a)(i\gamma_1+k_1'^a)}e^{-i(r+r'-2r_0)k_1'^a-\gamma_1(r-r')} \qquad (5.89b)
\end{aligned}$$

where we have used $k_1'^a = k_1' + i\gamma_1,\ k_3'^a = -k_2'^a = -(k_2' + i\gamma_1).\ C_2'(k') = \frac{\gamma_1^2+k'^2}{k'}\frac{1}{16\pi\gamma_2}$ is a number.

The finite time density correlator is given by

$$\begin{aligned}
&\phi^{<\xi}(r,r';t) = \frac{1}{8\pi}\int_0^{i\gamma_1} dk_1'^a exp(i(k_1'^a-i\gamma_1)(r-r') - 2i(k_1'^a-i\gamma_1)\frac{\gamma_1}{\gamma_2}t - \frac{1}{\gamma_2}(k_1'^a-i\gamma_1)^2 t) \\
&+\frac{1}{8\pi}\int_0^{i\gamma_1} dk_3'^a exp(i(-k_3'^a-i\gamma_1)(r-r') - 2i(-k_3'^a-i\gamma_1)\frac{\gamma_1}{\gamma_2}t - \frac{1}{\gamma_2}(-k_3'^a-i\gamma_1)^2 t) \\
&+\frac{1}{8\pi}\int_0^{i\gamma_1} dk_3'^a exp(i(-k_3'^a)(r+r'-2r_0)+\gamma_1(r-r') - 2i(-k_3'^a-i\gamma_1)\frac{\gamma_1}{\gamma_2}t - \frac{1}{\gamma_2}(-k_3'^a-i\gamma_1)^2 t) \\
&+\frac{1}{8\pi}\int_0^{i\gamma_1} dk_1'^a exp(-i(k_1'^a)(r+r'-2r_0)-\gamma_1(r-r') - 2i(k_1'^a-i\gamma_1)\frac{\gamma_1}{\gamma_2}t - \frac{1}{\gamma_2}(k_1'^a-i\gamma_1)^2 t) \\
&= -\frac{1}{8\pi}\int_{\gamma_1}^{0} dk_1'^b exp(k_1'^b(r-r'-2\frac{\gamma_1}{\gamma_2}t) + \frac{(k_1'^b)^2 t}{\gamma_2}) \\
&-\frac{1}{8\pi}\int_{\gamma_1}^{0} dk_2'^b exp(k_2'^b(r-r'-2\frac{\gamma_1}{\gamma_2}t) + \frac{(k_2'^b)^2 t}{\gamma_2}) \\
&-\frac{1}{8\pi}e^{\gamma_1(r-r')}e^{-\gamma_1(r+r'-2r_0)}\int_{\gamma_1}^{0} dk_2'^b exp(k_2'^b(r+r'-2r_0-2\frac{\gamma_1}{\gamma_2}t) + \frac{(k_2'^b)^2 t}{\gamma_2}) \\
&-\frac{1}{8\pi}e^{-\gamma_1(r-r')}e^{\gamma_1(r+r'-2r_0)}\int_{\gamma_1}^{0} dk_1'^b exp(-k_1'^b(r+r'-2r_0+2\frac{\gamma_1}{\gamma_2}t) + \frac{(k_1'^b)^2 t}{\gamma_2}) \qquad (5.90)
\end{aligned}$$

where we have used $k_3'^a = -k_2'^a = -k_2' - i\gamma_1,\ k_1'^b = ik_1',\ k_2'^b = ik_2'$. The integral in the upper equation gives error functions.

Results

We plot $\phi(r, r'; t)$ vs r for the case $E > \frac{F_0^2}{k_B T \Gamma}$ using equation 5.88. Here it is clear that with the increase of time the tails of $\phi(r, r'; t)$ (figures 5.1) spread in both sides from that at $t = 0$ and ϕ piles up at the hard core. $\phi(r, r'; t)$ tends to a peaked function around $r = r'$, when $t \to 0$. This is the initial condition.

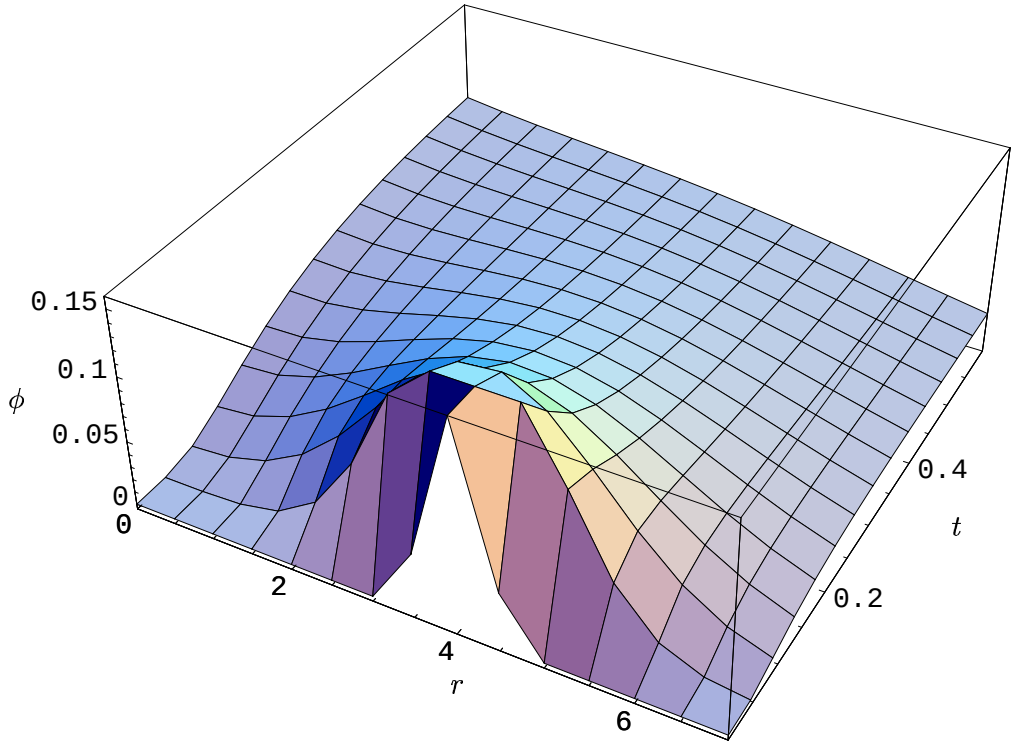

Figure 5.1: $\phi(r, r'; t)$ (from equation 5.88 for $E > \frac{F_0^2}{k_B T \Gamma}$) vs r and t. $\gamma_1 = -0.1,\ \gamma_2 = 0.1$ and the hard core is at $r = 0$. At $t = 0$, ϕ is peaked around $r = 4$.

5.1.5 Vortex antivortex pair dynamics in two-dimension

We can now discuss the problem of solving for the time dependent distribution function for vortex antivortex pair dynamics in two-dimension (2D). Here we recall the solution made by Carsten Timm [60]. In his solution he has excluded the zero (0) separation case as when vortices and antivortices come at 0 distance they recombine. But in our one dimensional (1D) analysis, explained above, we have proposed a finite distance hardcore for a vortex and antivortex separation. In 1D analysis our vortices and antivortices can not approach at $r < r_0$ because below r_0 the very high peaked barrier potential prohibits the particles from approaching towards each other.

Carsten Timm, in his calculation [60], got the following form for the probability density function $P(\mathbf{r}, \phi; \mathbf{r}', \phi'; t)$

$$P(r, \phi; r', \phi'; t) = \frac{1}{4\pi Dt}(\frac{r}{r'})^{\gamma} exp(-\frac{r^2 + r'^2}{4Dt}) \sum_{m=-\infty}^{\infty} e^{im(\phi-\phi')} I_{\sqrt{\gamma^2+m^2}}(\frac{rr'}{2Dt}) \quad (5.91a)$$

Doing the angular averaging ($P(r, r'; t) = \int d\phi P(r, \phi; r', \phi'; t)$, let $\phi' = 0$) we get only the $m = 0$ term in 2D case and this takes the following form

$$P(r, r'; t) = \frac{1}{4\pi Dt}(\frac{r}{r'})^{\gamma} exp(-\frac{r^2 + r'^2}{4Dt}) I_{\sqrt{\gamma^2}}(\frac{rr'}{2Dt}) \quad (5.91b)$$

Here I is a Bessel function. $\gamma = \frac{\gamma_T - 1}{2\gamma_T}$ with $\gamma_T = \frac{k_B T}{q^2}$ and q is the charge of a vortex.

Results

In the plot of the probability density function $P(\mathbf{r}, \mathbf{r}'; t)$ vs r/r', time being given by $\tau = \frac{t}{r'^2 D}$ (figure 5.2 using equation 5.91b) it is clear that two particles come closer to each other (the peak shifts towards shorter separation) with increasing time due to the effect of the attractive Coulomb potential between them. With the increase of the temperature (increase of $\gamma_T = \frac{k_B T}{q^2}$) the tail of the distribution function spreads towards increased r/r' which shows that more and more vortices become free due to thermal excitation. The curves corresponding to higher τ spread in both increasing and decreasing values of r/r' which explains that more and more particles become free (pair breaking) or collapse (recombination effect) with the increase of time.

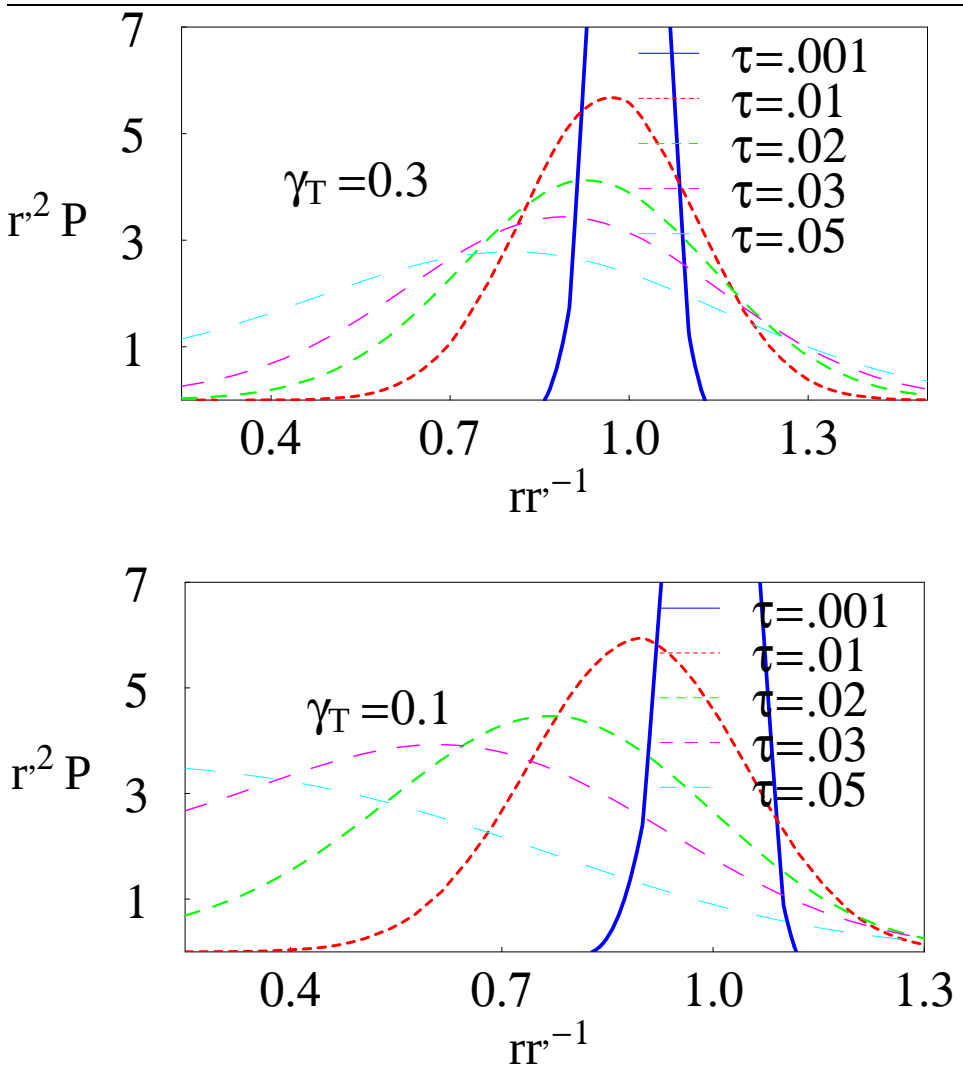

Figure 5.2: $r'^2 P(\mathbf{r}, \mathbf{r}'; t)$ vs r/r' (equation 5.91b) for different $\tau = \frac{t}{r'^2/D}$.

5.2 Conclusions

Time evolution of the probability density function of vortices and antivortices in two-dimensional JJAs has been discussed using a Fokker-Planck equation. Some collective effects namely screening of the long range Coulomb interaction, modification of purely diffusive dynamics and generalization of the friction function etc. have been extensively explained. We have then focussed on explaining vortex antivortex pair dynamics through the calculation of the time dependent probability density function where a finite hard core for the separation between two charged particles has been considered. We have also adopted Carsten Timm's approach of solving vortex antivortex pairdynamics where he considers that in the pair dynamics the pairing particles cannot recombine. Timm's approach gives justifiable results for the time dependent probability density

function in the case where two particles are prohibited from recombining with each other.

Chapter 6

Vortex-Antivortex Pair Dynamics in Regular two-dimensional Josephson junction arrays : Averaging over pair life time distribution

In this chapter we shall describe vortex-antivortex (VA) pair dynamics in two-dimensional (2D) Josephson junction arrays (JJAs) considering a distribution of VA pair life time. In chapter 2 we analysed VA pair dynamics through averaging over VA pair length distribution and calculated the susceptibility, mobility, dielectric function etc. for the vortex antivortex gas in 2D JJAs. Here we shall focus on calculating similar parameters but through a different approach of dealing VA pair dynamics namely through the consideration of a possible pair life time distribution.

6.1 Theoretical approach and basic definitions

The equation of motion (only radial motion for simplicity) for vortex in the overdamped limit (mass of vortex $M = 0$) in JJAs is

$$\gamma \frac{dx}{dt} = F(x) \tag{6.1}$$

where γ is the friction and we choose for the force

$$F(x) = \begin{cases} 0 & \text{for } x > \xi \\ -g & \text{for } a < x < \xi) \\ -f(x - r_0) & \text{for } r_0 < x < a \end{cases} \tag{6.2}$$

and corresponding to an interaction $V(x)$ $(F(x) = -\frac{dV(x)}{dx})$

$$V(x) = \begin{cases} const. & \text{for } x > \xi \\ V_1 + g(x-a) & \text{for } a < x < \xi) \\ V_0 + \frac{f}{2}(x-r_0)^2 & \text{for } r_0 < x < a \end{cases} \tag{6.3}$$

Here f and g are some parameters which are determined by the continuity of force at $x = a$ that is $f(a - r_0) = g$.

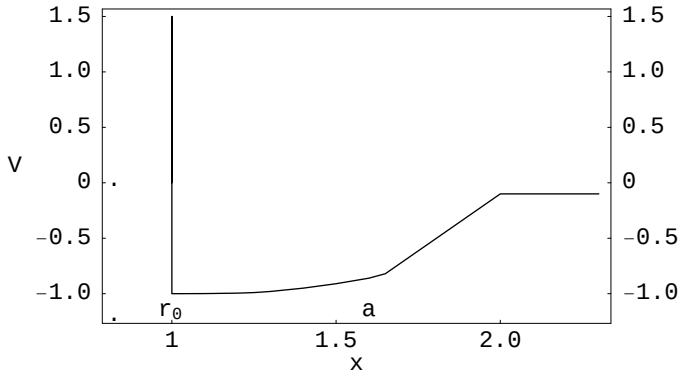

Figure 6.1: $V(x)$ vs x (equation 6.3).

Solution

(i) for $a < x < \xi$ $\quad \gamma\frac{dx}{xt} = -g \Rightarrow \quad x(t) = x(0) - \frac{g}{\gamma}t$

for $0 < t < t_a$ with $x(t_a) = a = x(0) - \frac{gt_a}{\gamma} \Rightarrow \quad t_a = \frac{\gamma(x_0 - a)}{g}$ with $x(0) = x_0$.

(ii) for $r_0 < x < a$ $\quad \gamma\frac{dx}{dt} = -f(x - r_0) \Rightarrow \quad x(t) = r_0 + (a - r_0)e^{-\frac{f}{\gamma}(t-t_a)}$. Here at $t = t_a$ $\quad x(t_a) = a$ and at $t \to \infty$ $\quad x(t) \to r_0$.

Pair susceptibility or polarisability

We now define the time dependent polarizability $\chi(t)$ of a stable vortex antivortex (VA) pair as

$$\chi(t) = \langle x(t)x(0)\rangle = \begin{cases} (x_0 - \frac{g}{\gamma}t)x_0 & \text{for } 0 \le t \le t_a \\ (r_0 + (a - r_0)e^{-\frac{f}{\gamma}(t-t_a)})x_0 & \text{for } t_a < t \end{cases} \tag{6.4}$$

Note We could use alternative forms for the force like e.g., $F(x) = -\frac{q_0^2}{x}$ with $a < x < \xi$ is one possibility.

We see the response of a pair through susceptibility $\chi(t - t')$ for the time $t - t' = \tau$ where $t' < t$. We consider the pairs of life time t_L. t_b and t_d are respectively the time of birth (pair making) and death (pair breaking) of a pair. So $t_d - t_b = t_L$. A given pair contributes to $\chi(\tau)$, if

(i) $\tau < t_L$

(ii) a pair survives between time t_b and t_d with $int(t', t) \subset int(t_b, t_d)$ i.e., $t_b < t'$ and $t < t_d$.

Now as $t_d = t_b + t_L$ and $t_b < t'(= t - \tau)$ we get $t_d < t - \tau + t_L$.

In this case we see the response of a pair which survives throughout the whole of the response collecting time. That means we consider the response of those pairs which took birth before we switch the response on and would die after the switch of the response is turned off. The *probability* of finding such a pair is

$$P(t < t_d < t - \tau + t_L) \propto t_L - \tau \tag{6.5}$$

limit: $t_L \to \infty$ *or* $\tau \to 0$ $\quad P \to N_p =$ number of pairs so

$$P(t < t_d < t - \tau + t_L) = N_p(1 - \frac{\tau}{t_L}) \tag{6.6}$$

The pair susceptibility $\bar{\chi}(\tau)$ is defined by

$$\bar{\chi}(\tau) = N_p(1 - \frac{\tau}{t_L})\theta(t_L - \tau)\chi(\tau) \tag{6.7}$$

where

$$\theta(t_L - \tau) = \begin{cases} 1 & \text{for } t_L > \tau \\ 0 & \text{for } t_L < \tau \end{cases} \tag{6.8}$$

Using Laplace transformation we get

$$\hat{\chi}(z, t_L) = N_p \int_0^{t_L} d\tau e^{-z\tau}(1 - \frac{\tau}{t_L})\chi(\tau) \tag{6.9}$$

We now average over pair life time t_L and get

$$\begin{aligned} \bar{\chi}(z) &= N_p \int dt_L p(t_L) \int_0^{\infty} dt\theta(t_L - t)e^{-zt}(1 - \frac{t}{t_L})\chi(t) \\ &= \int_0^{\infty} dt_L p(t_L) \int_0^{t_L} d\tau e^{-z\tau}(1 - \frac{\tau}{t_L})\chi(\tau) \end{aligned} \tag{6.10}$$

where we have considered $N_p = 1$.

Considering only the quadratic form for the interaction we get (see equations 6.3 and 6.4)

$$\chi(\tau) = r_0(1 + (c - 1)e^{-\frac{f}{\Gamma}\tau}) \tag{6.11}$$

Here $c = \frac{a}{r_0} \equiv$ follows from initial conditions.

We choose the expression for the pair life time distribution $p(t_L)$ from any of the following forms

$$(a) \qquad p(t_L) = A_1 e^{-\alpha(t_L - t_0)^2} \tag{6.12a}$$

$$(b) \qquad p(t_L) = \frac{A_2}{1 + (\frac{t_L}{t_0})^2} \tag{6.12b}$$

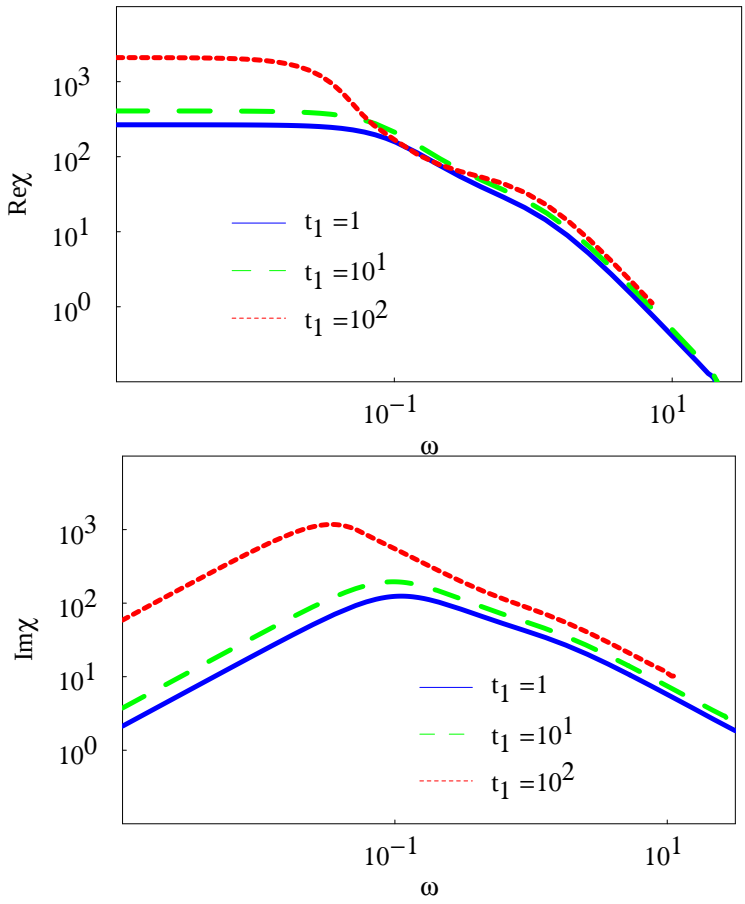

Figure 6.2: χ vs ω (equation 6.14a). $g = 1,\ c = 2,\ s = 10^{-2},\ \alpha_L = 10^{-3}$.

t_0 in equation (6.12a) is the initial condition and in equation (6.12b) is the upper limit of life time.

Normalisation : The values of A_1 and A_2 (in equation 6.12) follow from the following normalisation

$$(a)\ \int_0^\infty dt_L p(t_L) = \frac{A_1}{2}\int_{-\infty}^{\infty} dx e^{-\alpha x^2} = \frac{A_1}{2}\sqrt{\pi/\alpha} = 1 \tag{6.13a}$$

$$(b)\ \int_0^\infty dt_L p(t_L) = \int_0^\infty dt_L \frac{A_2}{1+b^2 t_L^2} = A_2\frac{\pi}{2b} = 1 \tag{6.13b}$$

We take the scale frequency $\omega_a = \frac{k_B T}{\Gamma r_0^2}$ and let $j = \frac{z}{\omega_a}$.

We do the following transformations: $\tau/t_L = x,\ t_L/t_0 = y,\ \omega_a t_0 = t_1,\ \alpha t_0^2 = \frac{\alpha}{\omega_a^2}t_1^2 = \alpha_L t_1^2,\ z\tau = j\omega_a t_L x = j\omega_a t_0 xy = jt_1 xy,\ \frac{f}{\Gamma}\tau = \frac{f}{\Gamma}\frac{t_1}{\omega_a}xy = gt_1 xy,\ \frac{f}{\Gamma\omega_a} = \frac{fa^2}{k_B T} \equiv g$. Now letting $j = -(i\omega - s)$ we get the following expressions of the average susceptibility for

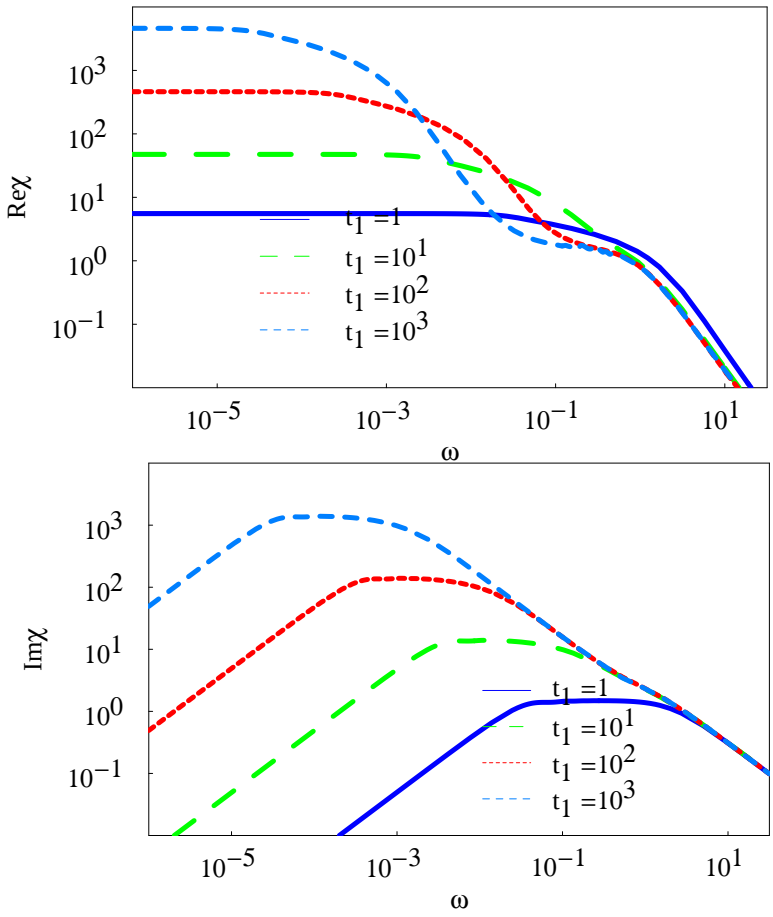

Figure 6.3: χ vs ω (equation 6.14b). $g = 1,\ c = 2,\ s_1 = 10^{-2}$.

two different forms of $p(t_L)$

$$\bar{\chi}(\omega) = \frac{2a}{\omega_a}\sqrt{\frac{\alpha_L}{\pi}}t_1^2\int_0^\infty dy e^{-\alpha_L t_1^2(y-1)^2} y \int_0^1 dx e^{(i\omega-s)t_1 xy}(1-x)(1+(c-1)e^{-gt_1 xy}) \tag{6.14a}$$

$$\begin{aligned}\bar{\chi}(\omega) \quad &= \frac{2a}{\pi\omega_a}t_1\int_0^\infty dy\frac{y}{1+y^2}\int_0^1 dx e^{(i\omega-s)t_1 xy}(1-x)(1+(c-1)e^{-gt_1 xy}) \\ &\approx \frac{2a}{\pi\omega_a}\int_0^\infty dy\frac{1}{1+y^2}\frac{1}{(i\omega-s)}(e^{(i\omega-s)t_1 y}-1 \\ &\qquad + \frac{c-1}{1-\frac{g}{i\omega-s}}(e^{(i\omega-s-g)t_1 y}-1))\end{aligned} \tag{6.14b}$$

In equation (6.14b) we have approximated the expression of $\bar{\chi}(\omega)$ replacing $(1-x)$ in it by 1. We let here a frequency dependent parameter $s = s_1\omega$ where s_1 is some number.

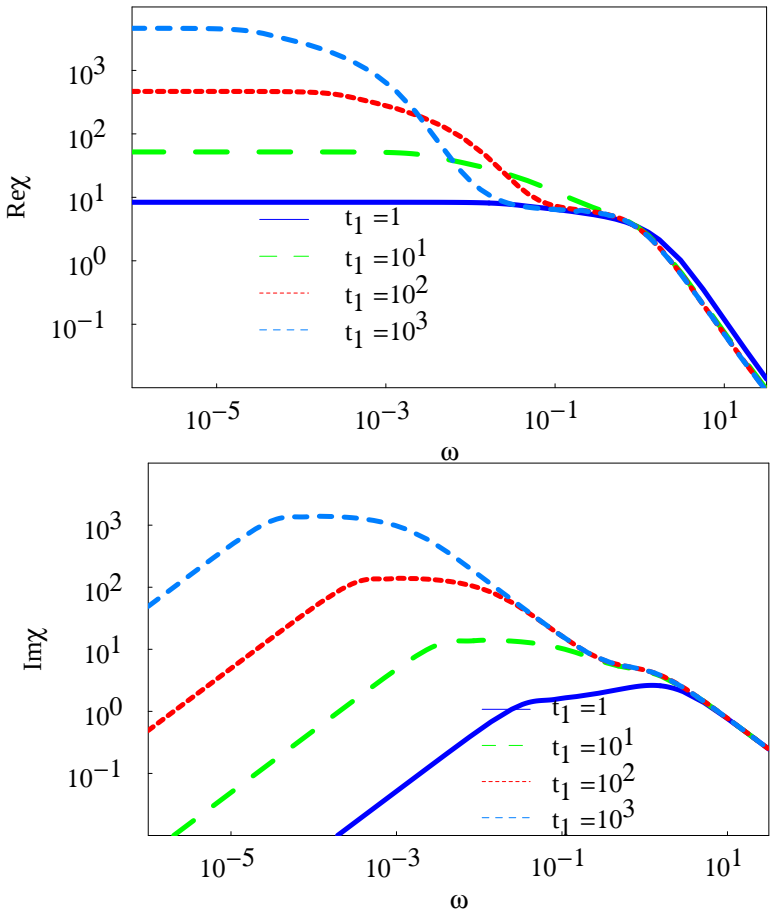

Figure 6.4: χ vs ω (equation 6.14b). $g = 1,\ c = 5,\ s_1 = 10^{-2}$.

Dielectric function

We define the frequency dependent dielectric function $\epsilon(z)$ (details are explained in chapter 2) as

$$\epsilon(z) = 1 + \frac{2\pi q_0^2 n}{z\gamma(z)} => \quad \epsilon(\Omega) = 1 + \frac{2\pi q_0^2 n \mu(\Omega)}{-i\Omega} = 1 + 2\pi q_0^2 n \bar{\chi}(\Omega) \tag{6.15}$$

where q_0 is the charge of a vortex, frequency $z = -i\Omega$, $\mu(\Omega) = \frac{1}{\gamma(\Omega)}$ is the inverse friction function which is called the vortex mobility. The friction function $\gamma(z)$ is defined by

$$\gamma(z) = \frac{1}{z}[\frac{1}{\bar{\chi}(z)} - \frac{1}{\bar{\chi}(0)}] \tag{6.16}$$

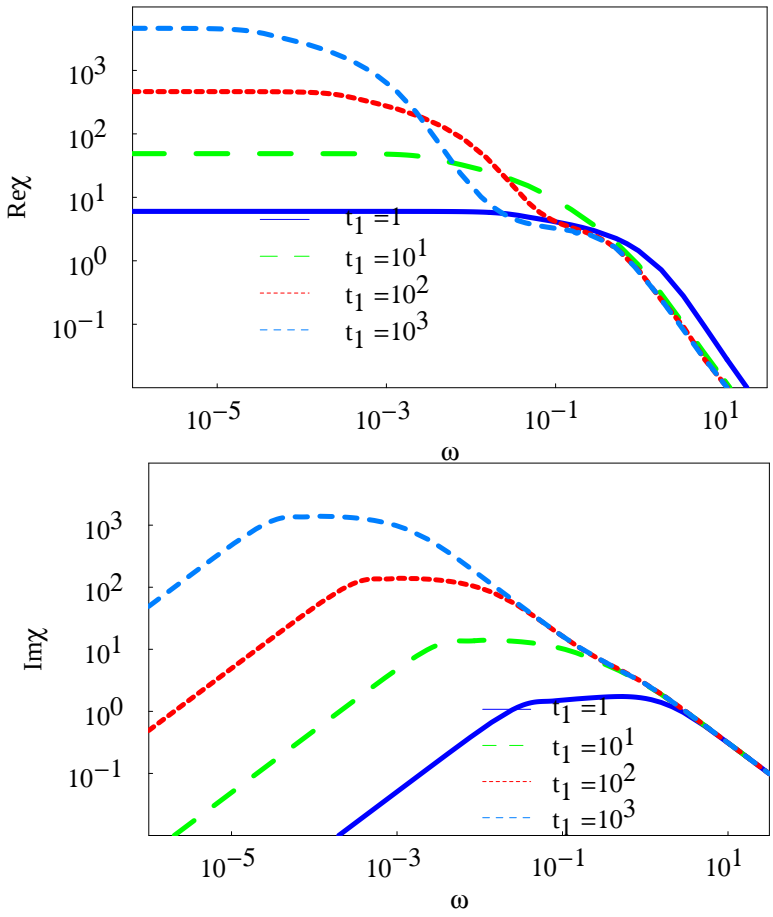

Figure 6.5: χ vs ω (equation 6.14b). $g = 0.5,\ c = 2,\ s_1 = 10^{-2}$.

Results

We have plotted the susceptibility for the vortex antivortex pair dynamics (explained above) using the expressions in equations (6.14a and 6.14b). Here at very low frequencies we see frequency independent behavior in the real part of the susceptibility. The constant value susceptibility falls to $Re\chi \propto \frac{1}{\omega^2}$ at very high frequency region. The exciting findings arise here in both the real and imaginary parts of the susceptibility in the mid frequency regime. At very low frequency $Im\chi \propto \omega$ and at very high frequency region $Im\chi \propto 1/\omega$ for both the choices of the pair life time distributions (equations 6.12a and 6.12b). But for the second (equation 6.12b) choice of $p(t_L)$ in equation 6.14b we see there is an extended flat region (almost constant) of $Im\chi$ in the mid frequency region (figure 6.3) which is almost absent in figure 6.2 using expression 6.14a where $p(t_L)$ is taken from equation 6.12a. This is comparable with the expressions for the susceptibility explained in chapter 2 of this thesis using our previous approach (equation 2.39 whose plot is shown here in figure 6.6 for the sake of comparison). This mid

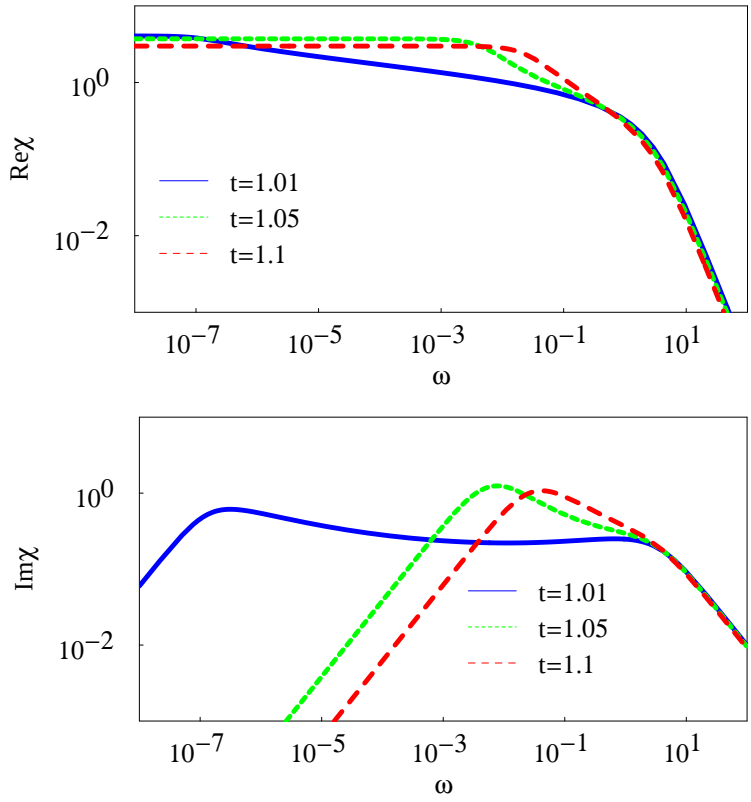

Figure 6.6: χ vs ω (equation 2.39) for different temperature $t = T/T_{BKT}$.

frequency flat region in $Im\chi$ finally becomes the origin of the $1/\omega$ flux noise for vortex antivortex pair dynamics. We have changed the values of the parameters c and g in the next two plottings namely in figure 6.4 ($c = 5$) and figure 6.5 (g=0.5). In both the changes we have got similar type of changes in the behaviors of $\chi(\omega)$. In both cases the mid frequency almost flat regions in $Im\chi$ change and some frequency dependent slowing down arise there. The high frequency universality of all the curves are also another important achievement which is also comparable with fig. 6.6 using other methods explained in chapter 2. Real parts of the susceptibility $Re\chi$ also behave a little differently in figures 6.3-6.5. In the mid frequency regime its smooth slowing down is changed very slightly with the introduction of different higher values of c and g and all curves ($Re\chi$) at higher values of t_1 fall down with increasing ω with a little downward bent and finally show a tendency of meeting at a common line at very high frequency regime. These (figures 6.3-6.5) are comparable with the real parts of χ in figure 6.6. The dielectric functions derived from this susceptibility are also plotted in figure 6.7. The Drude type $Re\epsilon^{-1} \propto \omega^2$ behavior is clear in this plot at low frequencies and at very high frequencies $Re\epsilon^{-1}$ is constant at the value 1. In the mid frequency regime we get anomalous type behavior in $Re\epsilon^{-1}$ while at very high values of t_1 Minnhagen

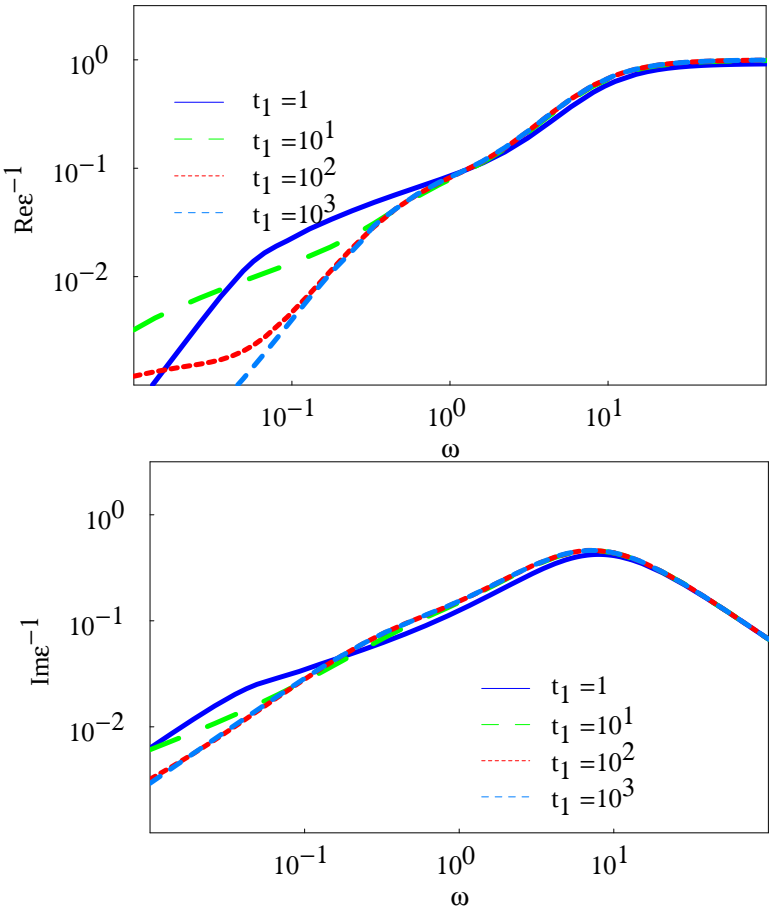

Figure 6.7: ϵ vs ω (equation 6.14b and 6.15). $g = 1,\ c = 2,\ s_1 = 10^{-2}$.

phenomenology $Re\epsilon^{-1} \propto \omega$ is achieved. We have finally plotted, in figure 6.8, the flux noise vs frequency. We see the frequency independent flux noise (white noise) for all t_1 at low frequency regime and a universal $S_\phi \propto \frac{1}{\omega^2}$ at very high frequency regime are achieved. In the intermediate frequency regime we get $S_\phi \propto \frac{1}{\omega^x}$ where $1/2 < x < 1$ and with the decrease of t_1 x approaches towards 1 that is we almost get $S_\phi \propto \frac{1}{\omega}$ flux noise in the intermediate frequency regime which is comparable with the experimental data [39,41] and our previous results explained in chapter 2.

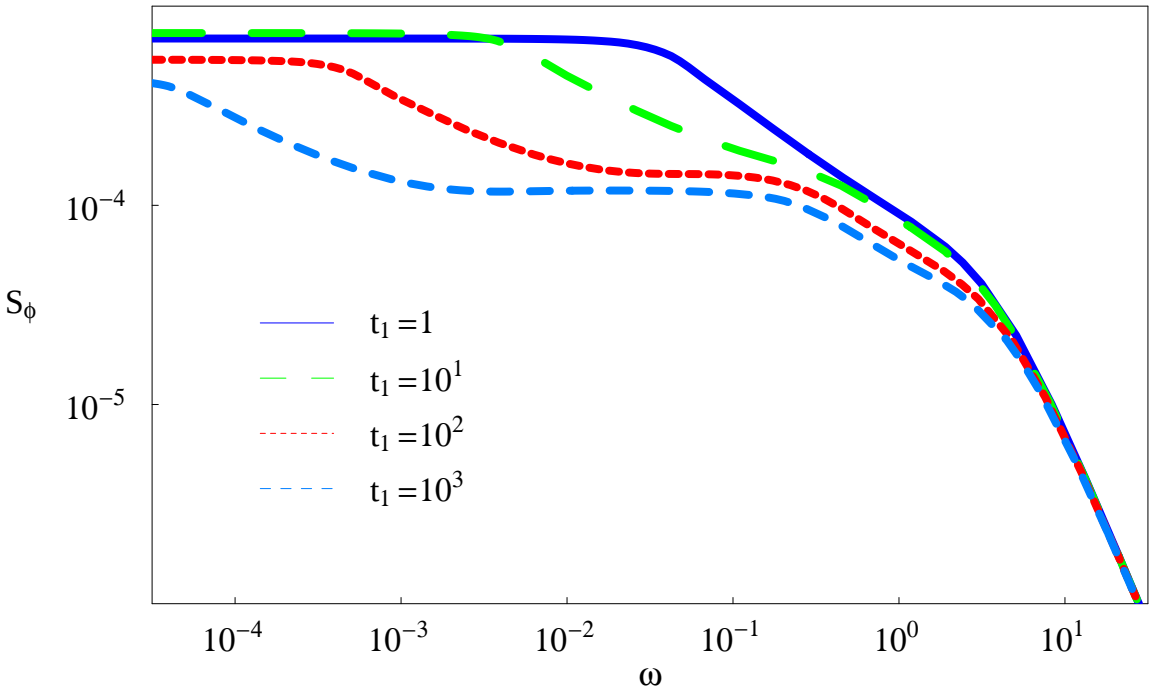

Figure 6.8: S_ϕ vs ω (derived from equation 6.14b. Details are in chapter 2 and equation 2.108 for the expression of the flux noise). $g = 1,\ c = 2,\ s_1 = 10^{-2}$.

6.2 Conclusions

We have presented here a new technique of solving vortex antivortex pair dynamics for calculating the susceptibility, mobility and dielectric function of vortex antivortex gas in two dimensional JJAs. We have dealt the pair dynamics averaging over the pair life time distribution which gives us resonably well results for the frequency dependence of mobility and dielectric function. We have used different forms for the pair life time distributions and have compared between the results coming out of those pair life time distributions. We have got some reasonable and comparable values in calculations on susceptibility, dielectric functions, flux noise etc. for vortex-antivortex pair dynamics in two dimensional Josephson junction arrays.

Chapter 7

Summary and discussion

In this thesis we have studied the dynamical phenomena of the topological excitations, vortices and antivortices, in two-dimensional (2D) Josephson junction arrays (JJAs) by numerical calculation, analytical analysis and Monte Carlo simulation of XY model. We have restricted our calculations to the case of thermally excited vortices and antivortices in the array of superconducting islands. Both regular and disordered arrays where the particles (vortex and antivortex) move randomly due to the influences of temperature and Coulomb interactions between the charges of the particles have been considered. Our central quantity is the charge density correlator which is related to the charge response function. We have also explained the time evolution of the probability density function which is related to the charge density correlator.

In chapter 2 the dynamical phenomena of the topological excitations (overdamped limit), present in two-dimensional classical Josephson junction arrays, are described in the framework of Ambekaokar et. al. for explaining the vortex antivortex pair dynamics in JJAs near Berezinskii-Kosterlitz-Thouless transition temperature considering a distribution of VA pair length. The vortex mobility for VA pair dynamics has been derived by averaging over the VA pair distribution function and the free V/A dynamical mobility has been taken from the calculation using the Mori technique. From the combined bound and free vortex mobility we have developped a formalism of calculating the flux noise and have got a good agreement with the experimental results. The theoretical results from these methodologies and their comparisons with the experimental results are explained in details. Here we have got that the anomalous Minnhagen phenomenology (MP) is a consequence of the motion of (unbound) vortices in a Coulomb potential which is screened by other *free* particles. The more this screening decreases upon approaching transition temperature, the more anomalous behavior is pronounced. However, MP does not lead to $1/\omega$ flux noise. Vortices and antivortices moving as *pair*, at short enough distances and up to some finite life time, yield an even more anomalous vortex dielectric constant with temperature-dependent frequency exponents. This effect, combined with a T-dependent pair structure factor indeed gives $1/\omega$ flux noise in an intermediate frequency range. That is the $1/\omega$ flux noise arises due to the vortex antivortex pair dynamics and $1/\omega$ part reduces with the increase of temperature

and finally is lost at very high temperature when almost all pairs break and screened interactions dominate.

We have calculated the charge structure factor in chapter 3 which has played an important role in explaining the flux noise in chapter 2. We used a Debye-Hückel model for the structure factor in chapter 2. The question arises whether the structure factors of such a vortex antivortex system depend on temperature. In order to find a concrete form for the structure factor we have used Monte Carlo simulation of XY model for temperature dependent vortex density and coordinates in a periodic array of Josephson junctions in two dimension. By examining the local phase configurations we have developped a method for calculating the coordinates of the vortices and antivortices in the array and have seen that the vortices and antivortices are not necessarily situated at the centers of the cells but any point inside the cell. The method of choosing the coordinates of a vortex or antivortex is explained in section 3.1. Using these coordinates we have calculated number and charge structure factors. The charge structure factor is zero for $k = 0$ which follows from the charge neutrality in a two dimensional Coulomb system but the number structure factor has a delta peak at $k = 0$. Both the structure factors end with the value of unity at very high wave numbers. For small values of the wavenumbers k's ($k > 0$) the charge structure factor grows as k^2 with some upward smooth peak before flattening to a constant value of unity indicating the structure of the system. We also see a small temperature dependence in the charge structure factors. At low k values the values of charge structure factor increases with the increase of temperature but the value of the structure factor decreases again if the temperature increases too much. A possible cause of this temperature effect is explained in the result section of chapter 3.

We have continued our analysis of vortex dynamics in Josephson junction arrays considering it to be not purely regular. So in chapter 4 we have raised the issue of investigating the effects of the missing superconducting sites in the arrays on the dynamics of free vortices and antivortices. Here we have developped, using the multiple trapping model, an expression for the mobility of vortices and have investigated the effects of the disorder on the conductance of the array through its relation with the vortex mobility near the critical percolation limit p_c. Using this mobility we have also calculated the flux noise expression in disordered array and have tried to see the disorder effects on the flux noise. In our results we see that sheet resistance R_s exhibits three frequency regimes. At very low and high frequency ω a white spectrum is observed with a much lower value for low ω than for large ω. For the time scale corresponding to the latter regime vortices remain either trapped in a hole or free outside any hole. Thus the mobility, and the corresponding response is given by the one of a regular array. At the opposite end, for very low frequencies, vortices get trapped many times during one excitation cycle, which strongly reduces their mobility. For intermediate frequency regime $R_s \propto \omega^x$ with x varying between $x = 1$ and $x = 2$. For higher temperatures the $R_s \propto \omega$ almost coincide, signalling some kind of universality. The inductive part $L_s^{-1} \propto \omega^2$ at low ω while for intermediate frequency regime L_s^{-1} is independent of ω. For large frequencies a tendency of L_s^{-1} to grow with frequency with some new exponent is also seen for higher values of percolation fraction p. The critical frequency for crossover

from $L_s^{-1} \propto \omega^2$ to constant L_s^{-1} decreases with the decrease of temperature T and p. We have also looked at the vortex resistance which is thermally activated at sufficiently high temperatures. The activation energy is seen to be on the order of 4 times the Josephson coupling between the existing superconducting sites but the values of the activation energy at lower temperatures are a little bit different from those at higher temperatures. The final calculation in chapter 4 has been on flux noise. $1/\omega$ noise is achieved for the intermediate frequencies separating the white noise part for small ω and $1/\omega^2$ noise for very high frequencies. Thus the presence of disorder leads to similar results as seen in regular arrays. However, very close to critical percolation fraction p_c the flux noise data has some unexpected flatenning before turing to $1/\omega^2$ part which is a consequence of the frequency dependence of the vortex mobility.

The time-dependent probability distribution function of vortices and antivortices in JJAs has been calculated in chapter 5 using a Fokker Planck equation. Some collective effects namely screening of the long range Coulomb interaction, modification of purely diffusive dynamics and generalization of the friction function have been extensively explained. Mori technique of solving one component Coulomb system is quite effective in explaining several things like free particle diffusion, friction function etc. but is not suitable to treat the screening in interaction problem in a fashionable way. Aiming at having all the solutions from one approach we have adopted Fokker-Planck methodology to solve a one component fluid (vortex system) in the beginning of chapter 5. We have later focussed on explaining vortex antivortex pair dynamics through the calculation of time dependent probability density function where a finite hard core for the interaction between two charged particles has been considered. The calculated distribution function has shown the time dependent behaviors of vortices and antivortices. With the evolution of time the vortex antivortex pair distribution slowly turns towards free particle distribution or recombination process takes place. We have also adopted Carsten Timm's approach of solving vortex antivortex pairdynamics where the pairing particles are prohibited from being recombined. This approach also gives justifiable results for the time dependent probability density function.

Finally in chapter 6 we have studied the vortex antivortex pair dynamics through calculation of the average susceptibility χ of a pair by averaging over different forms of the pair life time distribution. Using this technique we have worked on some aspects like the calculation of the frequency dependent susceptibility, mobility and dielectric function of vortex antivortex gas in two dimensional JJAs. At very low frequencies we see frequency independent behavior in the real part of the susceptibility. In the mid frequency regime it has some anomalous type behavior which finally falls to $Re\chi \propto \frac{1}{\omega^2}$ at very high frequency region. The exciting findings arise here in both the real and imaginary parts of the susceptibility in the mid frequency regime. At very low frequency $Im\chi \propto \omega$ and at very high frequency region $Im\chi \propto 1/\omega$ leaving some anomalies in the mid frequency regime. This anomalous behavior in the mid frequency regime is also visible in the $Re\chi$ plot. This mid frequency anomalous behavior produces some $1/\omega$ type flux noise as is shown in chapter 2. In the dielectric functions ϵ we see the Drude type $Re\epsilon^{-1} \propto \omega^2$ behavior at very low frequencies and at very high frequencies $Re\epsilon^{-1}$ is constant at the value 1. In the mid frequency regime we get anomalous

type behavior in $Re\epsilon^{-1}$ which under specific conditions are also satisfying with the Minnhagen phenomenology $Re\epsilon^{-1} \propto \omega$.

At the beginning of this project we aimed at understanding the dynamics of thermally created vortices in Josephson junction arrays. We have developped here several approaches. Most of the time we tried to compare our theoretical results with experimental observations available but due to the lack of experimental data for all the details we sometimes had to restrict on only theoretical explanations. We also opened some questions to be solved in coming time. When more and more experimental data will be available our theoretical methodologies can be extended towards more understanding of the dynamics of Josephson junction arrays.

Appendix A

Bibliography

[1] R.S.Newrock, C.J.Lobb,U.Geigenmüller, M.Octavio ; Solid State Physics 54, 263 (2000)

[2] P.Martinoli. C.Leemann ; Journal of Low Temperature Physics 118, 699 (2000)

[3] P.W.Anderson ; in ≪ Lectures on the Many-Body-Problem ≫, Vol 2, ed. E.R.Caianiello, Academic Press, New York (1964)

[4] E. Simanek ; ≪ Inhomogeneous superconductors ≫ , Oxford University Press, 1994, Ch. 4 and 5

[5] V.L.Berezinskii ; Sov Phys JETP 32, 493 (1971)

[6] J.M.Kosterlitz, D.J.Thouless ; J Phys C6, 1181 (1973)

[7] S.E.Korshunov, A.Vallat and H.Beck ; Phys Rev B51, 3071 (1995)

[8] E. Simanek ; Sol. State Comm. 31, 419 (1979)

[9] D. Ariosa, H.Beck, Phys Rev B45, 819 (1992)

[10] L.Jacobs, J.V.Jose, M.A. Novotny, A.M.Goldman, Phys Rev B38, 4562 (1988) and references therein

[11] M. Capezzali, D. Ariosa, H.,Beck; Physica B230-232, 962 (1997)

[12] K.H.Wagenblast, A.v Otterlo, G.Schn, G.T.Zimanyi ; Phys Rev Lett 78, 1779 (1997)

[13] J.M.Kosterlitz ; J.Phys C7, 1046 (1974)

[14] J.V. Jose, L.P. Kadanoff, S. Kirkpatrick, D.R. Nelson ; Phys Rev B 16, 1217 (1977)

[15] A.Vallat, H.Beck ; Phys Rev B 50, 4015 (1994)

[16] S.R.Shenoy ; J Phys C, Solid State Physics 18, 5163 (1985)

[17] P.Minnhagen ; Rev Mod Phys 59, 1001 (1987)

[18] D.Dominguez, J.V.Jose ; Int J Mod Phys B8, 3749 (1994)

[19] J.C.Ciria, C.Giovanella ; J Phys Cond Mat 10, 1453 (1998)

[20] G.Schön, A.D.Zaikin ; Physics Reports 198, 237 (1990)

[21] V.L.Pokrovsky, M.V.Feigel'man, A.M.Tsvelick ; ≪ Spin waves and magnetic excitations ≫, ed. A.S.Borovik-Romanov and S.K.Sinha ; Elsevier Science Publishers B.V. 1988, p. 67

[22] H.Beck, D.Ariosa ; Solid State Communications 80, 657 (1991)

[23] C.J.Lobb, D.Abraham, M.Tinkham ; Phys Rev B27, 150 (1983)
[24] U.Eckern, A.Schmid ; Phys Rev B 39, 6441 (1981)
[25] R.Fazio, H.van der Zaant ; Physics reports 355, 235 (2001)
[26] R Fazio, U Geigenmüller, G Schön ; in ≪ Quantum fluctuations in Mesoscopic and Macroscopic Systems ≫, eds. H.A.Caldeira et al, World scientific, Singapore, 1991, p. 214
[27] R. Fazio, G. Schön ; Phys Rev B 43, 5307 (1991), U Eckern, E B Sonin, Phys Rev B 47, 505 (1993)
[28] V.Ambegaokar, B.I.Halperin, D.R.Nelson, E.D.Siggia; Phys Rev Lett 40, 783 (1978) and Phys Rev B21, 1806 (1980)
[29] Md. Ashrafuzzaman and Hans Beck; Studies of High Temperature Superconductors (Nova Science, New York, 2002), Vol. 43
[30] Md. Ashrafuzzaman, M. Capezzali and H. Beck; Phys Rev B 68, 052502 (2003)
[31] V. Ambegaokar, S. Teitel; Phys Rev B19, 1667 (1979); D. Bormann; hand note and personal communication
[32] P. Minnhagen, Rev. Mod. Phys., Vol. 59, No 4 (October 1987)
[33] B. Jenneret, J.L. Gavilano, G.A. Racino, C. Leemann, P. Martinoli; Appl. Phys. Lett. 55, 2336(1989)
[34] O. Gallus, Diploma thesis, Institute of Physics, University of Neuchatel, Switzerland (1999)
[35] D. Bormann, H.Beck, O.Gallus, M.Capezzali ; J Phys IV France 10, Pr-447 (2000)
[36] M.Capezzali, H.Beck, S.R.Shenoy ; Phys Rev Lett 78, 523 (1997)
[37] Md. Ashrafuzzaman, P. Curty, M. Neef and H. Beck; Institute of Physics, University of Neuchatel, Switzerland (unpublished,2002)
[38] A. Jonsson and P. Minnhagen; Phys Rev B 55, 14 (1997)
[39] S. Candia, Ch. Leemann, S. Mouaziz and P. Martinoli, Physica C 369, 309 (2002)
[40] H.E.DeWitt, M.Schlanges, A.Y.Sakakura, W.D.Kraeft ; Phys Lett A197, 326 (1995)
[41] T.J.Shaw, M.J.Ferrari,L.L.Sohn, D.H.Lee, M.Tinkham, J.Clarke; Phs Rev Lett 76, 2551 (1996)
[42] Philippe Curty and Hans Beck, Institute of Physics, University of Neuchatel, Switzerland (unpublished)
[43] P.J. Flory, J. Am. Chem. Soc. 63, 3083 (1941).
[44] W.H. Stockmayer, J. Chem. Phys. 11, 45 (1943).
[45] S. R. Broadbend and J. M. Hammersley, Proc. Camb. Phil. Soc. 53, 629 (1957).
[46] B.B. Mandelbrot, The fractal geometry of nature, Freeman, San Francisco (1977).
[47] A. Bunde and S. Havlin, Fractal and Disorder Systems, Springer-Verlag, Berlin (1991).
[48] A.L. Eichenberger, J. Affolter, M. Willemin, M. Mombelli, H. Beck, P. Martinoli, S.E. Korshunov; Phys Rev Lett 77, 3905 (1996).

[49] Jérôme Affolter, PhD thesis, Institute of Physics, University of Neuchatel, Switzerland (2001), Unpublished.
[50] T. Nakayama, K. Yakubo, R.L. Orbach ; Rev Mod Phys 66, 381 (1994).
[51] M. Mombelli, H. Beck ; Phys Rev B57, 14'397 (1998).
[52] M.P.A. Fisher, Phys Rev Lett 62, 1415 (1989).
[53] M.V. Feigel'man, V.B. Geshkenbein, A.I. Larkin, V.M. Vinokur; Phys Rev Lett 63, 2303.
[54] M. Calame, S.E.Korshunov, Ch.Leemann, P.Martinoli ; Phys Rev Lett 86, 3630 (2001).
[55] H. Scher and E.W. Montroll, Phys Rev B12, 2455 (1975).
[56] Md. Ashrafuzzaman and Hans Beck, Journal of Magnetism and Magnetic Materials (JMMM), Vol 272-276P1 pp 284-285 (2003).
[57] A. D. Fokker, Ann. Physik 43, 810 (1914).
[58] M. Planck, Sitzber. Preuβ. Akad. Wiss. p. 324 (1917).
[59] H. Risken, The Fokker-Planck Equation (Methods of Solution and Application), Springer-Verlag, 2nd edition (1989).
[60] C. Timm, Physical Review B 55, 3241 (1997)